MULTI-FUNCTIONAL BIO-SYNTHETIC HYBRID NANOSTRUCTURES FOR ENHANCED CELLULAR UPTAKE, ENDOSOMAL ESCAPE AND TARGETED DELIVERY TOWARD DIAGNOSTICS AND THERAPEUTICS

A Dissertation

by

RITU SHRESTHA

Submitted to the Office of Graduate Studies of
Texas A&M University
in partial fulfillment of the requirements for the degree of

DOCTOR OF PHILOSOPHY

Approved by:

Chair of Committee,	Karen L. Wooley
Committee Members,	Kevin Burgess
	Paul S. Cremer
	Jaime C. Grunlan
Head of Department,	David H. Russell

December 2012

Major Subject: Chemistry

ABSTRACT

Applications of nanotechnology in medicine, also known as nanomedicine, is a rapidly growing field as it holds great potential in the development of novel therapeutics toward treatment of various diseases. Shell crosslinked knedel-like nanoparticles (SCKs) that are self assembled from amphiphilic block copolymers into polymeric micelles followed by crosslinking selectively throughout the shell domain have been investigated as theranostic agents for the delivery of nucleic acids and incorporation of imaging probes. The main focus of this dissertation is to design and develop unique multifunctional bio-synthetic hybrid nanoparticles that can carry agents for radiolabeling, moieties for inducing stealth properties to minimize protein adsorption *in vivo*, ligands for site-specific targeting, therapeutic payloads, and are optimized for efficient delivery of cargoes intracellularly and to the target sites toward constructing novel nanoscopic objects for therapy and diagnosis.

Alteration of polymeric building blocks of the nanoparticles provides opportunities for precise control over the sizes, shapes, compositions, structures and properties of the nanoparticles. To ensure ideal performance of nanoparticles as theranostic agents, it is critical to ensure high intracellular bioavailability of the therapeutic payload conjugated to nanoparticles. Special efforts were made by employing well-defined multi-step polymerization and polymer modification reactions that involved conjugation of peptide nucleic acids (PNAs) to chain terminus of poly(ethylene glycol) (PEG) chain grafts such that they were presented at the outermost

surface of SCKs. Additionally, chemical modification reactions were performed on the polymer backbone to integrate positive charges onto the shell of the nanoparticles to afford cationic SCKs (cSCKs) for facilitating cellular entry and electrostatic interactions with negatively charged nucleic acids. Covalent conjugation of F3, a tumor homing peptide, post-assembly of the nanoparticles enhanced cellular uptake and knockdown of nucleolin (a shuttling protein overexpressed at the sites of angiogenesis) and thus inhibiting tumor cell growth. Furthermore, these polymer precursors of the cSCKs were modified with partial to full incorporation of histamines to facilitate their endosomal escape for efficient delivery into the cytosol. The cSCKs were further templated onto high aspect ratio anionic cylinders to form hierarchically-assembled nanostructures that bring together individual components with unique functions, such as one carrying a therapeutic payload and the other with sites for radiolabeling. These higher order nanoobjects enhance circulation *in vivo*, have capabilities to package nucleic acids electrostatically and contain sites for radiolabeling, providing an overall advantage over the individual components, which could each facilitate only one or the other of the combined functions. Hierarchically-assembled nanostructures were investigated for their cellular uptake, transfection behavior and radiolabeling efficiency, as the next generation of theranostic agents.

DEDICATION

To my father, Prem Lal Shrestha, my mother, Maiya Milan Shrestha and my advisor, Karen Lynn Wooley

ACKNOWLEDGEMENTS

For the past five years, it has been my extreme privilege and a great pride to be working with Professor Karen Wooley toward completing my graduate studies. In the process of mentoring me to become an independent researcher, Karen has taught me invaluable life lessons, for which I am forever indebted to her. Her sharp acumen, attention to details, dedication, diligence and passion for her work are some of the many traits that make her an exceptional scientist. Karen's generosity, patience, understanding and sincere care toward her graduate students has been reflected countless times throughout my graduate career. The combination of her warm personality, modesty and creative imagination as a scientist is perhaps unparalleled. She is an epitome of excellence and holds really high standards for her work, which has influenced me to do the same in my career and my life. I will always remain grateful to have gained this opportunity to work with her. It has been a spectacular journey!

I would like to thank my committee members Dr. Kevin Burgess, Dr. Paul Cremer and Dr. Jaime Grunlan for their invaluable suggestions.

This work would not hold such a high impact without its biological evaluations, *in vitro* and *in vivo* experiments, for that, I thank our strong collaboration with the laboratories of Drs. John-Stephen Taylor, Steven L. Brody, Michael J. Welch, Jeffrey R. Leonard and Yongjian Liu at Washington University in Saint Louis. My friendship with Yuefei Shen, and our very fruitful collaboration that yielded in several publications has highly impacted in my scientific advances and her contribution to my work is greatly

appreciated. I would like to thank to Jack Xu, Aida Ibricevic, Sean Gunsten and Hannah Leuhmann for performing *in vitro* and *in vivo* evaluations and Dr. Ke Zhang for helpful insight in my project. Additionally, I am grateful to Dr. Mahmoud Elsabahy's collaborative efforts, insights and helpful suggestions that allowed me to gain an in depth understanding of biological assessment of nanomaterials.

I would like to extend my heartfelt gratitude to Dr. Andreas Nyström of Karolinska Institutet for initially mentoring me in the Wooley lab as a new graduate student, guiding me through polymerization techniques and providing me with innumerous helpful discussions, feedbacks and foresights to my research. Additionally, I would like to thank my colleagues in the Wooley Lab, mainly Dr. Jennifer Sorrells and Dr. Celine Besset for sharing their scientific experiences and friendship throughout these years. My list of appreciation for people affecting my graduate career would not be complete without extending my deepest gratitude to Sandani Samarajeewa, a dear friend and colleague from the Wooley lab, with whom I have shared joys and frustrations of research during my journey as a graduate student. Our joint experience in learning and exploring science has made a significant influence in my growth as a scientist. In addition to the scientific experience, I have gained a special friendship that will be valued for many years in the future.

The roots to my current academic endeavors trace to a very dedicated and motivating undergraduate advisor, Prof. George McKnight of Salem College, without whose encouragement, I would not have been here today. I will always remain thankful for his mentoring and constant guidance throughout my academic career.

I would like to thank my dear friends Dr. Hewan Belete, Dr. Nebiat Gebreselassie, Irina Kansakar, Doe Kumsa, Ei Ei Min, Dr. Nitika Paudel and Kanti Shrestha for allowing me to decompress my experiences from graduate school and providing me with constant motivation and words of encouragement. A very special recognition and thanks goes to Subin Shrestha for his patience and his belief in me, even at times when my beliefs were faltered. This process would have been much more difficult without his support. Lastly and most importantly, I would not have been able to pursue my further studies in the United States without the constant support and moral guidance from my family. The trust and liberty they have granted me throughout my life has kept me grounded and provided me with the strength to steadily move forward.

NOMENCLATURE

ALI	Acute lung injury
ATRP	Atom transfer radical polymerization
ARDS	Acute respiratory distress syndrome
CPP	Cell penetrating peptides
CuBr	Copper bromide
cSCK	Cationic shell crosslinked knedel-like
DA	Decyl acrylate
DDMAT	S-1-Dodecyl-S′-(α,α′-dimethyl-α″- acetic acid)trithiocarbonate
DIPEA	*N*,*N*-diisopropylethylamine
DNA	Deoxyribonucleic acid
DOTA	1,4,7,10-tetraazocyclododecane-*N,N',N'',N'''*-tetraacetic acid
DLS	Dynamic light scattering
DMF	Dimethylformamide
DMSO	Dimethyl sulfoxide
DSC	Differential scattering calorimetry
EDCI	1-(3'-dimethylaminopropyl)-3-ethylcarbodiimide methiodide
FITC	Fluorescein isothiocyanate
GPC	Gel permeation chromatography
HBTU	2-(1H-benzotriazol-1-yl)-1,1,3,3-tetramethyluronium hexafluorophosphate
HPLC	High pressure liquid chromatography

HOBT	Hydroxybenzotriazole
IL-lβ	Interleukin-lβ
iNOS	Inducible nitric oxide synthase
IR	Infrared
mRNA	Messenger ribonucleic acid
MWCO	Molecular weight cut-off
NO	Nitric oxide
ODA	Octadecyl acrylate
PAA	Poly(acrylic acid)
PAEA	Poly(acrylamidoethylamine)
PDI	Polydispersity index
PEG	Poly(ethylene glycol)
PMDETA	N,N,N',N'',N''-Pentamethyldiethylenetriamine
PNA	Peptide nucleic acid
P*t*BA	Poly(*tert*-butyl acrylate)
PS	Poly(styrene)
RAFT	Reversible addition-fragmentation chain transfer
RNAi	Ribonucleic acid interference
SATP	*N*-succinimidyl-S-acetylthiopropionate
SCK	Shell crosslinked knedel-like
siRNA	Small interfering ribonucleic acid

TEM	Transmission electron microscopy
TFA	Trifluoroacetic acid
THF	Tetrahydrofuran
TNF-α	Tumor necrosis factor-α
UV-vis	Ultraviolet-visible
TGA	Thermogravimetric analysis

TABLE OF CONTENTS

Page

Page

LIST OF FIGURES

FIGURE Page

FIGURE Page

LIST OF TABLES

CHAPTER I

INTRODUCTION

Nature has continued to awe and inspire scientists with its intricate designs integrated to form highly sophisticated systems with superior functions and complexities which are yet to be paralleled by their synthetic analogues.[1-3] Ubiquitous examples of such systems surround us in our daily lives where Nature has made alteration in compositions, structures and properties at a molecular level to provide attributes for enhanced performance. Proteins, such as histones exhibit efficient packaging and ordering of DNA to form structural units called nucleosomes that play a role in gene regulation. Furthermore, viruses are ultimate examples of highly efficient delivery vehicles for nucleic acids, as they are equipped with essential functionalities for binding to cells and consist of sophisticated structures facilitating cellular internalization while protecting the viral DNA.[4] Although Nature has seemingly effortless ways to create intricate systems with high levels of precision, duplicating such sophistication artificially is extremely challenging. Detailed comprehension of existing natural system requires synergy between multiple disciplines such as Biology, Chemistry and Physics, to bring together tools for understanding phenomenon at macroscopic and even more importantly, at nanoscopic levels, opening avenues toward development of new innovative technologies.

In 1959, an American physicist Richard Feyman, gave a talk at the American Physical Society titled "*There's plenty of room at the bottom*" which introduced the

concept of nanotechnology to the world.[5] It was his futuristic vision and imagination that currently allows us to manipulate matter at an atomic scale enabling us to create materials, devices and other structures sizing from 1 to 100 nm. The applications of nanotechnology are countless, ranging from their use to harness energy, develop advanced materials and groundbreaking discoveries in designing novel therapeutics. In the recent years, employment of nanotechnology in medicine, also known as nanomedicine, is one of the fastest growing areas in nanotechnology creating state-of-the-art efficient diagnostic and therapeutic tools for detection and treatment of various diseases.[6-9]

Over the past two decades nanoparticle based therapeutics have been introduced for the treatment of cancer, diabetes, inflammation, and neurodegenerative diseases.[10,11] Nanoparticles can be constructed from various materials (*e.g.* polymers, lipids, metals) and can host a wide range of active components such as chemotherapeutics, moieties for radiolabeling and ligands to impart stealth characteristics, nucleic acids, which promote their biomedical applications.[4,7,8,12-17] In particular, polymer based nanoparticles have received much attention due to their immense versatility in shapes, sizes, morphologies, ease in making chemical modification, providing internal volume for encapsulation of drugs, external surface area for conjugation of biologically active agents and multivalency.[9,14,18-21]

The most profound development nanomedicine has been underpinned by recent advances and collaboration between organic and polymer chemists, biologists and clinicians to provide functional materials along with chemical and biological techniques

for extensive analysis.[6,7,22] Progress made in polymerization techniques, mostly controlled radical polymerization techniques have dramatically improved the preparation of well-defined polymeric materials with control over their structures, functionalities and three dimensional architectures, thereby expanding the prospects of the types of nanoscopic assemblies that can be designed, developed and applied for various biomedical applications.[23]

Covalent interactions along with and supramolecular assembly has been exploited by Nature to fabricate functional macromolecular building blocks. Additionally, programmed assembly of block copolymers with structural and compositional variation by physical and chemical manipulation have enabled preparation of a myriad of morphologies like spheres, cylinders, toroids, vesicles and helices.[24-29] Our group has long standing interest in development of macromolecular functional nanoscopic objects from supramolecular assembly of amphiphilic block copolymer followed by chemical modification to afford well-defined core-shell nanoparticles known as shell crosslinked knedel-like (SCK) nanoparticles.[7,21,30-32] These nanoparticles have evolved as theranostic agents for imaging, diagnosis and delivery of therapeutic cargo such as chemotherapeutic and nucleic acids, thereby demonstrating great potential in biomedical applications toward treatment of various diseases.[14,33-37]

This dissertation is focuses on the design and development of multifunctional SCKs of various compositions, shapes, sizes and charges that have been tailored for their optimum performance for employment as nanoscopic objects for theranostic applications. Well-defined SCKs for these studies were prepared from self assembly of

amphiphilic block copolymers that were obtained by controlled radical polymerization techniques (RAFT and ATRP) followed by crosslinking selectively in the hydrophilic segment to provide stability in aqueous solution. Tuning the lengths and in turn the ratio of the hydrophilic and hydrophobic segments followed by altering the self assembly conditions dictated the sizes and shapes of the nanoparticles. Furthermore, selection of monomeric building blocks of the polymers allowed alteration in polymer composition which in turn affected the properties of nanoparticles. These nanoparticles were also optimized for circulation *in vivo* for a programmed period of time to increase their accumulation at the target sites.

In addition to the having precise control over structures and compositions, these nanoparticles can covalently or electrostatically carry therapeutic cargoes such as nuclei acids allowing it to mimic natural delivery systems (e.g.; viruses). Although nucleic acids exhibit great potential as therapeutics for treatment of various diseases, they face a series of hurdles, both extra- and intracellularly before reaching the cytosol of the cells[38,39] owing to their inherent negative charge, rapid enzymatic degradation and localization in endocytic vesicles during cellular uptake compromising their therapeutic potential. Employment of nanoparticles for complexation nucleic acids (PNAs and siRNAs) provides a great advantage as the positively charged nanocomplexes are partially protected against enzymatic degradation and enhances cellular uptake. Special efforts have been made in this dissertation to make optimization of nanoparticles for efficient delivery of nucleic acids into cells for superior transfection.

In Chapter 2, dual peptide nucleic acid- and peptide-functionalized nanoparticles were developed for their potential utility in the recognition and inhibition of mRNA sequences for inducible nitric oxide synthase (iNOS), which are overexpressed at the sites of inflammation, such as in cases of acute lung injury. Multifunctional nanoparticles with moieties to aid in radiolabeling, imparting stealth characteristics along with chemical functionalities for covalent conjugation of peptide nucleic acids and cell penetrating peptides were prepared and characterized. Special attention was provided to ensure that the biologically active ligands were available on the surface for interaction with mRNA, by conjugating the peptides to the chain end terminus of PEG after assembly of nanoparticles. These biosynthetic hybrid nanostructures were evaluated for their binding affinity to mRNAs by performing *in vitro* competition binding experiments which demonstrated that the K_d values of the PNAs were *ca*. an order of magnitude greater than the free PNAs, while the mismatched PNA showed no significant binding. This study was the preliminary step, where nanoparticles with optical and radio-labeling sites along with reactive functional handles for conjugation of ligands were prepared within well-defined nanoscopic domains toward the development of hierarchical nanostructures that hold great promise as antisense imaging agents and therapeutics. The ability to tune the particle composition allows tuning the PNA-RNA molecular recognition events while balancing the electrostatic binding and repulsions. However, the negative charge on the surface of the nanoparticles might induce repulsion with the cellular bilayer, hindering efficient uptake of these nanoparticles. Hence, this study was further extended with cationic nanoparticles carrying positive charge on the

shell that facilitates cellular internalization and enhancing transfection of genetic materials into the cells.

Building upon the extensive understanding of PAA based negatively charged nanoparticles investigated in Chapter 2 and integrating characteristics that enables efficient transport of nucleic acids into cells offered opportunities to broaden the prospect of these nanoparticles for treatment of various diseases. Chapter 3, reports the facile synthesis of cationic SCKs conjugated with fluorophore and tumor-homing F3 peptide for delivery of siRNA to brain tumor cells. Similar to the anionic SCKs prepared in the earlier studies, these cationic nanoparticles were prepared from self assembly of amphiphilic block copolymers followed by crosslinking selectively in the hydrophilic region to afford cSCKs. The alteration in charge was obtained by making compositional changes in the block copolymers which are the building blocks of the nanostructures. Cationic units were introduced *via* amidation reaction onto the amphiphilic block copolymer that allowed the nanoparticles to carry a positive charge at physiological pH which assisted in electrostatic interaction of negatively charged nucleic acids. Furthermore, F3 peptide that targets nucleolins overexpressed at the sites of angiogenesis, was covalently conjugated to the cSCKs and investigated for the cellular entry. These samples show similar physicochemical characterizations before and after conjugation to peptide as confirmed by DLS and TEM. *In vitro* studies demonstrated higher uptake of F3-targeted cSCKs into U87 glioma cells compared to control (cSCKs with scrambled peptides) samples. Additionally, confocal experiments of cSCKs complexed with nucleolin-siRNA, showed higher knockdown of nucleolin in U87

glioma cells. With the high levels of sophistication that are possible *via* simple iterations of controlled polymer chemistries, several functions can be incorporated for optimization of the biological performances for these bio-synthetic hybrid nanostructures.

Nanoparticles complexed with nucleic acids have to overcome several intra- and extra cellular barriers to reach their final destination *in vivo* hence continuous efforts have been ongoing for efficient delivery of nucleic acids into the cells. One of the ways of cellular uptake of nanoaparticles complexed with nucleic acids is by endocytosis, where the complexes are taken into cell by formation of vesicular structures known as endosomes formed by pinching off the bilayer. Materials entering the cells can be trapped into the endosomes and hence hindering effective delivery into the cells. The endosomal compartments have a unique pH environment that can be utilized to disrupt endosome to release the materials into the cytosol. Chapter 4 entails modification of cSCKs to incorporate various amounts of histamines and primary amines (as low- and high-pK_a functionalities) into their shells to achieve enhanced cell transfection with reduced toxicity, by absorbing protons at pH values between the physiological and endosomal pH range, resulting in disruption of endosomal membranes. These cSCKs were electrostatically complexed with siRNA and investigated for their cellular uptake, cytotoxicity, immunogenicity and endosomal escape in RAW 264.7 mouse macrophages and OVCAR-3 cells. *In vitro* studies demonstrated that increase in histamine content decreased the cytotoxicities of the nanoparticles. Incorporation of 15% histamine into the SCKs seemed to be optimum in this study to maintain its binding affinity with

siRNA while also being able to escape from the endosome into the cytosol for effective delivery of siRNA.

In the last part of this dissertation, we have extended the study of nucleic acid delivery from mere spherical cationic nanoparticles to hierarchically-assembled nanoparticles with cationic spheres template onto anionic cylinders. With the recent advances in nanotechnologies and a high level of interest in creating nanodevices that can bring together multiple desired components for coincident therapeutics and diagnostics toward developing candidates for nanomedicine, these hierarchically-assembled theranostic supramolecular structures act as a platform that allows for merging individual components with independent domains, such as sites for radiolabeling and functionalities for carrying payload to optimize them as a theranostic agents. In Chapter 6, we demonstrate the preparation of hierarchically-assembled theranostic (HAT) nanostructures from two different components-one carrying therapeutic payload and the other carrying sites for radiolabels, achieved by templating cationic SCKs (cSCKs) that can electrostatically bind siRNA, onto anionic shell crosslinked rods (SCRs) that provides sites for radiolabeling. These sophisticated nanostructures when investigated for their radiolabeling efficiency demonstrated superior radiolabeling compared to the negative-control sample. Evaluation of siRNA binding efficiencies along with their cytotoxicities and cellular uptake *in vitro* showed that the siRNA binding property of cationic SCKs were translated into the hierarchical assemblies. This simple procedure exhibits great potential as the next generation of theranostic agents by allowing a facile iterative process to bring together unique

individual components to form a higher order nanostructure that are optimized for their performance *in vivo* and provide an overall advantage to their individual units.

Nanoscopic objects serve as scaffolds for a combination of imaging, diagnostics and therapeutics. The ability to manipulate their sizes, shapes, morphologies and compositions by making alteration at a molecular level to optimize them for radiolabeling, increase loading capacities of drugs, impart stealth characteristics, tether interesting biological ligands allows the nanoobjects achieve therapeutic potential to treat different diseases. Furthermore, the ability to bring together multiple independent components together and integrate their properties into a hierarchical structure provides additional advantages and novel ways to mimic three dimensional structures present in Nature. The wide arrays of nanoparticles for numerous biomedical applications are discussed in the following chapters.

CHAPTER II

DUAL PEPTIDE NUCLEIC ACID-AND PEPTIDE-FUNCTIONALIZED SHELL CROSSLINKED NANOPARTICLES DESIGNED TO TARGET MRNA TOWARD THE DIAGNOSIS AND TREATMENT OF ACUTE LUNG INJURY*

2.1 Introduction

The mortality associated with acute lung injury (ALI) and acute respiratory distress syndrome (ARDS) remains high in the U.S. and around the world,[40] establishing the need for improved treatment and prevention strategies. ALI is an inflammatory process in the airspaces and lung parenchyma that is characterized by fluid accumulation (pulmonary edema) and it can progress to an acute stage that presents necrosis of the lung tissue.[41] One of the major indications of ALI is the overexpression of inducible nitric oxide synthase (iNOS), an enzyme that is found predominantly in the cells of epithelial origin. The production of iNOS is caused by the activation of proinflammatory cytokines such as interleukin-lβ (IL-lβ) and tumor necrosis factor-α (TNF-α), which are signaling molecules that are released as a part of the immune response due to the presence of bacterial products (*e.g.*, lipopolysaccharides (LPS)).[42] The upregulation of iNOS results in the production of nitric oxide (NO), which when

*Reprinted with permission from "Dual peptide nucleic acid- and peptide-functionalized shell cross-linked nanoparticles designed to target mRNA toward the diagnosis and treatment of acute lung injury" by Ritu Shrestha, Yuefei Shen, Kevin A. Pollack, John-Stephen A. Taylor, Karen L. Wooley, *Bioconjugate Chem*. **2012**, *23*, 574-585.

present in regulated amount can act as a mediator of vital biological functions in the lung.[43] However, the overexpression of this enzyme leads to the production of high concentrations of NO in an unregulated fashion, causing harm to cells and resulting in of NO and improves the symptoms of ALI.[44,45]

Because inducible nitric oxide synthase is both a biomarker and an exacerbating agent for ALI, there is great interest in the development of diagnostic agents and inhibitors for iNOS. Most of the work in this area has focused on imaging agents[46-48] and inhibitors for the iNOS protein[49] as well as imaging agents for detecting the formation of the nitric oxide that iNOS catalyzes.[50-52] An alternative strategy would be to target the mRNA encoding the iNOS protein with antisense agents that could have a dual function of both detecting iNOS mRNA expression level and inhibiting translation of the mRNA to the protein. One ideal class of antisense agents for this purpose are peptide nucleic acids (PNAs), which are synthetic analogs of DNA, in which the sugar phosphate backbone is replaced with an uncharged pseudopeptide backbone composed of *N*-(2-amino-ethyl) glycine units to which the nucleobases are linked through methylene carbonyl linkers.[53,54] Their attractiveness stems from their stability to degradation *in vivo*, high affinity for mRNA, and ability to block translation.[55-57] Additionally, PNAs are able to invade regions of secondary structure in the target mRNA, and the resulting PNA·RNA complexes are resistant to the action of RNase H which would otherwise degrade the mRNA and result in a loss of signal. While there are several reports on the use of PNAs to both inhibit [57] and image gene expression,[58-62] application of PNAs as regulators and imaging agents of gene expression *in vivo* has

been hampered by their poor cellular uptake and rapid clearance.[53,63,64] To overcome the permeability problems, PNAs have been conjugated to a variety of cell penetrating peptides and other ligands, which have been shown to improve their uptake in cell culture through endocytosis though they often remain trapped in endosomes.[65,66] In addition, simple cell penetrating PNA conjugates suffer from rapid clearance *in vivo* due to their small size. One way to circumvent these problems is to conjoin PNAs with nanoparticles having optimal cell penetrating, endosomal escape, pharmacokinetic, and biodistribution properties.

In our group, we have had long standing interest in developing novel polymeric systems and chemistries for the preparation of shell crosslinked knedel-like (SCK) nanoparticles [67-71] and fine tuning of existing nanostructures [20,25-28,72] for a diverse set of applications in biomedical research.[14,21,35,73-78] SCKs are composed of block copolymers with hydrophilic and hydrophobic segments, making them amphiphilic and prone to self assembly in selective solvents. Due to crosslinking between adjacent groups present in the shell, SCKs possess structural stability. Moreover, their tunable size, shape and ability to perform chemical modifications within selective sub-particle regions [16,79], allows for the conjugation of biologically active ligands, [74,76,80,81] such as PNAs,[82] to their surfaces, making them a versatile agent for gene delivery and transfection.[33,36,81,83,84] In the past, we have employed PNAs conjugated to SCKs to direct their assembly into higher order structures *via* selective and tunable binding interactions,[82] and for intracellular delivery of PNA through a bioreductively-cleavable linker.[33] The versatility of SCKs also allows for fine tuning of the core properties,

resulting in shape adaptable nanoparticles [85-88] that might enhance multi-valent binding recognition events. Herein, we report the design and synthesis of hierarchically-assembled, multi-functional SCKs that are conjugated with PNAs specific for iNOS mRNA to promote recognition and inhibit iNOS expression. These SCKs were also conjugated to the protein transduction domain of human immunodeficiency virus type 1 TAT protein to facilitate cellular entry, and to a fluorescent probe or DOTA for labeling with the PET imaging radionuclide ^{64}Cu for imaging purposes. The PNA-SCK conjugates were shown to sequence-specifically bind to iNOS mRNA with high affinity by comparing the binding of matched and mismatched PNA-SCK conjugates.

2.2 Materials and Methods

Polymerizations were performed on a double manifold with glassware and syringes that were dried in an oven (100 °C) for at least 1 h, and with syringes that were washed with N_2 (3 ×), prior to use. *tert*-Butyl acrylate (*t*-BA, 99%) was received from Sigma-Aldrich Company (St. Louis, MO), distilled over calcium hydride, and stored under N_2 prior to use. Octadecyl acrylate, decyl alcohol, trifluoroacetic acid (TFA, 95%; Aldrich), 2,2′-(ethylenedioxy)-bis(ethylamine) (97%, Aldrich), 1-(3′-dimethylaminopropyl)-3-ethylcarbodiimide methiodide (EDCI, 98%, Aldrich), hydroxybenzotriazole (HOBT, Aldrich), 2–(1H–benzotriazol–1–yl)-1,1,3,3-tetramethyluronium hexafluorophosphate (HBTU, Aldrich), Boc-NH-PEG_{3kDa}-NH_2 (Rapp Polymere, Tübingen, Germany), MeO-PEG_{2kDa}-NH_2 (Rapp Polymere, Tübingen, Germany), hydroxyl amine hydrochloride (98%, Aldrich), Sephadex G50 (Medium, GE Healthcare, Piscataway, NJ), *N*-succinimidyl-S-acetylthiopropionate (SATP) (Pierce,

Rockford, IL), and 4-maleimido butyric acid (Aldrich), N,N-diisopropylethylamine (DIPEA) (Aldrich), diethyl ether (anhydrous) (Aldrich), Alexa Fluor 633 hydrazide (Invitrogen) and O-(7-Azabenzo-triazol-1-yl)-1,1,3,3-tetramethyluronium hexafluorophosphate (HATU) were used as received. Fmoc-XAL PEG-PS resin was purchased from PerSeptive Biosystems (Ramsey, MN). GGYGRKKRRQRRR-maleimide was purchased from Chengdu Kaijie Bio-pharmaceuticals Co.,Ltd (Chengdu, China). PNA monomers (Fmoc-A-(Bhoc)-OH, Fmoc-C-(Bhoc)-OH, Fmoc-G-(Bhoc)-OH and Fmoc-T-OH) were obtained from Panagene (Daejeon, Korea). (S-1-dodecyl-S′-(α,α′-dimethyl-α′′-acetic acid)trithiocarbonate) (DDMAT) and Boc-protected DOTA-lysine (a lysine derivative of1, 4, 7, 10-tetraazocyclododecane-*N*, *N*', *N*'', *N*'''-tetraacetic acid (DOTA)) were synthesized as reported previously [14,21,35,89]. All other reagents were obtained from Sigma-Aldrich and used as received. Ellman's reagent kit (Pierce) was used for Ellman's assay, with the calibration curve constructed using cysteine monohydrate in aqueous buffer (100 mM PBS, 0.1 M NaCl, 10 mM EDTA, pH 7.4) at 412 nm. Spectra/Por membrane tubes were purchased from Spectrum Medical Industries, Inc., and were used for dialysis. Nanopure water (18 MΩ•cm) was acquired by means of a Barnstead Nanopure ultrapure water purification system (Thermo Scientific, Asheville, NC).

^{1}H NMR and ^{13}C NMR spectra were recorded on an Inova 300 or Mercury 300 spectrometer interfaced to a UNIX computer using VnmrJ software. Samples were prepared as solutions in $CDCl_3$, CD_2Cl_2, or DMF-d_7 and solvent protons were used as internal standard. IR spectra were recorded on an IR Prestige 21 system (Shimadzu Corp., Japan). A small amount of sample was placed to cover the ATR crystal for IR measurements. Data were analyzed using IRsolution software. UV-vis absorption measurements were made using a UV-2550 system (Shimadzu Corp., Japan) using PMMA cuvettes. Spectra were analyzed with UV-Probe 2.33 software.

Gel permeation chromatography was conducted on a system equipped with a Waters Chromatography, Inc. (Milford, MA) model 1515 isocratic pump and a model 2414 differential refractometer with a three-column set of Polymer Laboratories, Inc. (Amherst, MA) Styragel columns (PL_{gel} 5μm Mixed C, 500 Å, and 10^4 Å, 300 x 7.5 mm columns) and a guard column (PL_{gel} 5μm, 50 x 7.5 mm).

The system was equilibrated at 40 °C in tetrahydrofuran (THF), which served as the polymer solvent and eluent (flow rate set to 1.00 mL/min). The differential refractometer was calibrated with Polymer Laboratories, Inc. polystyrene standards (300 to 467,000 Da). Polymer solutions were prepared at a concentration of *ca*. 3 mg/mL with 0.05% vol toluene as flow rate marker and an injection volume of 200 μL was used. Data were analyzed using Empower Pro software from Waters Chromatography Inc.

Differential scanning calorimetry studies were performed on a Mettler Toledo DSC822 calibrated according to the standard procedures using Indium. The heating rates were 10 °C min^{-1} and cooling rates were 5 °C min^{-1} with a temperature range of -120–150 °C. The crystalline melting point (T_m) and crystallization temperature (T_c) were determined during the second heating or cooling cycles, respectively. Thermogravimetric analysis was performed under Ar atmosphere using a Mettler Toledo model TGA/DSC1 with a heating rate of 10 °C/min. Measurements were analyzed using Mettler Toledo STARe software v.10.00.

Samples for TEM were prepared by depositing 5 µL of sample to glow discharged carbon coated copper grids. Excess sample was wicked off using filter paper and the grids were allowed to dry in air for 1 minute. The grids were then stained with 5 µL of 2% uranyl acetate and excess stain was wicked off using filter paper. Specimens were observed on a JEOL 1200EX transmission electron microscope operating at 100 kV and micrographs were recorded at calibrated magnifications using an SIA-15C CCD camera. The final pixel size was 0.42 nm/pixel. The number-average particle diameters

(D_{av}) and standard deviations were generated from the analysis of particles from at least two different micrographs.

Dynamic light scattering (DLS) measurements were conducted using Delsa Nano C from Beckman Coulter, Inc. (Fullerton, CA) equipped with a laser diode operating at 658 nm. Size measurements were made in water (n = 1.3329, η = 0.890 cP at 25 ± 1 °C; n = 1.3293, η = 0.547 cP at 50 ± 1 °C; n = 1.3255, η = 0.404 cP at 70 ± 1 °C). Scattered light was detected at 165° angle and analyzed using a log correlator over 70 accumulations for a 0.5 mL of sample in a glass sizing cell (0.9 mL capacity). The photomultiplier aperture and the attenuator were automatically adjusted to obtain a photon counting rate of *ca*. 10 kcps. The calculations of the particle size distribution and distribution averages were performed using CONTIN particle size distribution analysis routines. Prior to analysis, the samples were filtered through a 0.45 μm Whatman Nylon membrane filter (Whatman, Inc.). The samples in the glass sizing cell were equilibrated at the desired temperature for 5 min before measurements were made. The peak average of histograms from intensity, volume or number distributions out of 70 accumulations was reported as the average diameter of the particles.

PNA synthesis was carried out on an automated ABI 8909 synthesizer (Applied Biosystems, Carlsbad, CA) with a PNA option. High-pressure liquid chromatography (HPLC) of PNAs was carried out on Beckman Coulter System Gold 126 HPLC system. Matrix-assisted laser desorption ionization (MALDI) mass spectra of PNA conjugates were measured on a PerSeptive Voyager RP MALDI-time of flight (TOF) mass

spectrometer using CHCA as a matrix and calibrated versus insulin (average [M + H] = 5734.5) which was present as an internal standard.

DNA was 5'-labeled by [γ-^{32}P]-ATP with T4 polynucleotide kinase. DNA, T4 polynucleotide kinase buffer, H_2O, [γ-^{32}P]-ATP and T4 polynucleotide kinase were mixed together and incubated for 1 h at 37 °C, followed by boiling for 20 min to inactivate the kinase. Radiolabeled DNA bands with corrected sizes were purified from polyacrylamide gel and taken forward for further experiments.

Synthesis of poly(*tert*-butyl acrylate) (P*t*BA$_{140}$) (1)

To a 100 mL Schlenk flask equipped with a stir bar, DDMAT (284 mg, 0.779 mmol) was added as a chain transfer agent followed by AIBN (6.40 mg, 39.0 μmol) and 2-butanone (11.2 g, 156 mmol). Monomer *t*BA (20.0 g, 156 mmol) was added and the Schlenk flask was then sealed with a rubber septum. The reaction mixture was allowed to stir at room temperature to ensure homogeneity. After performing four freeze-pump-thaw cycles, the reaction mixture was allowed to equilibrate to room temperature before being inserted into a preheated oil bath at 60 °C. The kinetics of polymerization were monitored by analyzing aliquots at predetermined times *via* ^{1}H NMR spectroscopy. After 2 h, the desired conversion was achieved and the reaction was quenched by immersing the Schlenk flask into liquid N_2. A minimum amount of THF was used to dissolve the reaction mixture which was precipitated three times into a mixture of methanol and ice to afford the homopolymer of P*t*BA. The polymer was dissolved in dichloromethane and dried over magnesium sulfate. Finally, the solvent was removed under vacuum to yield (13.0 g, 68 % yield, based upon 80% conversion) of poly(*tert*-

butyl acrylate) as a bright yellow powder. $(M_n)_{NMR}$ = 18.3 kDa. $(M_n)_{GPC}$ = 23.6 kDa. $(M_w)_{GPC}$ = 26.4 kDa. PDI = 1.12. IR: 2920, 2830, 1716, 1443, 1364, 1285, 1125, 813, 745 cm^{-1}. ^1H NMR (CD_2Cl_2) δ: 0.85 (t, J = 7.0 Hz, C***H***$_3CH_2$-), 1.20-1.85 (br, -CHC***H***$_2$- of the polymer backbone, alkyl chain initiator and HOOCC(C***H***$_3)_2$-), 2.20 (br, -C***H***CH_2- of the polymer backbone), 3.20 (t, J = 7.0 Hz, -SCSC***H***$_2$-), 4.6-4.7 (br, -CH_2C***H***S-) ppm. ^{13}C NMR (CD_2Cl_2) δ: 12.5, 22.7, 27.9, 29.5, 36.1, 37.3, 41.9-42.4, 80.2, 173.9-174.1 ppm. DSC: (T_g) = 48 °C. TGA: T_{onset} = 186 °C, $T_{decomposition}$: (186-228 °C) 37.5 % mass loss; (228-307 °C) 7.5% mass loss; (307-472 °C) 27% mass loss; 28% mass remaining.

Synthesis of poly(*tert*-butyl acrylate)$_{140}$-*b*-poly(octadecyl acrylate$_{16}$-*co*-decyl acrylate$_{43}$) (P*t*BA$_{140}$-*b*-P(ODA$_{16}$-*co*-DA$_{43}$) (2)

To a 50 mL flame–dried Schlenk flask equipped with a stir bar, ODA (1.67 g, 5.14 mmol) was added followed by DA (2.95 g, 13.9 mmol), P*t*BA (3.50 g, 0.190 mmol) and a stock solution of AIBN (1.56 mg, 9.50 μmol) prepared in toluene. The monomers and macrochain transfer agent were allowed to dissolve in toluene (3.50 g, 38.0 mmol). The reaction mixture was degassed by three freeze pump thaw cycles and allowed to warm to room temperature. Polymerization was facilitated by immersing the Schlenk flask into a preheated oil bath at 70 °C. Progress of polymerization was monitored by ^1H NMR spectroscopy of aliquots at pre-determined times. Upon attaining the desired degree of polymerization, after 1.5 h, the reaction was quenched by immersing the reaction flask into liquid N_2. The reaction mixture was dissolved in a minimum amount of THF (6.00 mL) and three consecutive precipitations were performed in methanol in

an ice bath. After the final precipitation, a yellow powder (3.35 g, 70% yield, based on 60% conversion) was obtained after removal of solvent and subsequent drying *in vacuo.* $(M_n)_{NMR}$ = 32.6 kDa. $(M_n)_{GPC}$ = 26.8 kDa. $(M_w)_{GPC}$ =29.7 kDa. PDI = 1.10. IR: 2920, 2830, 1716, 1443, 1364, 1285, 1125, 813, 745 cm^{-1}. ^1H NMR (CD_2Cl_2) δ: 0.88 (t, J = 6.9 Hz, -C***H***$_3CH_2$- of ODA, DA and chain transfer agent), 1.35-1.76 and 1.70-1.98 (br, -C***H***$_2$CH-backbone of PODA, PDA, CTA and HOOCC(C***H***$_3)_2$-), (2.05-2.40 (br, -CH_2C***H***-), 4.00 (br, -OC***H***$_2CH_2$-, PODA, PDA) ppm. ^{13}C NMR (CD_2Cl_2) δ: 13.8, 22.7, 25.9, 27.7-27.8, 28.7, 29.4, 29.6, 31.9, 34.5-37.5, 41.4-41.9, 64.6, 80.2, 173.8-174.1 ppm. DSC: (T_g) = 41 °C. (T_m) = -2.2 and 9.1 °C. (T_c) = -6.8 and 3.4 °C. TGA: T_{onset} = 209 °C, $T_{decomposition}$: (209-250 °C) 11 % mass loss; (250-485 °C) 70% mass loss; 20% mass remaining.

Synthesis of poly(acrylic acid)$_{140}$-*b*-poly(octadecyl acrylate$_{16}$-*co*-decyl acrylate$_{43}$) (PAA$_{140}$-*b*-P(ODA$_{16}$-*co*-DA$_{43}$)) (3)

A round bottom flask equipped with stir bar was charged with **2** (1.00 g, 30.7 μmol). Dichloromethane (10 mL) was added followed by dropwise addition of TFA (10 mL) and the reaction mixture was allowed to stir for 24 h at RT. The solvent was removed under vacuum and the polymer was allowed to dissolve in a minimum amount of THF. Upon extensive dialysis against nanopure water and lyophilization, a pale white fluffy solid of PAA$_{140}$-*b*-P(ODA$_{16}$-*co*-DA$_{43}$) (**3**) (0.74 g, 98%) was obtained. $(M_n)_{NMR}$ = 24.7 kDa. IR: 3600-2350, 1716, 1443, 1250, 1159, 830, 750 cm^{-1}. ^1H NMR (DMF-d_7) δ: 0.86 (t, J = 6.6 Hz, -C***H***$_3CH_2$- of ODA, DA and chain transfer agent), 1.15-1.4 (br, -C***H***$_2$-alkyl chain of PODA, PDA, CTA and HOOCC(C***H***$_3)_2$-), 1.95-2.1 (br, -C***H***$_2$CH-

backbone of PODA, PDA and CTA), 2.05-2.20 (br, -$CH_2C\boldsymbol{H}$- backbone of PODA, PDA and CTA), 4.00 (br, -$OC\boldsymbol{H}_2CH_2$-, PODA, PDA) ppm. ^{13}C NMR (DMF-d_7) δ: 14.5, 23.5, 27.0, 29.5, 30.5, 31.0, 33.0, 35.1-37.5, 41.5-43.0, 65.0, 174.1-175.1, 175.9 ppm. DSC: (T_g) = 129.5 °C. (T_m) = 6.3 °C, (T_c) = 3.1 °C. TGA: T_{onset} = 190°C, $T_{decomposition}$: (190-294 °C) 18 % mass loss; (294-495 °C) 68% mass loss; 14% mass remaining.

Synthesis of poly(acrylic acid$_{137}$)-*g*-DOTA$_3$-*b*-poly(octadecyl acrylate$_{16}$-*co*-decyl acrylate$_{43}$) (PAA$_{137}$-*g*-(CONH-lysine-DOTA-Boc)$_3$-*b*-P(ODA$_{16}$-*co*-DA$_{43}$)) (4)**

General procedure for amidation, involving the attachment of DOTA: A 50 mL flame-dried RB flask equipped with a stir bar was charged with **3** (350 mg, 14.1 μmol) and DMF (5.00 g). Stock solutions of HOBT, HBTU and CONH-lysine-DOTA-Boc were prepared in dry DMF. After the polymer was allowed to dissolve completely, HBTU (56.1 mg, 0.148 mmol), HOBt (19.9 mg, 0.148 mmol) and DIPEA (6.19 mg, 0.148 mmol) were added at intervals of 30 min. DOTA-lysine (51.7 mg, 73.8 μmol) was added and the solution was stirred for 24 h at RT. The reaction mixture was then transferred to dialysis tubing (MWCO *ca.*6000-8000 Da) presoaked in nanopure water. Extensive dialysis against nanopure water followed by lyophilization afforded a white powder of **3** (235 mg, 89.0%, 3 DOTA-lysine per chain, 60% coupling efficiency). M_n=26.7 kDa. IR: 3400-2570, 1715, 1580, 1477, 1250, 1160, 978, 830, 750 cm^{-1}. ^{1}H NMR (DMF-d_7) δ: 0.86 (t, J = 6.6 Hz, -C$\boldsymbol{H}_3CH_2$- of ODA, DA and chain transfer agent, C$\boldsymbol{H}_3$- *tert*-butyl groups of DOTA), 1.15-1.4 (br, -C$\boldsymbol{H}_2$-alkyl chain of PODA, PDA, CTA and HOOCC(C$\boldsymbol{H}_3$)$_2$-), 1.95-2.1 (br, -C$\boldsymbol{H}_2$CH- backbone of PODA, PDA and CTA) 2.05-2.20 (br, -$CH_2C\boldsymbol{H}$- backbone of PODA, PDA and CTA), 2.3-2.4 (br, DOTA), 2.95-3.10

(br, DOTA), 4.00 (br, -OC***H***$_2$CH$_2$-, PODA, PDA) ppm. ^{13}C NMR (DMF-d$_7$) δ: 14.5, 23.5, 27.0, 29.5, 30.5, 31.0, 33.0, 35.1-37.5, 41.5-43.0, 53.0, 56.0, 65.0, 82.0, 174.1-175.1, 177.6 ppm. DSC: (T_g) = 131.8 °C. (T_m) = 1.0 °C, (T_c) = -3.0 °C. TGA: T_{onset} = 112 °C, $T_{decomposition}$: (112-190°C) 9 % mass loss; (190-247 °C) 7% mass loss; (264-278 °C) 7% mass loss; (278-395 °C) 38% mass loss; (395-500 °C) 19% mass loss; 20% mass remaining.

Synthesis of poly(acrylic acid)$_{131}$-*g*-(PEG$_{3\ kDa}$-Boc)$_3$-*g*-(mPEG$_{2\ kDa}$)$_3$-*g*-(CONH-lysine-DOTA-Boc)$_3$-*b*-poly(octadecyl acrylate$_{16}$-*co*-decyl acrylate$_{43}$) (PAA$_{131}$-*g*-(PEG$_{3\ kDa}$-Boc)$_3$-*g*-(mPEG$_{2\ kDa}$)$_3$-*g*-(CONH-lysine-DOTA-Boc)$_3$-*b*-P(ODA$_{16}$-*co*-DA$_{43}$)) (5)

A reaction mixture of **4** (97.0 mg, 3.63 μmol), HBTU (19.4 mg, 51.1 μmol), HOBt (12.1 mg, 51.1 μmol), DIPEA (6.58 mg, 51.1 μmol), 2 kDa mPEG-NH_2 (25.8 mg, 12.8 μmol), and 3 kDa Boc-NH-PEG-NH_2 (82.3 mg, 12.8 μmol) in DMF was allowed to undergo reaction under the general procedure outlined for amidation above to yield an amorphous white solid of **5**, PAA$_{131}$-*g*-(PEG$_{3\ kDa}$-Boc)$_3$-*g*-(mPEG$_{2\ kDa}$)$_3$-*g*-(CONH-lysine-DOTA-Boc)$_3$-*b*-P(ODA$_{16}$-*co*-DA$_{43}$) (133 mg, 88%), having ca. 3 of each type of PEG per chain, 75 % coupling efficiency. $(M_n)_{NMR}$ = 41.6 kDa. IR: 3600-2580, 1715, 1543, 1455, 1250, 1160, 1114, 966, 807, 760 cm^{-1}. ^{1}H NMR (DMF-d$_7$) δ: 0.86 (t, J = 6.6 Hz, -C***H***$_3$CH$_2$- of ODA, DA and chain transfer agent, C***H***$_3$- *tert*-butyl groups of DOTA), 1.15-1.4 (br, C***H***$_2$-alkyl chain of PODA, PDA, CTA and HOOCC(C***H***$_3$)$_2$-), 1.95-2.10 (br, -C***H***$_2$CH- backbone of PODA, PDA and CTA) 2.05-2.20 (br, 3 H, -CH$_2$C***H***- backbone of PODA, PDA and CTA), 2.30-2.4 (br, DOTA), 2.95-3.10 (br,

DOTA), 3.20 (s, -OC***H***$_3$, PEG), 3.50 (-C***H***$_2$-,br, PEG), 4.00 (br, -OC*H*$_2$CH$_2$-, PODA, PDA) ppm. ^{13}C NMR (DMF-d$_7$) δ: 14.5, 23.5, 27.0, 29.5, 30.5, 31.0, 33.0, 35.1-37.5, 41.5-43.0, 52.0, 56.0, 58.6, 65.0, 70.8, 82.0, 174.6, 176.8 ppm. DSC: (T_m) = -43.8 °C, (T_m) $_{(ODA\text{-}co\text{-}DA)}$ = 8.2 °C, (T_m) $_{(PEO)}$ = 33.6 °C, (T_c) = -44.3 and 3.8 °C. TGA: T_{onset} = 150 °C, $T_{decomposition}$: (150-438 °C) 68% mass loss; (438-500 °C) 6% mass loss; 26% mass remaining.

Synthesis of poly(acrylic acid)$_{131}$-*g*-(PEG$_{3\ kDa}$-NH$_2$)$_3$-*g*-(mPEG$_{2\ kDa}$)$_3$-*g*-(CONH-lysine-DOTA-COOH)$_3$-*b*-poly(octadecyl acrylate$_{16}$-*co*-decyl acrylate$_{43}$) (PAA$_{131}$-*g*-(PEG$_{3\ kDa}$-NH$_2$)$_3$-*g*-(mPEG$_{2\ kDa}$)$_3$-*g*-(CONH-lysine-DOTA-COOH)$_3$-*b*-P(ODA$_{16}$-*co*-DA$_{43}$)) (6)

In a round bottom flask was placed **5** (90.0 mg, 2.16 μmol) and TFA (6.00 mL) was added dropwise. The reaction mixture was allowed to stir for 24 h at RT. The TFA was then removed under a flow of N_2, the polymer was dissolved in THF, the solution was then dialyzed against nanopure water, and the polymer was isolated by lyophilization to obtain **6** as a fluffy white powder (55 mg, 65%). (M_n) $_{NMR}$ = 41.0 kDa. IR: 3600-2600, 1715, 1590, 1430, 1250, 1135, 945, 820, 760 cm^{-1}. ^{1}H NMR (DMF-d$_7$) δ: 0.86 (t, J = 6.6 Hz, -C***H***$_3$CH$_2$- of ODA, DA and chain transfer agent), 1.15-1.4 (br, C***H***$_2$- alkyl chain of PODA, PDA, CTA and HOOCC(C***H***$_3$)$_2$-), 1.95-2.1 (br, -C***H***$_2$CH- backbone of PODA, PDA and CTA), 2.05-2.20 (br, -CH$_2$C***H***- backbone of PODA, PDA and CTA), 2.3-2.4 (br, DOTA), 2.95-3.10 (br, DOTA), 3.20 (s, -OC***H***$_3$, PEG), 3.50 (-C***H***$_2$-,br, PEG), 4.00 (br, 4 H, -OC***H***$_2$CH$_2$-, PODA, PDA) ppm. ^{13}C NMR (DMF-d$_7$) δ: 14.5, 23.5, 27.0, 29.5, 30.5, 31.0, 33.0, 35.1-37.5, 41.5-43.0, 52.0, 58.0, 58.6, 65.0, 70.5,

174.1-175.1, 176.8 ppm. DSC: (T_m) = -43.5 °C, $(T_m)_{(ODA\text{-}co\text{-}DA)}$ = 10.8 °C, $(T_m)_{(PEO)}$ = 29.8 °C, (T_c) = -35.2 and 3.9 °C. TGA: T_{onset} = 150 °C, $T_{decomposition}$: (150-438 °C) 68% mass loss; (438-500 °C) 6% mass loss; 26% mass remaining.

Synthesis of poly(acrylic acid)$_{131}$-*g*-(PEG$_{3\ kDa}$- NHCO-C_2H_4-$SCOCH_3$)$_3$-*g*-(mPEG$_{2\ kDa}$)$_3$-*g*-(CONH-lysine-DOTA-COOH)$_3$-*b*-poly(octadecyl acrylate$_{16}$-*co*-decyl acrylate$_{46}$) (PAA$_{131}$-*g*-(PEG$_{3\ kDa}$-NHCO-C_2H_4-$SCOCH_3$)$_3$–*g*-(mPEG$_{2\ kDa}$)$_3$-(CONH-lysine-DOTA-COOH)$_3$-*b*-P(ODA$_{16}$-*co*-DA$_{43}$)) (7)

In a round bottom flask, **6** (30 mg, 0.68 μmol) was dissolved in dry DMF (4.00 mL), SATP (4.74 mg, 20.5 μmol), DIPEA (20 μL, 0.1 μmol) was added and the reaction mixture was stirred at RT. The reaction mixture was then transferred into presoaked dialysis tubing (MWCO *ca.* 6000-8000 Da) to remove small molecule impurities. After extensive dialysis and lyophilization **7** was obtained (25 mg, 82%). $(M_n)_{NMR}$ = 41.7 kDa. IR: 3600-2600, 1715, 1590, 1415, 1250, 1120, 920, 820, 730 cm^{-1}. ^{1}H NMR (DMF-d_7) δ: 0.86 (t, J = 6.6 Hz, -C***H***$_3$CH$_2$ of ODA, DA and chain transfer agent), 1.15-1.40 (br, C***H***$_2$- alkyl chain of PODA, PDA, CTA and HOOCC(C***H***$_3$)$_2$), 1.95-2.10 (br, -C***H***$_2$CH- backbone of PODA, PDA and CTA), 2.05-2.20 (br, -CH$_2$C***H***- backbone of PODA, PDA and CTA), 2.30-2.40 (br, DOTA), 2.71-2.75 (br, -C***H***$_2$S-), 2.95-3.10 (br, DOTA), 3.50 (-OC***H***$_2$-C***H***$_2$O-,br, PEG) 4.00 (br, -OC***H***$_2$CH$_2$-, PODA, PDA) ppm. ^{13}C NMR (DMF-d_7) δ: 14.5, 23.5, 27.0, 29.5, 30.5-31.5, 33.0, 35.1-37.5, 41.5-43.0, 55.8, 57.5, 65.0, 70.5, 174.1-175.1, 176.5 ppm. DSC: (T_m) = -44.3 °C, $(T_m)_{(ODA\text{-}co\text{-}DA)}$ = 11.3 °C, $(T_m)_{(PEO)}$ = 27.8 °C, (T_c) = -36.4 and 6.1 °C. TGA: T_{onset} = 170 °C, $T_{decomposition}$: (170-283 °C) 4% mass loss; (283-460 °C) 87.3% mass loss; 8.7% mass remaining.

Procedure for the preparation of micelles (8)

To **7** in DMF (8.0 mg, 1.0 $mgmL^{-1}$) was added an equal volume of nanopure water dropwise *via* a syringe pump over the course of 3 h. The mixture was allowed to stir for 16 h at RT and was then transferred to presoaked dialysis tubing (MWCO *ca.* 6000-8000 Da) and dialyzed against nanopure water for *ca*. 4 d to remove the organic solvent and give a final polymer concentration of 0.32 $mgmL^{-1}$. $(D_h)_n$ (DLS) = 43 ± 8 nm; $(D_h)_{vol}$ (DLS) = 63 ± 6 nm; $(D_h)_{int}$ (DLS) = 124 ± 20 nm; D_{av} (TEM) = 36 ± 4 nm.

Procedure for the preparation of SCKs (9)

To a solution of micelles (**8**) (15 mL, 0.32 $mgmL^{-1}$) was added 2, 2`-(ethylenedioxy)bis(ethylamine) (0.63 mg, 4.3 μmol, to achieve nominally crosslinking through 20% of the COOH groups) from a stock solution *via* a syringe pump over 30 min. The reaction mixture was allowed to stir at RT for 30 min and EDCI (1.17 mg, 3.93 μmol) was added as a solution in water *via* syringe pump over 15 min. The reaction mixture was allowed to stir at RT for 24 h and was then transferred to presoaked dialysis tubing (MWCO *ca.* 6000-8000 Da) and dialyzed for *ca*. 4 d to afford the SCK solution with a final concentration of 0.29 $mgmL^{-1}$. $(D_h)_n$ (DLS) = 48 ± 7 nm; $(D_h)_{vol}$ (DLS) = 79 ± 10 nm; $(D_h)_{int}$ (DLS) = 123 ± 9 nm; D_{av} (TEM) = 41 ± 4 nm.

Conjugation of Alexa Fluor 633 hydrazide to SCKs (10)

To a SCK solution (8.0 mL, 0.29 $mgmL^{-1}$) at 0 °C was added a stock aqueous solution of EDCI (2.41 mg, 8.10 μmol) over a period of 3 min, and the mixture was allowed to stir for 20 min. Sulfo-NHS (1.78 mg, 8.10 μmol) was added from a stock solution prepared in nanopure water and the reaction was stirred for 2 h. The pH of the

solution was adjusted to 7.2 using PBS buffer (pH 8.86, 0.2 M) and Alexa Fluor 633 hydrazide (72.0 μg, 0.064 μmol) was added to the reaction mixture from a stock solution in DMSO. The reaction mixture was allowed to stir for 24 h in the dark and was then transferred to presoaked dialysis tubing (MWCO *ca.* 6000-8000 Da) and dialyzed against NP water for 5 d in an Al-foil-wrapped beaker. The concentration of dye was found to be 12.0 μM from UV-vis spectroscopy. $(D_h)_n$ (DLS) = 60 ± 16 nm; $(D_h)_{vol}$ (DLS) = 79 ± 30 nm; $(D_h)_{int}$ (DLS) = 125 ± 53 nm; D_{av} (TEM) = 40 ± 4 nm.

Deprotection of masked thiols of Alexa Fluor 633 hydrazide labeled SCKs (11)

Hydroxyl amine hydrochloride (75.0 μL, 0.5 M) in aqueous buffer (100 mM, 150 mM NaCl) was added to a stirred solution of SCK **10** (5.0 mL) suspended in buffer (100 mM, 150 mM NaCl) and the reaction mixture was allowed to stir for 3 h at RT. The solution was assayed by Ellman's assay and the thiol content was determined to be 33 ± 4 μM. The solution was immediately used for conjugation with maleimide-functionalized PNAs and CPPs.

Synthesis of maleimide-PNA conjugates (12)

PNAs were synthesized continuously on universal support XAL-PEG-PS resin at a 2 μmol scale with standard solid phase Fmoc chemistry on an Expedite 8909 Synthesizer. After completion of automated synthesis, PNAs were cleaved from the solid support and the bases were deprotected using trifluoroacetic acid: m-cresol (4:1, v/v) for 3 h and then precipitated with diethyl ether. The crude products were purified by HPLC and characterized by MALDI-TOF. PNAs were then dissolved in NMP: dimethylsulfoxide (DMSO) (7:3, v/v) with 15 min vigorous stirring. Maleimide

dissolved in NMP was added to the PNA solution followed by addition of DIEA (16 μL) and the reaction mixture was maintained at room temperature for 2.5 h with gentle shaking. Excess cold diethyl ether (anhydrous) was added to precipitate the PNA-maleimide conjugates. The PNA-maleimide conjugates were dried under nitrogen and characterized by MALDI-TOF mass spectrometry.

General procedure for conjugation of SCKs with iNOS PNAs with and without TAT (13)

To a SCK solution (750 μL, 0.29 $mgmL^{-1}$) suspended in buffer (100 mM PBS, 150 mM NaCl, pH 7.2), citric acid buffer (pH 5.12) was used to adjust the pH to 6.5. A concentrated solution of iNOS PNA (Maleimide-TTTCCTTTTCCTCTTTCA or Maleimide-TGTCCTCCTTTTCTTTCA) (5.0 nmoles in DMF) in (100 mM PBS, 150 mM NaCl, pH 7.4) was added to the SCK solution to prepare SCKs with mismatch or match PNAs. Additionally, TAT (Maleimide-GGYGRKKRRQRRR) (6.7 nmoles from a stock solution in DMF) was added to the reaction mixture of SCKs with either match or mismatch PNA sequences to prepare PNA-SCK-TAT conjugates. The reaction mixture was stirred at room temperature for 6 h and remaining thiols were capped by addition of 4-maleimido-butyric acid (1 mg suspended in 100 mM PBS, 150 mM NaCl, pH 7.4). The reaction was stirred for 16 h before being purified by Sephadex®G-50 gel column. D_{av} (TEM) = 28 ± 5 nm.

Preparation of biotinylated iNOS mRNA (14)

Image CloneID 4978648 containing the iNOS mRNA sequence (Gene Bank BC062378, ATCC cloning NO. 10470196) was obtained from ATCC. The plasmid

DNA was purified and linearized at the unique XbaI site before transcription. Transcription reactions were carried out using the Promega RiboMAX Large Scale RNA production system utilizing the SP6 promoter (Promega). Transcription proceeded with SP6 RNA polymerase, NTPs and Bio-UTP (Roche) for 4 h at 37 °C, and followed by DNase I treatment, phenol:chloroform: isoamylalcohol (25:24:1) extraction and ethanol precipitation. The final purified iNOS RNA was quite homogeneous and corresponded in size to the expected 4 Kb transcript.

Binding affinity of ODNs to iNOS mRNA by a Dynabead-based binding assay

The radiolabeled ODN (100 pM) was incubated with biotinylated mRNA (0.01, 0.1, 1, 10, 100 nM) and 1 µL of RNase inhibitor for 4h at 37°C in a total volume of 100 µL. Streptavidin coated Dynabeads were added and mixed for 30 min. The beads were then separated by a magnet, washed twice and resuspended in 100 µL of hybridization buffer (5m M Tris-HCl, pH 7.0, 1 mM EDTA, 0.1 M NaCl). Solutions were then counted by liquid scintillation to give bound fractions directly.

The dissociation constants were determined by non-linear fitting of the fraction bound versus RNA concentration data to the analytical expression shown below for a two state binding equilibrium using the Kaleidagraph program.

$$F_B = NSB + \frac{SB*(([L]+K_d+[RNA])-\sqrt{([L]+K_d+[RNA])^2-4*[RNA]})}{2*[L]} \quad (1)$$

where F_B is the experimentally determined fraction of bound ODN, NSB is the fraction of ODN that is nonspecifically bound, SB is the fraction of ODN that can be specifically

bound and was set equal to (1-NSB), [L] is total ODN concentration, K_d is dissociation constant of the ODN and [RNA] is total RNA concentration.

Binding affinity of iNOS PNA-SCK-TAT for iNOS mRNA by a competition assay

Biotinylated mRNA (10 pM) was incubated with 1000 pM radiolabeled ODN and 1 μL of RNase inhibitor for 4 h at 37 °C, to which unlabeled competitor PNAs (0, 0.001, 0.01, 0.1, 1, 10 nM) or iNOS PNA-SCK-TAT (0, 0.01, 0.1, 1, 10, 100 and 1000 nM, concentration calculated based on PNA concentration) were added. The streptavidin coated Dynabeads were added and mixed for another 30 min at 37 °C. Following incubation, the reaction mixture was separated by a magnetic field, washed twice and resuspended in hybridization buffer (5 mM Tris-HCl, pH 7.0, 1 mM EDTA, 0.1 M NaCl). The solution containing bound ODNs was counted by liquid scintillation. Additionally, SCK-TAT alone served as a control group.

The fraction of antisense ODN bound to the RNA (B) was then plotted against the competitor PNA concentration ([PNA]), and an IC_{50} value is determined (the concentration of competitor PNA that reduces binding of the ODN by 50%) by fitting the data according to a standard equation. Once the IC_{50} values are obtained, the K_ds for the PNAs can be determined using a simple relationship involving the IC_{50} and the K_d for the antisense ODN.

$$B = B_{min} + \frac{B_{max} - B_{min}}{1+10^{\log[PNA] - \log(IC_{50})}} \quad (2)$$

$$K_d(PNA) = \frac{IC_{50}}{1+\frac{[ODN]}{K_d(ODN)}} \quad (3)$$

2.3 Results and Discussion

Design of the PNA nanoparticles

The PNA nanoparticles were designed to meet a number of criteria for future applications as imaging and knock down agents for iNOS expression. The first was that the nanoparticle be able to enter cells efficiently so as to be able to engage the iNOS mRNA in the cytoplasm. The second was that the attached PNAs would be able to freely interact with the mRNA. The third was that the nanoparticle would be capable of being detected by both fluorescent and PET imaging modalities. The fourth was that the nanoparticles avoid detection by the mononuclear phagocytic system (MPS), also referred to as the reticuloendothelial system (RES), which would otherwise result in their rapid clearance from the blood. To meet these criteria, a PEGylated shell crosslinked nanoparticle was chosen in which the PNAs and the TAT peptide would be attached to the ends of the PEG chains, while the imaging agents would be conjugated to the polyacrylate shell. PEGylation has been previously shown to impart stealth character to SCKs and prolong their retention in the blood [14,21], presumably by shielding the polyacrylate core from components of the MPS. The TAT peptide was chosen to facilitate endocytosis of the SCKs [90,91], and to enable TAT to interact with the cell surface, it was attached to the ends of the PEG chains, using a thiol coupling strategy [16]. Likewise, the PNAs were designed to also be attached to the ends of the PEG chains to enable them to interact with the mRNA in the cytoplasm. The imaging agents were

designed to be attached to the polyacrylate shell to minimize their exposure to the MPS. The polyacrylate shell was also expected to serve additional functions to serve as a robust network for maintaining the nanoparticle structure and to, potentially, facilitate rupture of the endosome upon lowering of the pH during endosomal acidification [92].

Synthesis of the SCK nanoparticles

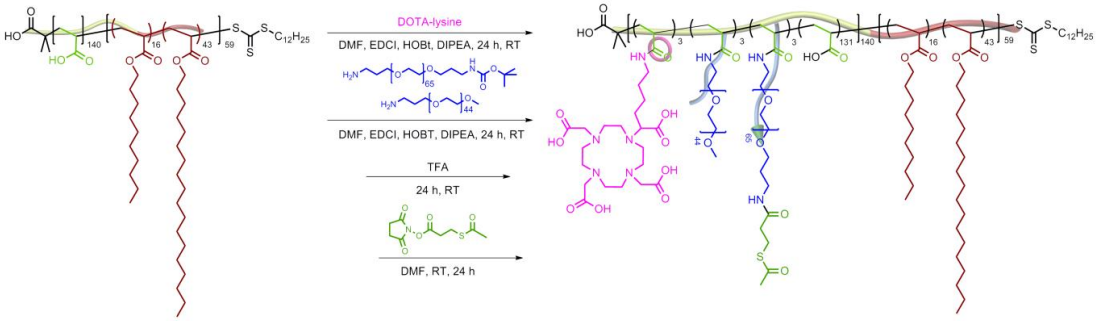

Figure 2.1. Schematic representation of synthesis of amphiphilic functional block graft copolymer, **7**.

The block copolymer precursor used in this study was prepared by a two-step reversible addition-fragmentation chain transfer (RAFT) polymerization process, followed by deprotection (Fig. 2.1), as described in previous work by our group [85]. *S*-1-dodecyl-*S'*-(α, α'-dimethyl-α''-acetic acid) trithiocarbonate (DDMAT) was used as a chain transfer agent to synthesize an initial P*t*BA$_{140}$ **1** homopolymer, which served as a macrochain transfer agent. This macrochain transfer agent was then employed during the copolymerization of octadecyl acrylate and decyl acrylate to afford P*t*BA$_{140}$-*b*-P(ODA$_{16}$-*co*-DA$_{43}$), **2**, having a narrow molecular weight distribution (PDI < 1.10) (Fig

2.2). The *tert*-butyl protecting groups were removed *via* acidolysis with TFA in CH_2Cl_2 to yield the amphiphilic block copolymer of PAA_{140}-*b*-P(ODA_{16}-*co*-DA_{43}), **3**. The PAA_{140}-*b*-P(ODA_{16}-*co*-DA_{43}) polymer was further functionalized with chelators and PEO grafts to provide for terminal coupling sites for attachment of the biologically-active ligands (PNA and TAT) and to allow for direct, future translation to *in vivo* studies. The block copolymer was first functionalized with Boc-protected DOTA-lysine *via* amidation of acrylic acid repeat units of the polymer to afford **4** with *ca*. 3 DOTA-lysines per polymer backbone. DOTA serves as a chelator for ^{64}Cu which will allow the resulting nanoparticles to be used for PET imaging *in vivo*.[14,21,35,93] Furthermore, different lengths of PEO grafts (2 kDa and 3 kDa) were appended to the polymer backbone to obtain **5**, using similar amidation chemistry to yield *ca*. 3 of each type of PEO per polymer chain. The 2 kDa PEO grafts provide stealth properties for the nanoparticles, while the 3 kDa PEO chains, after chain terminus deprotection and modification, additionally, provide reactive sites. The Boc-protecting groups from DOTA and 3 kDa PEOs were removed using TFA in a global deprotection step revealing amines at their termini. In the last step, methyl ester protected sulfohydryl groups were introduced at the NH_2- termini of the 3 kDa PEOs by reaction with SATP to yield functional block graft copolymers, **7** (Table 2.1). After each chemical transformation of the amphiphilic block copolymers, purification was performed *via* extensive dialysis against nanopure water and the polymers were isolated by lyophilization.

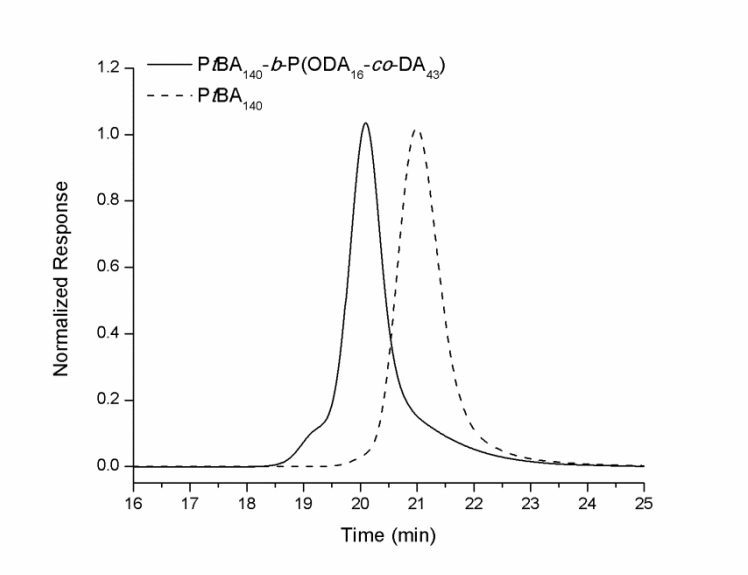

Figure 2.2. GPC traces for PtBA 1 and PtBA-*b*-P(ODA-*co*-DA) **2.**

Table 2.1. Summary of polymers prepared.

	Polymer	DOTA	PEG	$SCOCH_3$	M_n [Da] ^{1}H NMR	M_n [Da] GPC	M_w [Da] GPC	PDI GPC
1	P*t*BA_{140}	-	-	-	18,300	12,000	13,200	1.1
2	P*t*BA_{140}-*b*-P(ODA_{16}-*co*-DA_{43})	-	-	-	32,600	20,800	25,500	1.2
3	PAA_{140}-*b*-P(ODA_{16}-*co*-DA_{43})	-	-	-	24,700	-	-	-
4	PAA_{137}-*g*-(CONH-lysine-DOTA-Boc)$_3$-*b*-P(ODA_{16}-*co*-DA_{43})	3	-	-	26,700	-	-	-
5	PAA_{131}-*g*-($PEG_{3\ kDa}$-Boc)$_3$-*g*-($mPEG_{2\ kDa}$)$_3$-*g*-(CONH-lysine-DOTA-Boc)$_3$-*b*-P(ODA_{16}-*co*-DA_{43})	3	3	-	41,600	-	-	-
6	PAA_{131}-*g*-($PEG_{3\ kDa}$-NH_2)$_3$-*g*-($mPEG_{2\ kDa}$)$_3$-*g*-(CONH-lysine-DOTA-COOH)$_3$-*b*-P(ODA_{16}-*co*-DA_{43})	3	3	-	41,000	-	-	-
7	PAA_{131}-*g*-($PEG_{3\ kDa}$-NHCO-C_2H_4-$SCOCH_3$)$_3$–*g*-($mPEG_{2\ kDa}$)$_3$-(CONH-lysine-DOTA-COOH)$_3$-*b*-P(ODA_{16}-*co*-DA_{43})	3	3	3	41,700	-	-	-

Preparation of functionalized and labeled nanoparticles

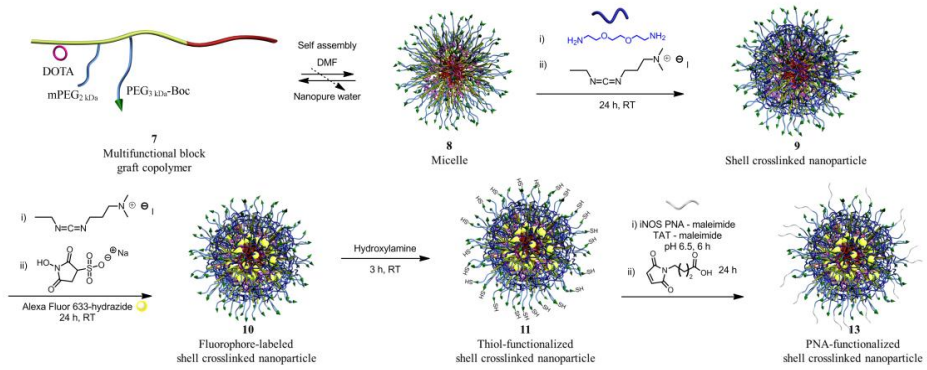

Figure 2.3 Schematic representation of self assembly of the multi-functional block graft copolymer **7** into micelle **8**, crosslinking into SCK **9**, conjugation of Alexa Fluor 633 hydrazide **10**, and functionalization with PNAs and TAT to give the final bio-synthetic hybrid nanostructure **13**.

SCKs were prepared by the solution-state assembly of the amphiphilic block graft copolymers in water followed by crosslinking reactions selectively throughout the hydrophilic shell layer (Fig. 2.3). After dissolving **7** in DMF at a concentration of 1 $mg \cdot mL^{-1}$, self assembly was induced by gradual addition of an equal amount of water over a period of 3 h. The aqueous micelle solution was allowed to stir overnight and was then transferred to dialysis tubing (MWCO 6-8 kDa) and dialyzed against nanopure water for 4 d to remove organic solvent. The SCKs were obtained by crosslinking approximately 20% of the acrylic acid segments by amidation with the amine groups of the crosslinker (2, 2'-ethylenedioxy)bis(ethylamine), in the presence of EDCI, followed by extensive dialysis to remove unreacted small molecule starting materials and reaction by products.

Alexa Fluor 633 hydrazide was attached to the SCKs, to serve as a fluorescent probe, by performing post-assembly conjugation of the hydrazide group of the dye to EDCI-activated acrylic acids in the shell of the SCKs at 0 °C. The reaction was carried out for 24 h in the dark and the fluorescently-labeled SCKs were purified by extensive dialysis for 5 d against nanopure water to remove unconjugated dye molecules.

Bioconjugation of TAT and PNAs to the SCK nanoparticles

By introducing a masked thiol on to the end of the 3 kDa PEO terminus, a surface functional nanoparticle was designed and prepared that could undergo conjugation with biomacromolecules, *e.g.,* proteins,[16] peptides and nucleic acid sequences, through efficient reactions, such as thiol-maleimide, thiol-haloacetyl or disulfide couplings. The acetyl protecting groups of the masked thiols were removed by reaction with the addition of a 0.1 M hydroxylamine solution for 4 h (Fig. 2.3).

The thiol content of the nanoparticles was then evaluated using Ellman's assay and was determined to be 33 ± 4 μM. Ellman's assay of SCKs before reacting with hydroxylamine showed undetectable concentration of –SH. The resulting reactive –SH sites were expected to be presented on the surface of the SCK nanostructures, allowing for surface availability of biologically-active ligands, and were therefore, utilized for conjugation of the PNAs as mRNA recognition elements and TAT CPPs for cell entry. These SCKs were subjected to reaction, coincidentally, with PNAs and TAT that were functionalized with maleimide, at pH 6.5 for 6 h at 0 °C. Two anti-iNOS PNAs, PNA240 and PNA480, and mismatch controls were selected for conjugation to the SCKs (Table 2.2), from a set of PNAs previously shown to have similar affinity for iNOS mRNA, but differing abilities to inhibit iNOS expression [94]. In each case, the unreacted thiols were capped using 4-maleimido butyric acid. The nanoparticle conjugates were purified with Sephadex G-50 columns and the amounts of PNAs incorporated into the SCK samples were calculated by UV-vis spectroscopy (Figures 2.4 A and B) using the inherent wavelength of 260 nm for PNAs.

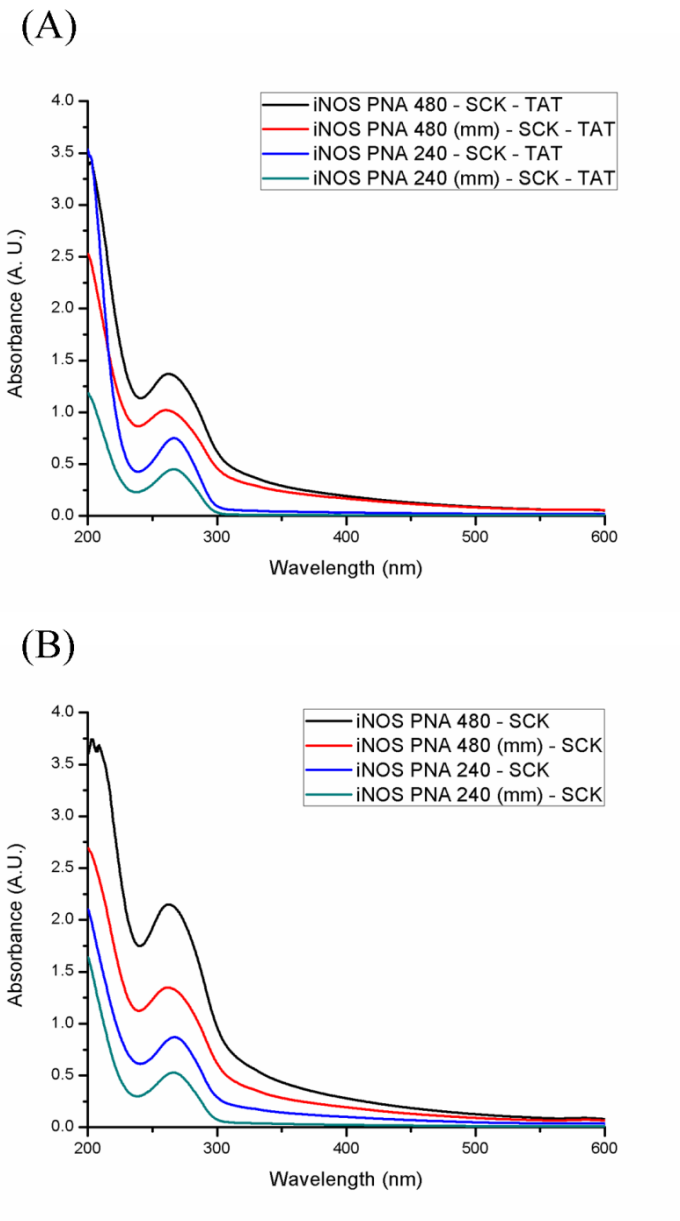

Figure 2.4. (A) UV-vis spectra of iNOS PNA-SCK conjugates, (B).UV-vis spectroscopy of iNOS PNA-SCK-TAT conjugates.

Table 2.2. ODN and PNA sequences used.

Sequence ID	Sequence (5'-3' or amino-carboxy)
240	5'- TGT CCT TTT CCT CTT TCA -3'
240 (mm)	5'- TGT CCT CCT TTT CTT TCA -3'
480	5'- TGA AAT CCG ATG TGG CCT-3'
480(mm)	5'-TAG AAT CCA GTG GTG CCT- 3'

Characterization of nanoparticles

The size and shape of the SCKs were determined using DLS and TEM. DLS analysis showed that the hydrodynamic diameters of the SCKs were slightly larger than were the diameter values determined by TEM, due to the hydration of the hydrophilic shell in aqueous conditions. The micelles and SCKs were 48 ± 7 nm by DLS and 41 ± 4 nm by TEM (Fig. 2.5). The average core diameter of the nanoparticles after conjugation with PNAs and TAT were determined using TEM and were found to be *ca.* 28 ± 5 nm (S1).

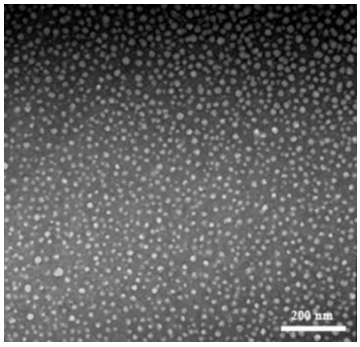

Figure 2.5. TEM image of SCKs **9**.

Binding affinity of the PNA and PNA-SCK conjugates for iNOS mRNA

The binding affinities of the PNA and PNA-SCK conjugates were determined by a competition assay against radiolabeled ODNs targeting the same site on the mRNA. To carry out this assay, we first determined the binding affinity of the ODNs targeting the same site as the PNA using a Dynabead assay that we had previously developed for this purpose.[95] The target mRNA was produced by transcription from an iNOS cDNA clone *in vitro* with Bio-dUTP to incorporate biotin groups into the RNA to enable it to be retrieved with streptavidin coated magnetic beads. The 5'-radiolabeled antisense ODNs were then incubated with the iNOS RNA and allowed to equilibrate for 4 h, after which the Dynabeads were added to bind to the mRNA, which could then be immobilized with a magnetic field. The solution containing the free ODNs was removed from the reaction tube and both the free and bound fractions were quantified by liquid scintillation counting. The ratio of bound to free ODN *vs* concentration was then fit to a standard equation (Equation 1), from which the dissociation constant (K_d) could be determined. As can be seen in Table 2.3, ODNs designed on the basis of binding sites identified by the RT-ROL mapping assay (iNOS240, iNOS480) [94] showed very high affinity with dissociation constants (K_d's) of 7.3 ± 1.2 and 5.2 ± 2.5 nM (Table 2.3).

Table 2.3. Binding affinities of ODNs, PNAs, PNA-SCK and iNOS PNA-SCK-TAT conjugates.

Sequence ID	ODN (nM)	PNA (nM)	PNA-SCK (nM)	PNA-SCK-TAT (nM)
240	7.3 ± 1.2	0.10 ± 0.052	3.2 ± 2.0	1.4 ± 0.5
240mm	-	>10000	>1000	>1000
480	5.2 ± 2.5	0.086 ± 0.026	1.1 ± 0.3	1.7 ± 1.0
480mm	-	>10000	>1000	>1000
No PNA	-	-	>1000	>1000

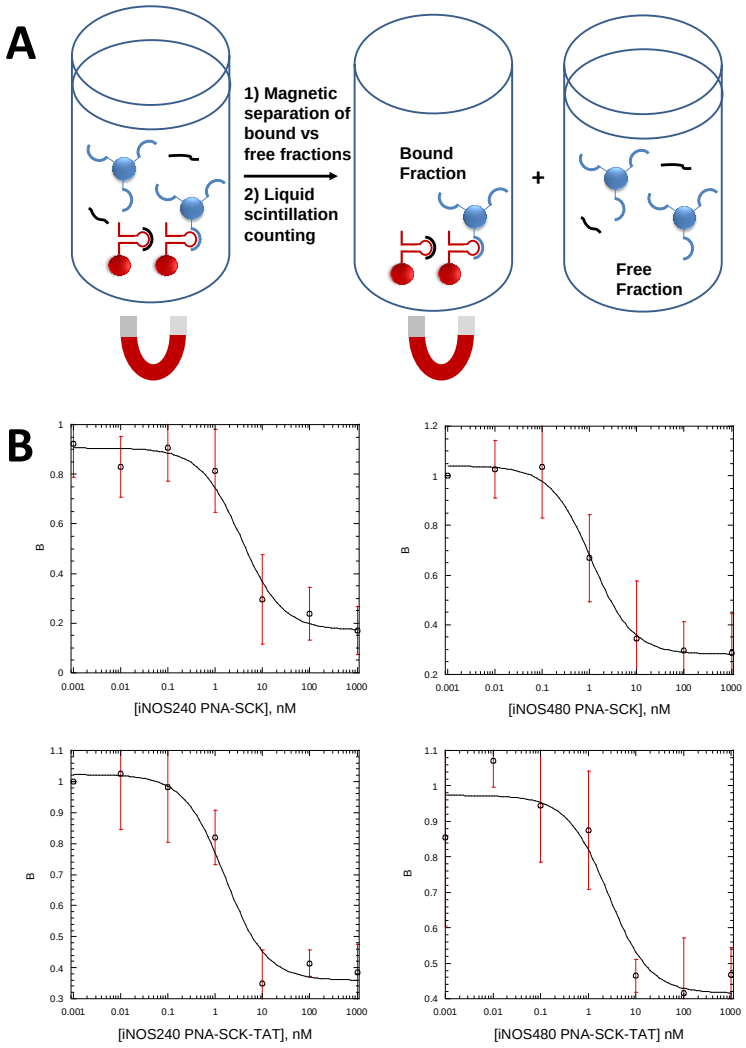

Figure 2.6. Dynabead competition assay to determine iNOS mRNA binding affinity of SCK-PNA conjugates. A) Biotinylated iNOS mRNA (10 pM) bound to streptavidin coated Dynabeads were incubated with 1 nM 5'-radiolabeled 240 or 480 antisense ODN and increasing concentrations of the corresponding SCK-PNA conjugate. After incubation for 4 h, the bound *versus* free fractions were separated by a magnet and the radioactivity in each fraction was quantified by liquid scintillation counting. B) Plots of the average fraction of mRNA bound by radioactively labeled ODN *vs.* the SCK-PNA conjugates from three experiments fit to the analytical expression 2) described in the experimental section from which the IC_{50} was extracted. The data in Table 3 was obtained from averaging fits to each independent experiment (See supporting information).

Once the binding affinity of the ODNs was established, the binding affinity of PNAs and PNA-SCK conjugates to iNOS mRNA could be determined by a competition assay in which the concentration of ODN was held constant and the concentration of the PNA or PNA-SCK was varied (Fig. 2.6-2.11). The K_d could then be calculated from the IC_{50}. As can be seen in Table 2.3, the two PNAs, PNA-240 and PNA-480 showed similar K_d's of 101 ± 52 and 86 ± 26 pM, while the mismatched PNAs had K_d's of > 10 nM. When conjugated to the SCKs, the binding affinity of the PNAs appeared to decrease about 30 to 10-fold, respectively, to 3.2 ± 2.0 and 1.1 ±0.3 nM, while the mismatched PNAs showed no significant affinity. The decrease in affinity of the PNAs upon conjugation could be due to a number of factors, such as electrostatic repulsion between the SCK and the RNA, or steric interference by a bound RNA molecule. The binding affinity of the iNOS PNA-SCK-TAT conjugates, which could have been expected to be higher due to the positive charge of the TAT peptide, was not significantly different from the conjugates lacking the TAT peptide.

2.4 Conclusions

SCKs covalently conjugated with iNOS PNAs and CPPs have been prepared and their binding affinities with complementary mRNAs post-conjugation were evaluated. Specific effort was made to have these biologically-active units presented from the outer most surface of the SCKs, by employing well-defined multi-step polymerization and polymer modification reactions that involved combinations of stealthy PEG chain grafts. The binding affinity measurements demonstrated that the PNAs retain molecular recognition selectivity even after undergoing coupling onto the nanoscopic SCK objects. The shapes and sizes of SCKs remained almost the same in the resulting nanoconjugates. By partitioning various optical and radiolabeling sites and reactive functionalities for conjugation of biological ligands within a size-, shape- and flexibility-controlled nanoscopic framework, these bio-synthetic hybrid materials provide preliminary steps towards the development of hierarchical nanostructures that hold great promise as antisense imaging agents and therapeutics. The availability of particles with tunable compositions and properties will allow us to fine-tune the PNA-RNA molecular recognition events, while balancing the electrostatic binding and repulsion.[36,83] With the high levels of sophistication that are possible *via* simple iterations of controlled polymer chemistries, there are several functions whose biological performances are yet to be evaluated. Extended *in vitro* and *in vivo* studies are underway.

2.5 Acknowledgements

This material is based upon work supported by the National Heart Lung and Blood Institute of the National Institutes of Health as a Program of Excellence in Nanotechnology (HHSN268201000046C) and by the Office of Naval Research (N00014-10-1-0527). The Welch Foundation is gratefully acknowledged for support through the W. T. Doherty-Welch Chair in Chemistry, Grant No. A-0001.

2.6 Supporting Information

Supplementary Figures.

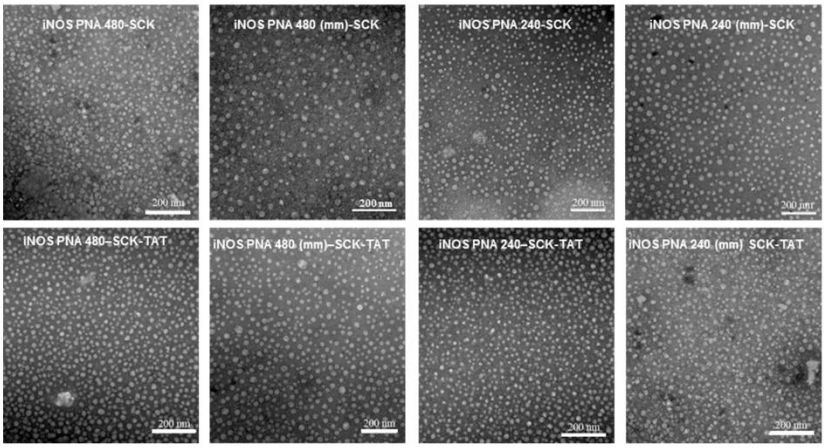

Figure 2.7. TEM images of iNOS PNA-SCK conjugates with and without TAT.

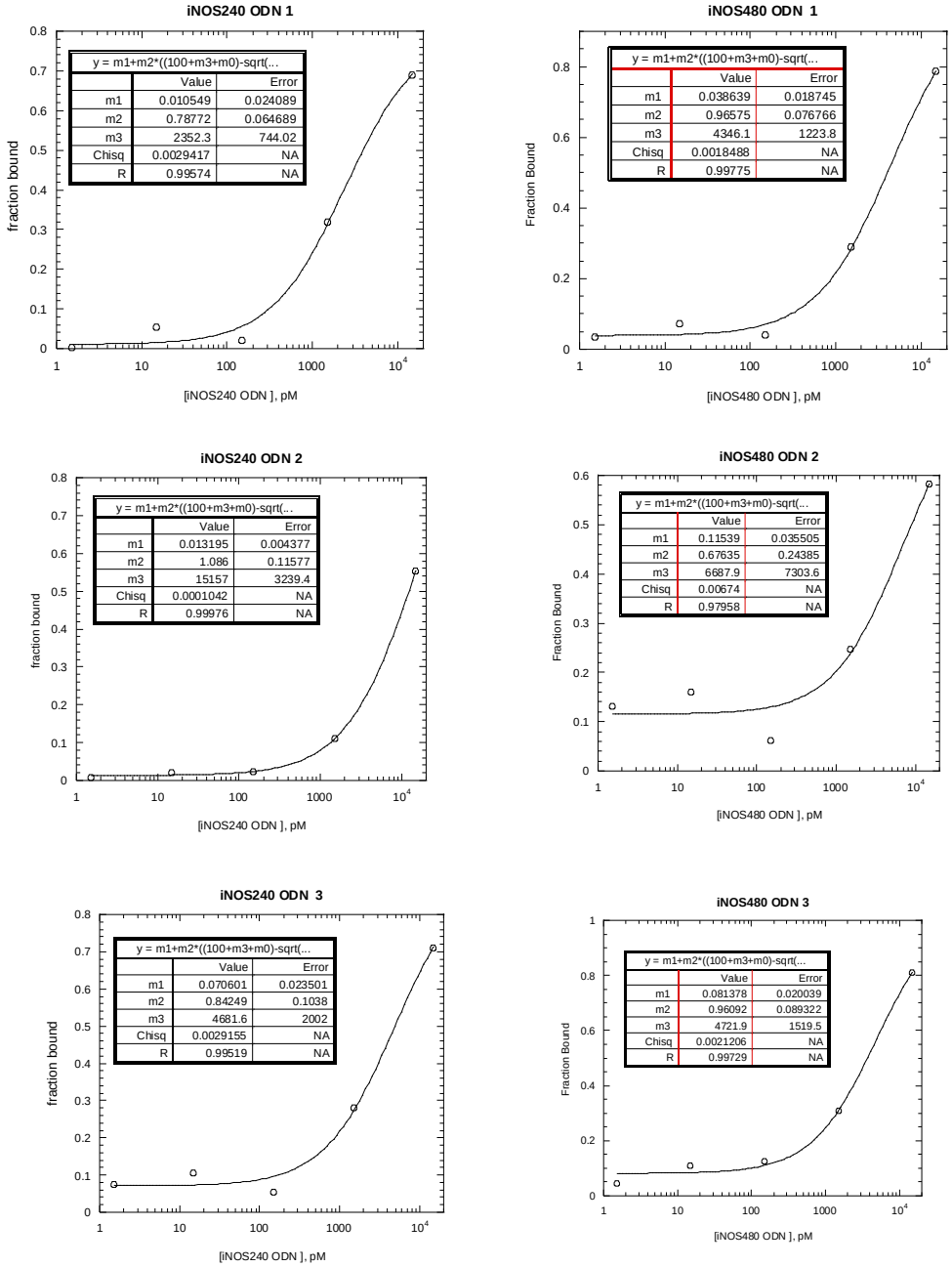

Figure 2.8. Determination of ODN 240 and 480 binding affinity for iNOS mRNA. Fits of fraction ODN bound to the iNOS mRNA from a Dynabead binding assay to equation 1) as described in the experimental section. The concentration of ODN was 100 pM.

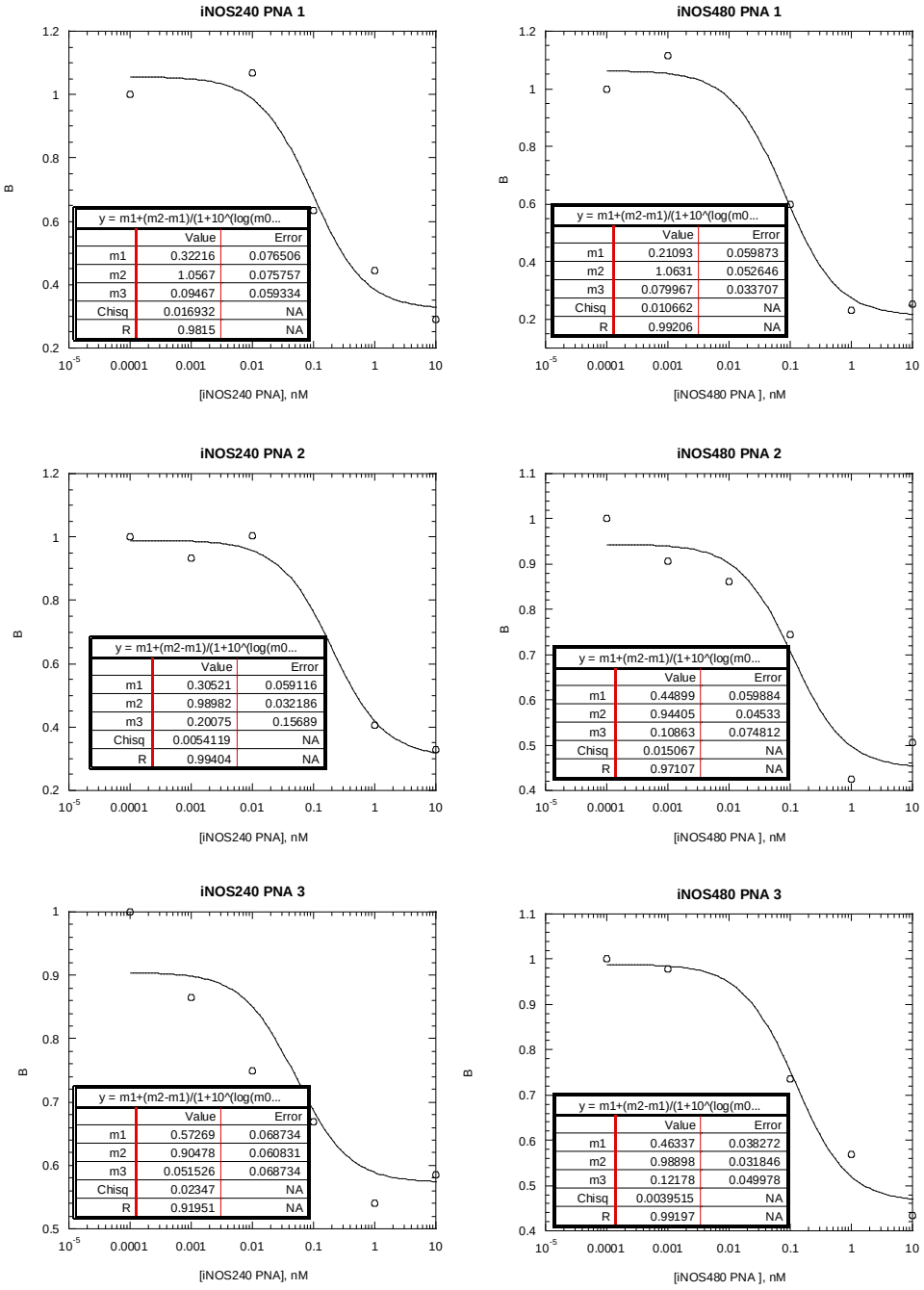

Figure 2.9. Determination of PNA 240 and 480 binding affinity for iNOS mRNA through a Dynabead competition assay as described in the experimental section. The fraction of mRNA (10 pM) bound to 5'-radiolabeled ODN (1 nM) as a function of PNA concentration (nM) was fit to equation 2) to determine the IC_{50}. The K_d for PNA binding was then determined from the K_d for the ODN and the IC_{50} for the PNA according to equation 3).

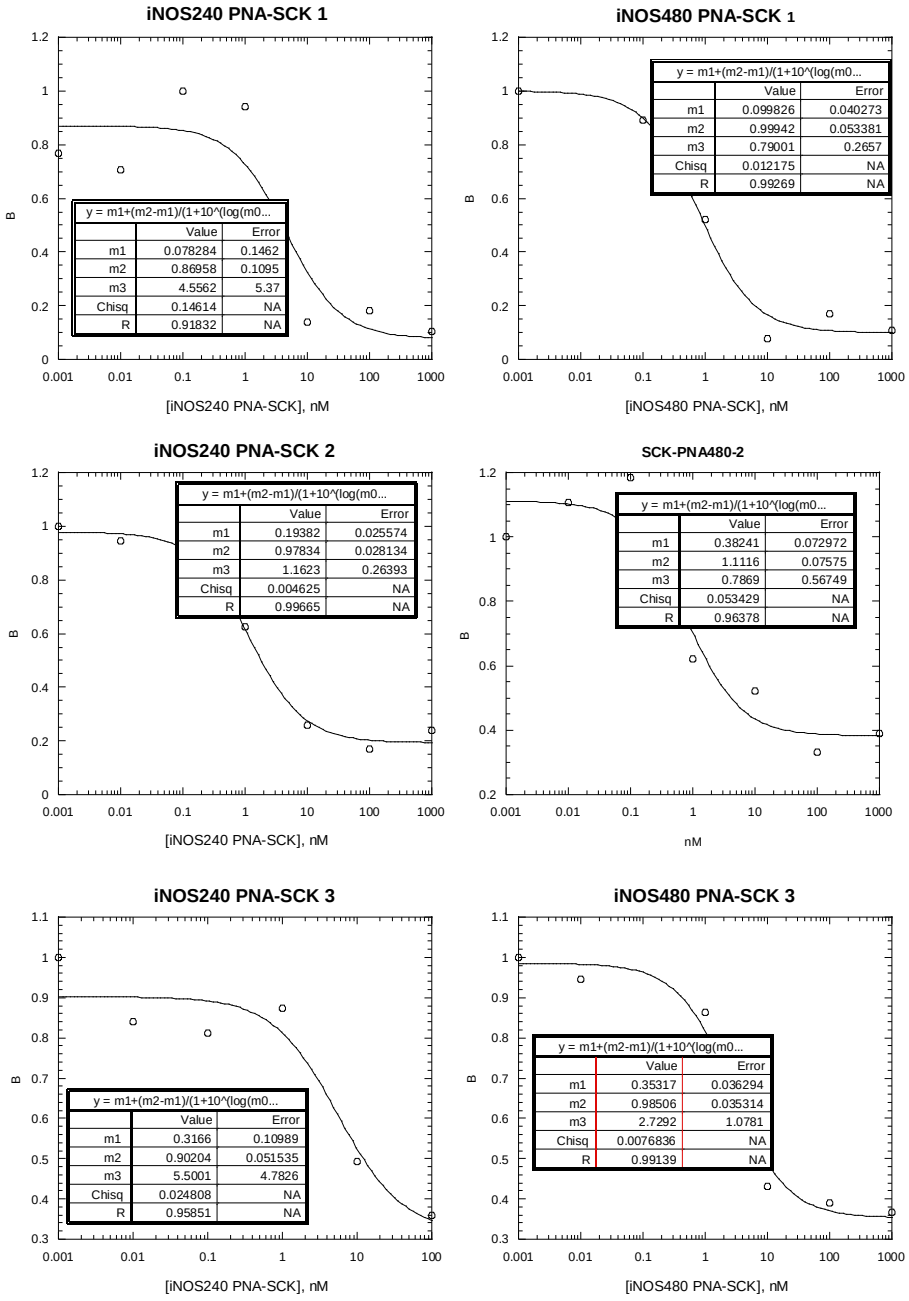

Figure 2.10. Determination of SCK-PNA 240 and 480 binding affinity for iNOS mRNA through a Dynabead competition assay as described in the experimental section. The fraction of mRNA (10 pM) bound to 5'-radiolabeled ODN (1 nM) as a function of SCK-PNA concentration (nM) was fit to equation 2) to determine the IC_{50}. The K_d for SCK-PNA binding was then determined from the K_d for the ODN and the IC_{50} for the SCK-PNA according to equation 3).

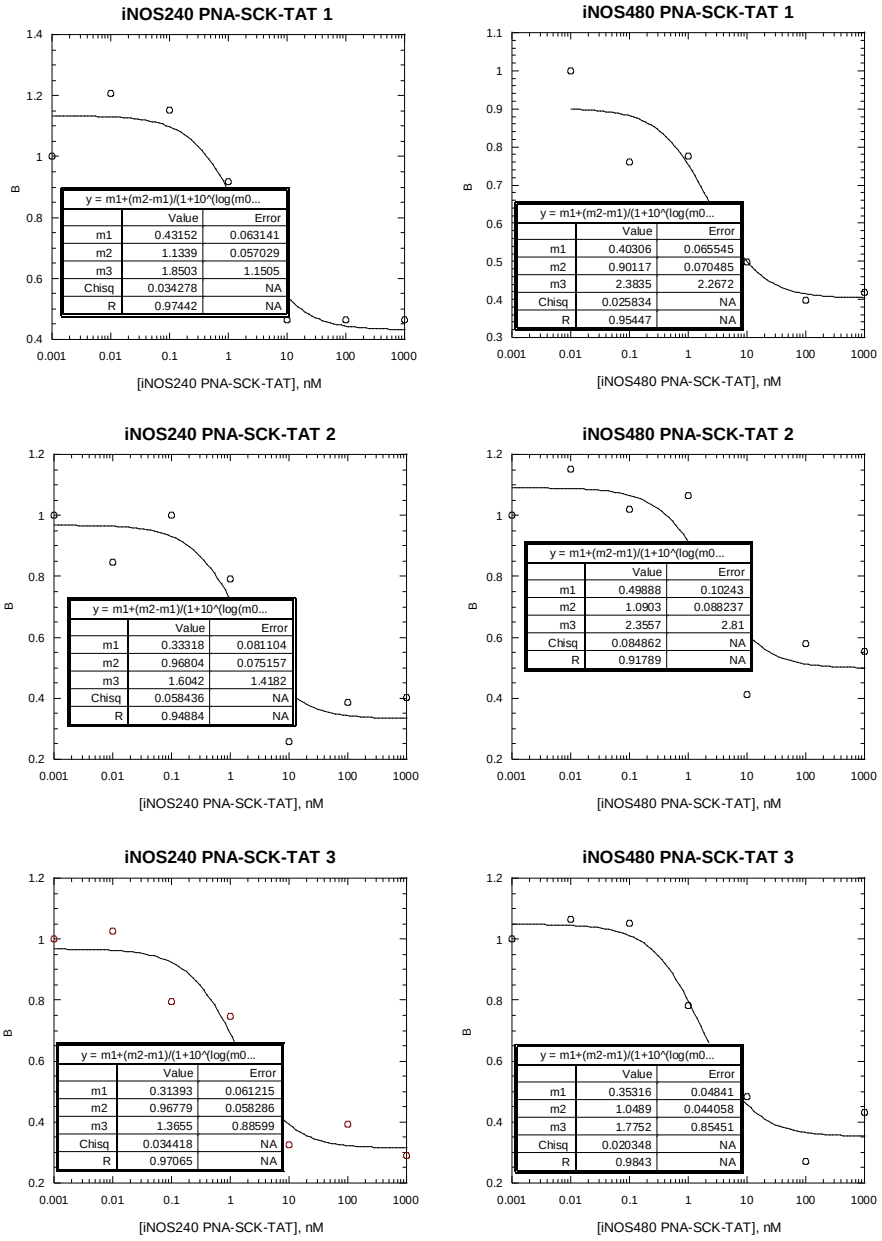

Figure 2.11. Determination of TAT-SCK-PNA 240 and 480 binding affinity for iNOS mRNA through a Dynabead competition assay as described in the experimental section. The fraction of mRNA (10 pM) bound to 5'-radiolabeled ODN (1 nM) as a function of TAT-SCK-PNA concentration (nM) was fit to equation 2) to determine the IC50. The K_d for TAT-SCK-PNA binding was then determined from the K_d for the ODN and the IC50 for the TAT-SCK-PNA according to equation 3).

CHAPTER III

ENHANCED CELLULAR UPTAKE OF F3 PEPTIDE- AND FLUOROPHORE-TETHERED CATIONIC SHELL CROSSLINKED NANOPARTICLES FOR TARGETING NUCLEOLIN AND SELECTIVE DELIVERY OF SMALL INTERFERING RNA TOWARD THE TREATMENT OF PEDIATRIC BRAIN TUMORS

3.1 Introduction

The fatalities associated with adult and pediatric brain tumors remain high in the United States, establishing a need for an improved and effective alternative treatment strategy.[55] Brain tumor occurs due to the unlimited proliferation of cells.[96] Approximately 66,290 new cases of brain and central nervous system tumors are expected to be diagnosed in 2012, among which 4,200 are projected to be pediatric incidences.[55] Despite modern advances in chemo- and radiotherapy, methods of treatment, in general, are non-selective and have many adverse effects.[97] Therefore, there is a need for alternative strategies for more effective and targeted therapy toward the treatment of brain tumors.

In recent years, RNA interference (RNAi) has received much attention due to its potential in the treatment of various diseases.[38] RNAi is a gene silencing mechanism where small interfering RNA (siRNA) downregulates the expression of a specific gene providing this technology with a high level of selectivity and efficiency, and hence, offering it a great advantage over other forms of therapeutics.[98] However, employing siRNAs for clinical applications imposes a limitation, owing to their large size and inherent negative charge resulting in low cellular uptake.[38,99,100] Additionally, the rapid enzymatic degradation of siRNA by extra- and intracellular nucleases compromises its

therapeutic potential. One way to circumvent this challenge is to complex the negatively-charged siRNA with positively-charged lipids/polymers, where the electrostatic interactions between siRNA and cationic lipids/polymers result in the formation of positively-charged nanocomplexes, which partially protects the siRNA against degradation and enhances cellular uptake.

Recent advances made with synthetic chemistry provide opportunities for the construction of well-defined, sophisticated materials having precise control over charges, sizes and three dimensional structures, resembling nanoscopic objects as formed in Nature[22] and extending significantly the types of materials that are available for nucleic acid packaging, protection and delivery strategies, among other nanomedicine applications. The design and development of nanomaterials have extended beyond mere fundamental investigations, to potentially translatable, medically-relevant nanotechnologies for the detection, diagnosis and treatment of cancer and other diseases.[20,31,101] Several platforms, such as liposomes,[102] magnetic nanoparticles,[103] and quantum dots[104,105] have been explored, however, our group has a long standing interest in developing novel polymeric systems and chemistries for the preparation of shell crosslinked knedel-like (SCK) nanoparticles,[30,106] and fine tuning of existing nanostructures for a diverse set of applications in biomedical research.[7,9,14,93,107,108] SCKs are core-shell morphology nanoparticles composed of block copolymers that consist of a hydrophilic and a hydrophobic segment, making them amphiphilic and prone to self assembly in selective solvents. Furthermore, selective crosslinking throughout the adjacent chains in the hydrophilic shell layer allows SCKs to possess structural and

kinetic stabilities. These nanomaterials have emerged as a powerful tool for providing novel non-viral vectors for effective delivery of therapeutics.[33,109]

Extending the application of nanotechnology for the delivery of siRNA therapeutics, specifically, includes several challenges that the SCK nanoparticle platform has the potential to address, including effective packaging of the nucleic acids, protection against enzymatic degradation and allowing the targeted delivery of siRNA to the tumor site as well as intracellularly into the cytoplasm of cancer cells toward the treatment of brain tumors. Here, we take advantage of our ability to exploit the properties of nanoparticles by performing manipulations at early stages of their design, to incorporate positive charges along the hydrophilic segment of the block copolymer precursor to yield cationic SCKs (cSCKs). cSCKs have been engineered[33,110,111] with positive charges in the shell domain of the nanoconstructs to impart cationic character and enhance cellular uptake, while allowing also for electrostatic attractive interactions for binding siRNA to conduct RNAi. Moreover, efficient and effective RNAi can occur by directing the siRNA not to the entire cell population but to selected target cells. This process requires engineering a platform that provides dual advantage such that it carries positive charges on the surface and additionally, is tethered with ligands allowing it to identify specific cell types.

With our current interest in developing multifunctional nanoparticles capable of delivery of diagnostic and therapeutic agents to tumors, we have focused on the highly promising F3 peptide ligand, which can bind to overexpressed nucleolin as an angiogenesis marker, and has been shown to effectively traffick nanoparticles to brain

tumors *in vivo*.[112] F3 peptide is a 31-amino acid peptide that has demonstrated to have cell penetrating properties and is a promising candidate for drug-targeting and gene-therapy applications.[113-115] Covalent conjugation of F3 peptide onto nanoparticles allows for enhanced cellular uptake[116,117] of the nanostructures and targeted delivery of therapeutics, resulting in an increased efficacy, reduced side effects and, hence, improved overall efficiency of delivery. Herein, cSCKs conjugated with fluorophore and decorated with F3 peptide were prepared as bio-synthetic hybrids that were mixed with negatively-charged nucleolin-siRNA and investigated for their differential cellular uptake and knockdown of nucleolin expression in U87 glioma cells *in vitro*.

3.2 Materials and Methods

Synthesis of poly(tert-butyl acrylate)$_{160}$ (PtBA$_{160}$) (1)

Bulk polymerization of *tert*-butyl acrylate by atom transfer radical polymerization: To a flame dried 100 mL Schlenk flask, *tert*-butyl acrylate (56.6 g, 44.2 mmol) was added along with copper (I) bromide (0.41 g, 2.86 mmol). The reaction mixture was sealed and three freeze pump thaw cycles were performed to ensure the removal of air. N,N,N',N',N''-pentamethyldiethylenetriamine (0.49 g, 2.87 mmol) and 2-ethylbromo propionate (0.40 g, 2.21 mmol) were added to the reaction mixture *via* a syringe and the reaction mixture was allowed to undergo two more freeze pump cycles. The reaction mixture was brought to room temperature and stirred to ensure homogeneity. Following this, the Schlenk flask was immersed into a preheated oil bath at 50 °C. Aliquots were taken at predetermined time interval and conversion was monitored *via* NMR and GPC. After the expected conversion was reached, the

polymerization was quenched by immersing the reaction flask into liquid nitrogen. The reaction mixture was passed through a short alumina plug to remove copper and three consecutive precipitations were performed in methanol and ice (80:20). After the final precipitation, a white gooey polymer (18.0 g, 50% yield) was obtained after removal of solvent and subsequent drying under *vacuo*. $(M_n)_{NMR}$ = 21.2 kDa. $(M_n)_{GPC}$ = 14.9 kDa. $(M_w)_{GPC}$ = 17.7 kDa. PDI= 1.18. IR: 3000, 2920, 1710, 1500, 1370, 1220, 1150, 880, 810 cm^{-1}. ^{1}H-NMR (CD_2Cl_2): δ 1.5 (s, $(C\boldsymbol{H}_3)_3COC$-), 1.8, (br, -$C\boldsymbol{H}CH_2$-), 2.2 ((br, -$CHC\boldsymbol{H}_2$-), 4.1 ($CH_3C\boldsymbol{H}_2OCO$-) ppm. ^{13}C NMR (CD_2Cl_2): δ: 26.7, 31.6 – 38.0, 80.2, 174.6 ppm. DSC: (T_g) = 58 °C. T_{onset} = 118 °C, $T_{decomposition}$: [(118 - 248 °C) 31 % mass loss; (248 - 457 °C) 43% mass loss; 26% mass remaining].

Synthesis of poly(*tert*-butyl acrylate)$_{160}$-*b*-poly(styrene)$_{30}$ (P*t*BA$_{160}$-*b*-PS$_{30}$) (2)

Amphiphilic block copolymer of poly(*tert*-butyl acrylate)$_{160}$-*b*-poly(styrene)$_{30}$ (P*t*BA$_{160}$-*b*-PS$_{30}$) was prepared using atom transfer radical polymerization. To a flame dried 25 mL Schlenk flask, P*t*BA$_{164}$ (8.00 g, 0.37 mmol) was added along with copper (I) bromide (108 mg, 0.75 mmol), styrene (1.96 g, 18.9 mmol) and anisole (8.00 g). The reaction mixture was sealed and three freeze pump thaw cycles were performed to ensure the removal of air. N, N, N', N', N''-pentamethyldiethylenetriamine **(**130 mg, 0.75 mmol) was added to the reaction mixture *via* a syringe and the reaction mixture was allowed to undergo two more freeze pump thaw cycles. The reaction mixture was brought to room temperature and stirred to ensure homogeneity. Following this, the Schlenk flask was immersed into a preheated oil bath at 82 °C. Aliquots were taken at predetermined time interval and conversions were monitored *via* ^{1}H - NMR and GPC.

After the expected conversion was reached, the polymerization was quenched by immersing the reaction flask into liquid nitrogen. The reaction mixture was passed through a short alumina plug to remove copper and three consecutive precipitations were performed in methanol and ice (80:20). After the final precipitation, a white powder (6.08 g, 97% yield) was obtained after the removal of solvent and subsequent drying under *vacuo*. $(M_n)_{NMR}$ = 24.4 kDa. $(M_n)_{GPC}$ = 23.4 kDa. $(M_w)_{GPC}$ = 25.9 kDa. PDI= 1.11. IR: 3000, 2945, 1730, 1460, 1380, 1280, 1150, 870, 770 cm^{-1}. ^{1}H-NMR (CD_2Cl_2): δ 1.5 (s, $(CH_3)_3COC$-), 1.8, (br, -$CHCH_2$-), 2.2 ((br, -$CHCH_2$-), 4.1 (CH_3CH_2OCO-), 6.2-7.3 (br, Ar***H***) ppm. ^{13}C NMR (CD_2Cl_2): δ: 26.7, 31.6 – 38.0, 80.2, 126.4 – 128.1, 174.6 ppm. DSC: (T_g) = 51 °C. T_{onset} = 136 °C, $T_{decomposition}$: [(136 - 245 °C) 36 % mass loss; (245-464 °C) 43% mass loss; 21% mass remaining].

Synthesis of poly(acrylic acid)$_{160}$-*b*-poly(styrene)$_{30}$ (PAA_{160}-*b*-PS_{30}) (3)

Block copolymer **2** (2.10 g, 0.09 mmol) was dissolved in trifluoroacetic acid (70.0g, 0.61 mol) and stirred at room temperature for 16 h. The next day, TFA was evaporated and polymer was dissolved in THF and transferred to a presoaked dialysis bag (MWCO 6-8000 Da). The mixture was extensively dialyzed for 4 days against nanopure water followed by lyophilization to obtain white fluffy polymer of PAA_{164}-*b*-PS_{31} (1.02 g, yield = 78.0%). $(M_n)_{NMR}$ = 15.2 kDa. IR: 3700-2400, 1720, 1488, 1280, 1205, 860 cm^{-1}. ^{1}H-NMR (DMSO-d_6) δ: 1.0-2.0 (br, polymer backbone), 2.2 (br, -$CHCH_2$-), 4.1 (CH_3CH_2OCO-), 6.2 - 7.3 (br, Ar***H***), 12.2 (br, COO***H***) ppm. ^{13}C NMR (DMSO-d_6) δ: 31.6 – 38.0, 126.4 – 128.1, 175.6 ppm. DSC: (T_g) = 49 °C, 127 °C. T_{onset}

= 154 °C, $T_{decomposition}$: [(154 - 289 °C) 6 % mass loss; (289-482 °C) 40% mass loss; 40% mass remaining].

Synthesis of poly(acrylamidoethylamine-boc)$_{160}$-*b*-poly(styrene)$_{30}$ (PAEA-boc$_{160}$-*b*-PS$_{30}$) (4)

General procedure for conjugation of *N*-boc-ethylenediamine: Lyophilized polymer, **3** (150 mg, 9.86 μmol) was allowed to dissolve in DMF (7.50 mL) for 30 mins prior to the addition of HOBT (324 mg, 2.39 mmol) and HBTU (912 mg, 2.39 mmol) in a DMF solution. The reaction was stirred for 30 mins and diisopropylethylamine (180 mg, 1.34 mmol) was added along with *N*-boc-ethylenediamine (389 mg, 2.39 mmol). The reaction was stirred overnight at room temperature for 24 h and dialyzed against 150 mM NaCl solution for 2 days, then against nanopure water for 5 days. After dialysis the solution was filtered to obtain a white powder (380 mg, 95.0% yield). $(M_n)_{NMR}$ = 38.7 kDa. $(M_n)_{GPC}$ = 47.0 kDa. $(M_w)_{GPC}$ = 60.1 kDa. PDI= 1.27. IR: 3630-3120, 2960, 2910, 1650, 1620, 1540, 1450, 1380, 1260, 1180, 1030, 890, 830 cm^{-1}. ^{1}H-NMR (DMSO-d_6) δ: 1.0 - 2.0 (br, polymer backbone, boc), 2.2 ((br,-CHC***H***$_2$-), 2.8 - 3.4 (br,-NC***H***$_2$C***H***$_2$N-) 6.2 - 7.3 (br, Ar***H***) ppm. ^{13}C NMR (DMSO-d_6) δ: 26.7, 31.6 – 41.0, 56.5, 80.2, 126.4 – 128.1, 145.5, 175.3 ppm. DSC: (T_g) = 28 °C, 106 °C. T_{onset} = 132 °C, $T_{decomposition}$: [(132 - 239 °C) 29 % mass loss; (239-475 °C) 47% mass loss; 24% mass remaining].

Synthesis of poly(acrylamidoethylamine)$_{160}$-*b*-poly(styrene)$_{30}$ (PAEA$_{160}$-*b*-PS$_{30}$) (5)

General procedure for the removal of Boc groups: A white powder of **4,** (153 mg, 3.54 μmol) was dissolved in TFA (7.00 g, 61.4 mmol) and stirred at room temperature

overnight. The next day, TFA was the removed under *vacuo.* The polymer was then dissolved in DMSO and dialyzed against nanopure water followed by lyophilization to obtain the deprotected polymer. $(M_n)_{NMR}$ = 22.1 kDa. IR: 4000-2360, 1670, 1560, 1470, 1190, 1130, 855, 810, 750 cm^{-1}. ^{1}H-NMR (DMSO-d_6): δ 1.0-2.0 (br, polymer backbone), 2.2 (br,-CHC***H***$_2$-), 2.8- 3.4 (br,-NC***H***$_2$C***H***$_2$N-) 6.2-7.3 (br, Ar***H***), 7.2 - 8.4 (br, N***H***) ppm. ^{13}C-NMR (DMSO-d_6): δ: 26.7, 31.6 – 38.0, 40.5, 126.4 – 128.1, 145.5, 175.0 ppm. DSC: (T_g) = 29 °C, 109 °C. T_{onset} = 173 °C, $T_{decomposition}$: [(173 - 296 °C) 14 % mass loss; (296-484 °C) 48% mass loss; 38% mass remaining].

Preparation of micelles (6)

To **5** (5.05 mg), DMSO (3.40 mL) was added and the reaction was stirred for 1 h. The solution was then transferred into a presoaked dialysis tubing (MWCO *ca.* 6000-8000 Da) and dialyzed against nanopure water for 4 d to remove residual solvent and impurities to afford clear micellar solution at a concentration of 530 μgmL^{-1}. $(D_h)_{num}$ (DLS) = 168 ± 163 nm; $(D_h)_{vol}$ (DLS) = 29 ± 19 nm; $(D_h)_{int}$ (DLS) = 19 ± 5 nm. Zeta potential = 50 ± 2 mV (pH 5.5).

Preparation of cSCKs (7)

To **6** (6.00 mL), sodium carbonate (20 μL of 1.0 M solution) was added to adjust the pH to *ca*. 8.0. A diacid crosslinker (2.0 mg) was activated with HOBT (1.7 mg, 2.2 equiv. per COOH) and HBTU (4.8 mg, 2.2 equiv. per COOH) in 300 μL of DMF for 30 min. The activated crosslinker solution was slowly added to the micellar solution to crosslink *ca.* 5 % of the amines. The reaction mixture was stirred overnight, and then transferred to a dialysis tube (MWCO *ca.* 6000-8000 Da) and dialyzed against nanopure water for 3 days to obtain clear cSCK solution at 520 μg/mL. $(D_h)_{num}$ (DLS) = 252 ± 221 nm; $(D_h)_{vol}$ (DLS) = 45 ± 31 nm; $(D_h)_{int}$ (DLS) = 29 ± 8 nm. Zeta potential = 35 ± 2 mV (pH 5.5).

Conjugation of Cy3 – NHS to cSCKs (8)

To **7** (4.00 mL), sodium carbonate (20 μL of 1.0 M solution) was added to adjust the pH to *ca*. 8.0. Cy3–NHS (0.3 μL) was added from a stock solution (200 mM) in DMSO to tether *ca*. 1 dye per polymer chain. The reaction mixture turned magenta as soon as the dye was added. The reaction was stirred overnight, and then transferred to a dialysis tube (MWCO *ca.* 6000-8000 Da) and dialyzed against 10 mM PBS buffer in dark for 3 days to obtain magenta solution of cSCK solution with a concentration of 580 μgmL^{-1}. Dye concentration was quantified by UV-vis spectrophotometer and found to be 3.35 μM. $(D_h)_{num}$ (DLS) = 515 ± 594 nm; $(D_h)_{vol}$ (DLS) = 28 ± 21 nm; $(D_h)_{int}$ (DLS) = 20 ± 5 nm. Zeta potential = 35 ± 2 mV (pH 5.5).

Modification of F3 peptide to bear maleimide units (9)

F3 peptide (FITC-Ahx-KDEPQRRSARLSAKPAPPKPEPKPRKAPAKK) and scrambled sequence (FITC-Ahx-KDEARALPSQRSRKPAPPKPEPKPKKAPAKK) labeled with FITC were modified to append maleimide onto the lysine units of the peptide backbone. To each peptide (10.0 mg, 2.54 μmol) in 10 mM PBS buffer (500 μL), succinimidyl-N-maleimidoethyl carboxylate (7.10 mg, 26.7 μmol) was added from a stock solution in DMF along with DIPEA (4 μL). After 2h, the reaction was transferred to a Zeba desalting column that was washed and equilibrated with 10 mM PBS buffer to remove small molecule impurities.

Conjugation of F3 peptides to Cy3 – cSCKs (10)

To **8** (1.50 mL)**,** sodium carbonate (20 μL of 1.0 M solution) was added to adjust the pH to *ca*. 8.0 followed by the addition of **9 (**FITC-F3-maleimide) (250 μL of stock solution). The reaction was stirred for 24 h followed by purification using Sephadex G-75 to remove unreacted F3 – peptide affording dark pink solution of Cy3 – cSCK – F3 – FITC conjugate. The reaction was analyzed by UV-vis spectrophotometer to confirm the presence of Cy3 on the cSCKs and FITC on the peptide. $(D_h)_{num}$ (DLS) = 194 ± 207 nm; $(D_h)_{vol}$ (DLS) = 26 ± 17 nm; $(D_h)_{int}$ (DLS) = 17 ± 5 nm. Zeta potential = 81 ± 14 mV (pH 5.5).

3.3 Results and Discussion

Dual F3 peptide- and Cy3-labeled cSCKs were prepared from amphiphilic block copolymers in a stepwise process, allowing for an increasing level of complexity at each stage of modification that enhanced the structural function of the resulting nanostructures. As illustrated throughout Figures 3.1, 3.2, 3.3 and 3.5, controlled radical polymerization, post-polymerization chemical modification reactions, supramolecular assembly in water, and intramicellar crosslinking reactions afforded cSCKs, which then underwent conjugation reactions of fluorescent labels and biologically-active targeting ligands with reactive sites in the shells of the cSCKs to produce bio-synthetic hybrid nanoparticles.

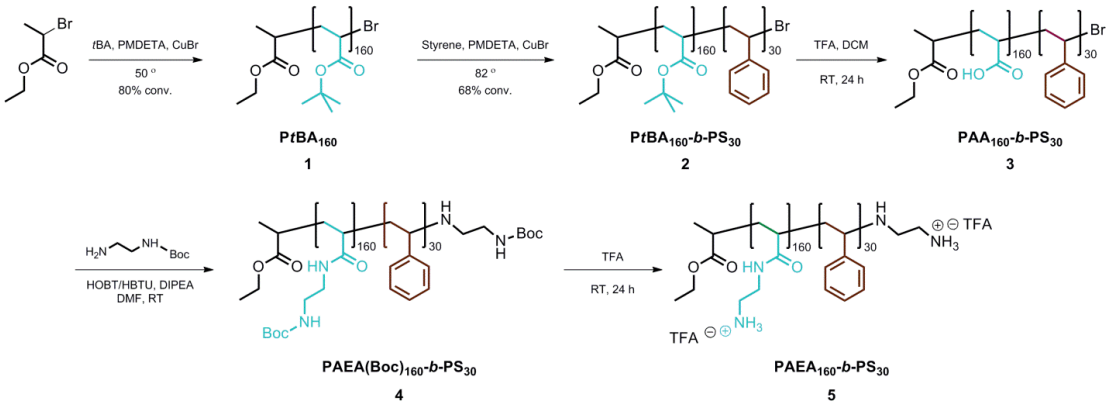

Figure 3.1. Schematic representation of preparation of cationic amphiphilic block copolymer in a stepwise process by sequential atom transfer radical polymerization of tert-butyl acrylate and styrene followed by deprotection, amidation of N-boc ethylene.

The amphiphilic block copolymer precursor to the cSCK was prepared by a sequential atom transfer radical polymerization of *tert*-butyl acrylate and styrene

followed by a sequence of selective acidolysis and amidation reactions. The P*t*BA$_{160}$ (**1**) macroinitiator was afforded through the bulk polymerization of *t*BA at 50 °C for 4 h using ethyl 2-bromopropionate as the initiator and CuBr/PMDETA catalytic system (Fig. 3.1). The homopolymer was chain extended to afford the block copolymer P*t*BA$_{160}$-*b*-PS$_{30}$ (**2**), employing **1** and styrene in the presence of CuBr/PMDETA in anisole. By allowing the reaction to proceed under conditions of high dilution and low conversion, the polymer was prepared with narrow molecular weight distribution (PDI<1.10) (Fig. 3.2). Furthermore, the *tert*-butyl protecting groups were removed *via* acidolysis with TFA in CH_2Cl_2 to yield the amphiphilic block copolymer of PAA$_{160}$-*b*-PS$_{30}$ (**3**). The acrylic acid repeat units were then converted to acrylamides, each carrying a protected amino group, by using an excess of *N*-Boc ethylene diamine in the presence of HOBT, HBTU and DIPEA in DMF, yielding P(AEA-Boc)$_{160}$-*b*-PS$_{30}$ (**4**). In the final step, the Boc protecting groups were removed by direct dissolution of **4** in TFA overnight, followed by removal of the TFA under a N_2 stream, to afford the block graft copolymer PAEA$_{160}$-*b*-PS$_{30}$ (**5**).

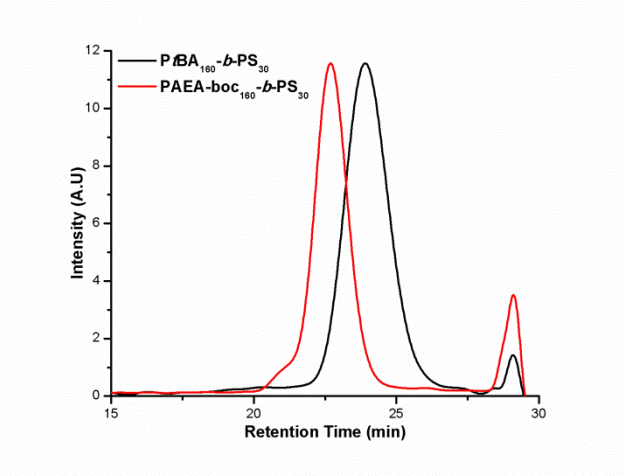

Figure 3.2. Gel permeation chromatograms of P*t*BA$_{160}$-*b*-PS$_{30}$ (**2**) and P(AEA-Boc)$_{160}$-*b*-PS$_{30}$ (**4**).

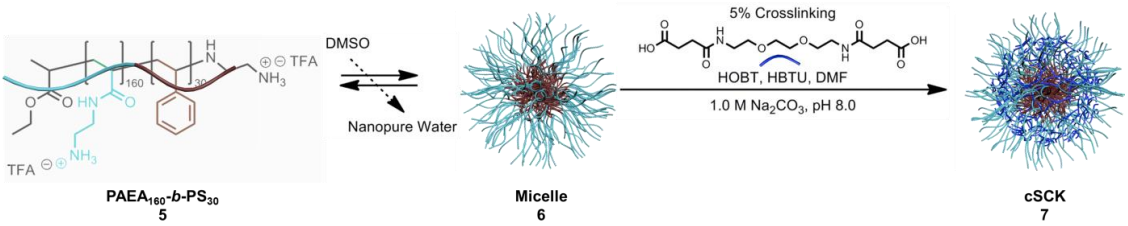

Figure 3.3 Schematic representation of self assembly of amphiphilic block graft copolymer PAEA$_{160}$-*b*-PS$_{30}$ (**5**) on transitioning from organic solvent to water, followed by crosslinking selectively of the hydrophilic shell to afford cationic SCK (**7**).

cSCKs were prepared by the solution-state assembly of the amphiphilic block copolymers **5** in water followed by crosslinking reactions selectively throughout the hydrophilic shell layer. After dissolving **5** in DMSO at a concentration of 2 mgmL^{-1}, self assembly was induced by direct dialysis of the polymer solution in DMSO against molecular biology grade water, using a dialysis membrane (MWCO 6-8 kDa), where gradual exchange of DMSO by water occurred (Fig. 3.3). Due to the nanoscopic size of the assemblies, the micelle solution remained clear at 0.70 mg mL^{-1}. The cSCKs were

obtained by crosslinking approximately 5% of the amino groups along the hydrophilic segments by amidation with activated carboxylic acids (activated using 2.2 equiv. of both HOBT and HBTU relative to the COOH groups in the crosslinker in DMF) of the diacid crosslinker (4,15-dioxo-8,11-dioxa-5,14-diazaoctadecane-1,18-dioic acid) at pH *ca*. 8 (adjusted using 1.0 M Na_2CO_3(aq.)). The crosslinking reaction was allowed to proceed overnight, followed by extensive dialysis to remove unreacted small molecule starting materials and reaction by-products.

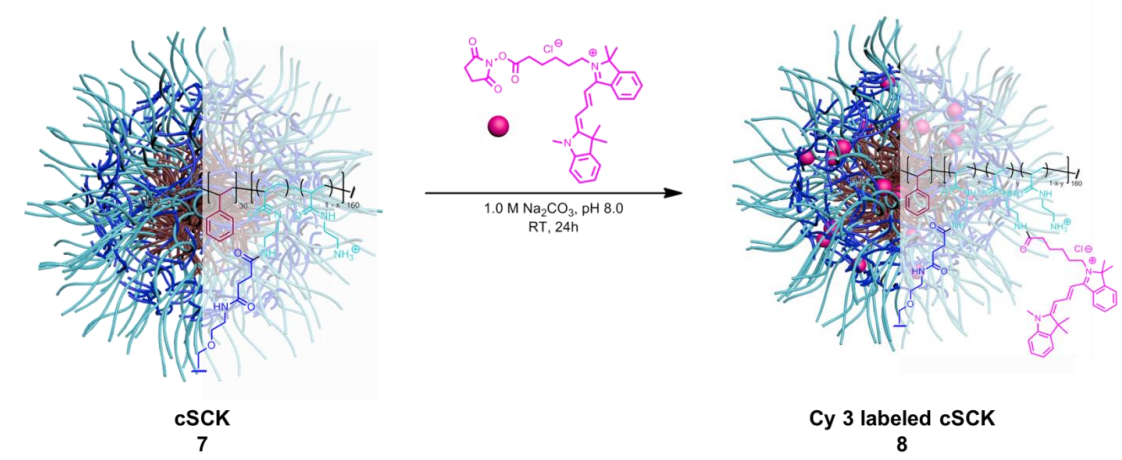

Figure 3.4 Schematic representation of preparation of Cy3-labeled cSCK by covalent conjugation of Cy3-NHS with amines along the hydrophilic segments within the shells of cSCKs at pH 8.0.

Cy3-NHS was attached to the cSCKs, to serve as a fluorescent probe, by performing post-assembly conjugation of the activated ester of the dye to amines in the shells of the cSCKs at pH *ca*. 8.0 (adjusted using 1.0 M Na_2CO_3(aq)) (Fig. 3.4). The reaction was carried out for 24 h in the dark, followed by purification by extensive

dialysis against 150 mM NaCl for 1 d and nanopure water for additional 3 d to remove unconjugated dye and small molecule by-products, and afford the fluorescently-labeled cSCKs having ~0.2 dye molecules per polymer chain comprising the cSCKs, as determined by UV-vis spectroscopy with observation at the Cy3 λ_{max}.

FITC-labeled, tumor-homing F3 peptide, which has demonstrated cell penetrating properties, was conjugated to the cSCKs in this study to target nucleolin, overexpressed at tumor cell surfaces and tumor vasculature, and facilitate enhanced cellular uptake. FITC-F3 was modified to bear maleimide functionalities on the peptide backbone (Fig. 3.5), to provide a functional handle for conjugation of the peptide to the cSCKs (Scheme 3.6).

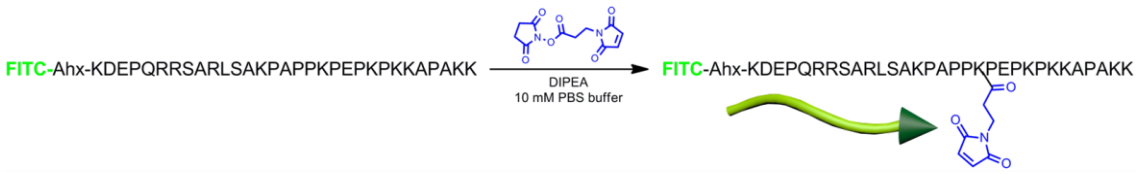

Figure 3.5 Schematic representation of modification of FITC-F3 peptide using succinimidyl-N-maleimidoethyl carboxylate as a bifunctional coupling agent to install maleimide groups for attachment to the cSCKs. Although the maleimide connection is shown only on one lysine, several maleimides groups could be present.

FITC-F3 underwent reaction with a 10-fold excess of bi-functional coupling agent (succinimidyl-N-maleimidoethyl carboxylate) with a NHS ester on one end and maleimide on the other terminus. F3 peptide (FITC-Ahx-KDEPQRRSARLSAKPAPPKPEPKPRKAPAKK) has several lysine units that can undergo reaction with the activated ester of the bifunctional reagent to install maleimide groups along the peptide backbone. The reaction was purified by spin column to remove unreacted small molecules and byproducts to obtain a bright fluorescent solution of modified FITC-F3 peptide.

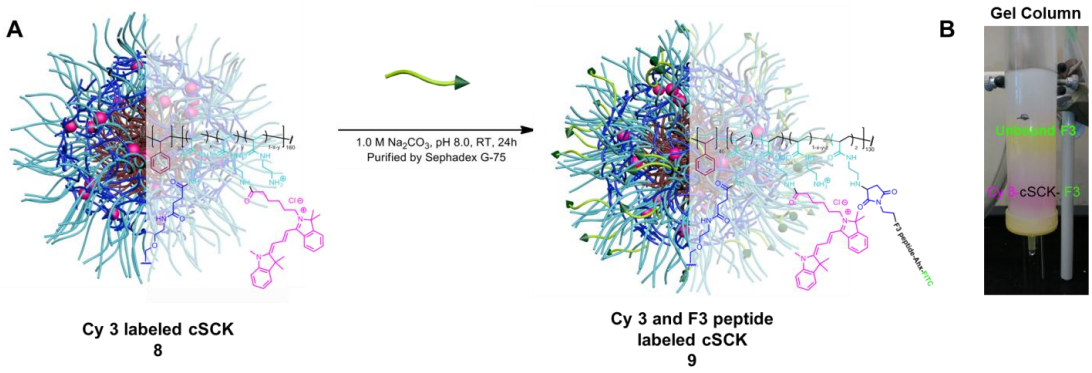

Figure 3.6 Schematic representation of (**A**) Preparation of F3 peptide-tethered cSCK by conjugating maleimide-modified FITC-F3 onto Cy3-cSCK. (**B**) Purification of Cy3-cSCK-F3-FITC conjugates (pink band) using Sephadex G-75 to remove unconjugated F3 peptide (yellow-green band).

The objective of tethering F3 peptide onto the Cy3-labeled cSCKs was to create surface functional nanoparticles for their use as targeting entities for tissue-specific targeting and delivery. Maleimide-functionalized F3 peptides, and their scrambled analogs, were subjected to undergo reactions with amine functionalized cSCK at pH *ca*. 8.0 overnight (Fig. 3.6A) to afford the targeted and non-targeted (control) cSCK samples, respectively. The nanoparticle conjugates were purified with Sephadex G-75 columns that allowed for visualization of the unconjugated peptide as a bright yellow-green band on the column (Fig. 3.6B). The amounts of F3 peptide incorporated into the cSCK samples were calculated by UV-vis spectroscopy (Fig. 3.7 A and B) using the inherent wavelength of 488 nm for FITC on the F3 peptide. Scrambled F3 peptide was employed, as a control sequence, to investigate the differential uptake of the nanoparticles in the presence of the peptide. From UV-vis measurements, *ca*. 0.2 dye molecules and 0.3 peptides were conjugated per polymer chain.

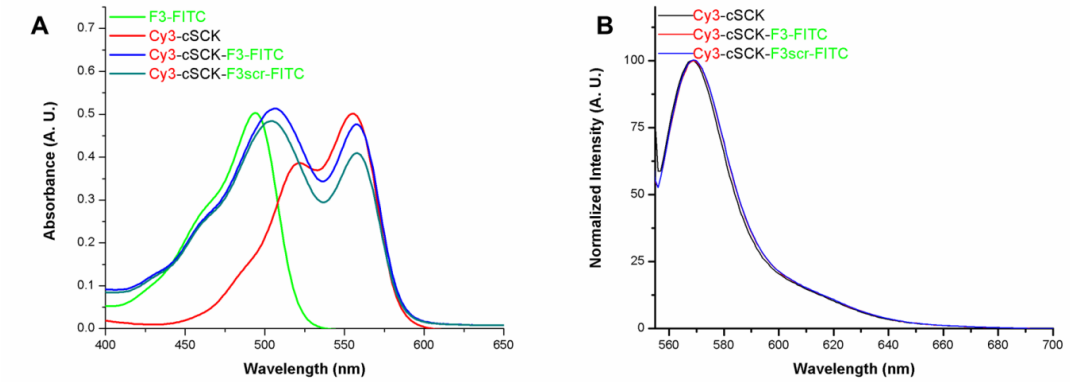

Figure 3.7 (**A**) UV-vis spectra of FITC-labeled F3 peptide, Cy3-labeled cSCK, Cy3- and F3 peptide-conjugated cSCKs, and Cy3- and scrambled F3 peptide-conjugated cSCKs. (**B**) Fluorescence emission spectra (excitation at 546 nm) of Cy3-labeled cSCK, Cy3- and F3 peptide-conjugated cSCKs, and Cy3- and scrambled F3 peptide-conjugated cSCKs. All samples were analyzed as solutions in molecular biology grade water.

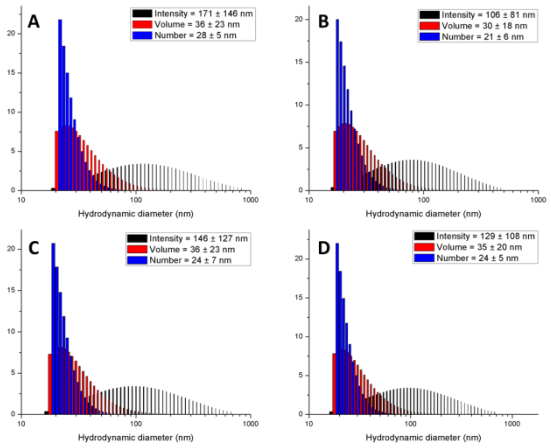

Figure 3.8 Dynamic light scattering of (A) micelles, (B) cSCKs, (C) Cy3- and F3-tethered cSCKs and (D) Cy3- and scrambled F3-tethered cSCKs.

The sizes and charges of the cSCKs were determined using dynamic light scattering (Fig. 3.8) and zeta potential measurements. The micelles and cSCKs were *ca*. 21 nm as measured by DLS prior to conjugation of the peptides and *ca*. 25 nm post-

peptide conjugation. The sizes of the particles remained the same *ca*. 21-25 nm, within the experimental error, across the series of conjugations of the Cy3 and the F3 peptide. The zeta potential values of the micelles and cSCKs, *ca*. 30 mV (at pH 5.5, in nanopure water), confirmed the positive surface charge density. After covalent conjugation to peptides, the zeta potential values were found to be *ca*. 43 mV (at pH 5.5, in nanopure water), perhaps due to incorporation of several lysine units present on the peptide backbone that contributed to the increase in cationic character of the peptide-cSCK conjugates.

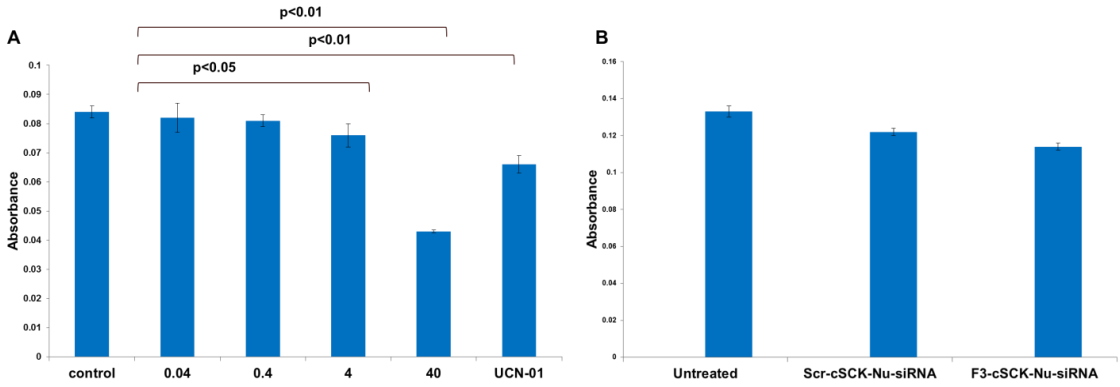

Figure 3.9. (**A**) Absorbance levels from U87MG glioma cell viability studies using the MTT assay of cSCKs at various concentrations (μgmL-1). (**B**) Absorbance levels from cell viability studies using the MTT assay of cSCKs at 2 μgmL-1 loaded with nucleolin targeting siRNA to illustrate significant inhibition of U87MG glioma cell growth for the F3-targeted cSCKs.

The Cy3-labeled F3-cSCK conjugates, **9** and **10**, were used to perform *in vitro* studies to investigate their cellular uptake behavior in U87MG glioma cells. Previously, we found that compared to normal human astrocytes, human glioma tumor cells (U87MG) showed significant amounts of nucleolin expression. Additionally, F3

peptide-based protein HMGN2 sequence has demonstrated significant binding to human malignant tumors including human glioma cells. We, therefore, hypothesized that conjugation of F3 peptide onto cSCK nanoparticles would enhance cellular uptake of F3 peptide-conjugated cSCKs into U87MG cells compared to scrambled F3-peptide conjugated cSCKs. The cytotoxicity profiles of unconjugated cSCKs on U87MG glioma cell lines were first examined to determine the non-toxic concentration levels. At a concentration of 4 μgmL^{-1}, cSCK nanoparticles exhibited slightly lower cell viability compared to the control sample, as determined by MTT assay (Fig. 3.9A). However, at a higher concentration (40 μgmL^{-1}), the cSCKs showed much lower cell viability and, therefore, a concentration of 2 μgmL^{-1} was selected to treat U87MG cells for investigation of cellular uptake of F3 peptide- and scrambled F3 peptide-conjugated cSCKs using confocal microscopy. As shown in Fig. 3.10, remarkable cellular uptake was observed for F3 peptide-conjugated cSCK nanoparticles, **9**, compared to scrambled F3 peptide-conjugated cSCKs, **10**. As expected, cells treated with unconjugated, **8**, or **10** also showed moderate amounts of uptake.

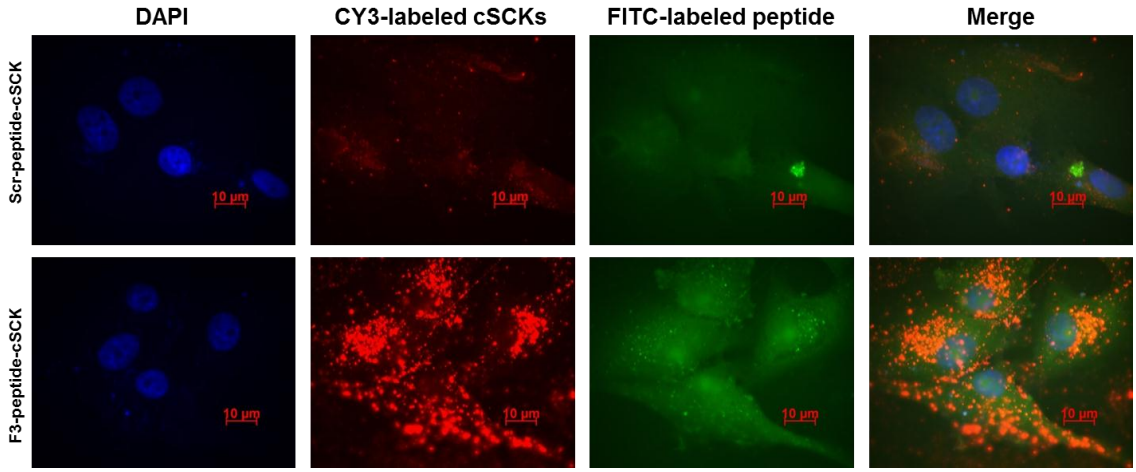

Figure 3.10 Confocal fluorescence microscopy images of U87MG cells, incubated with **9** or **10**, and observed with filters that allow for visualization of DAPI nuclear stain, Cy3 and FITC, indicating enhanced cellular uptake of F3 peptide-conjugated cSCKs, **9**, in U87MG glioma cells, compared to scrambled peptide conjugated cSCKs, **10**.

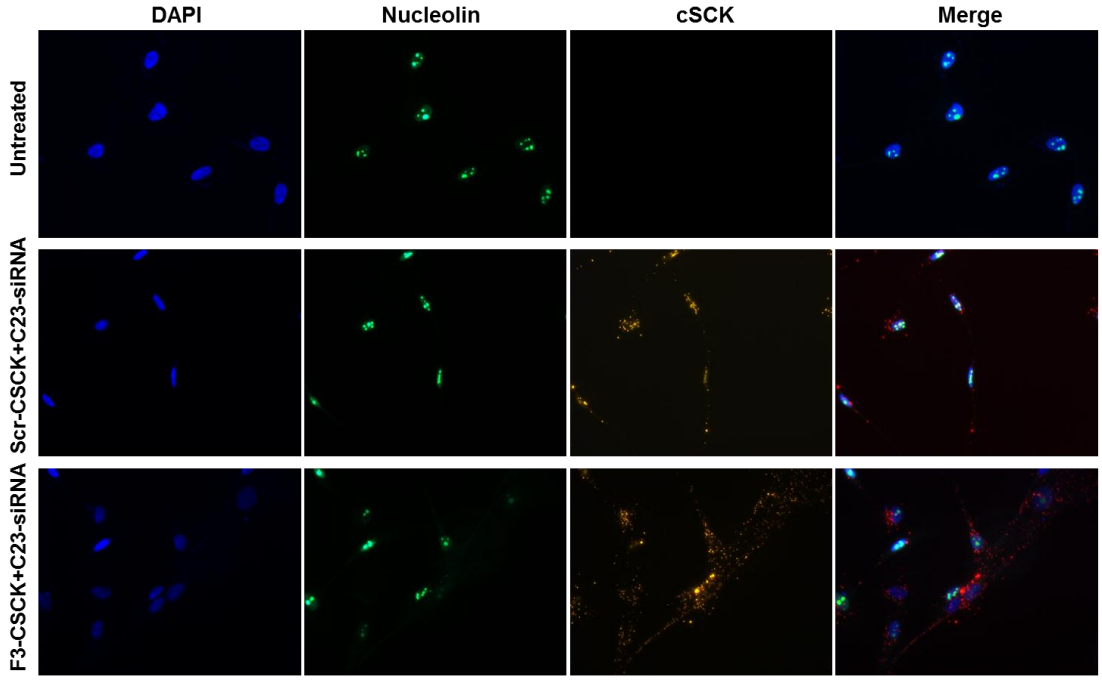

Figure 3.11 Enhanced cellular uptake of F3 peptide conjugated cSCKs and nucleolin-siRNA in U87MG glioma cells.

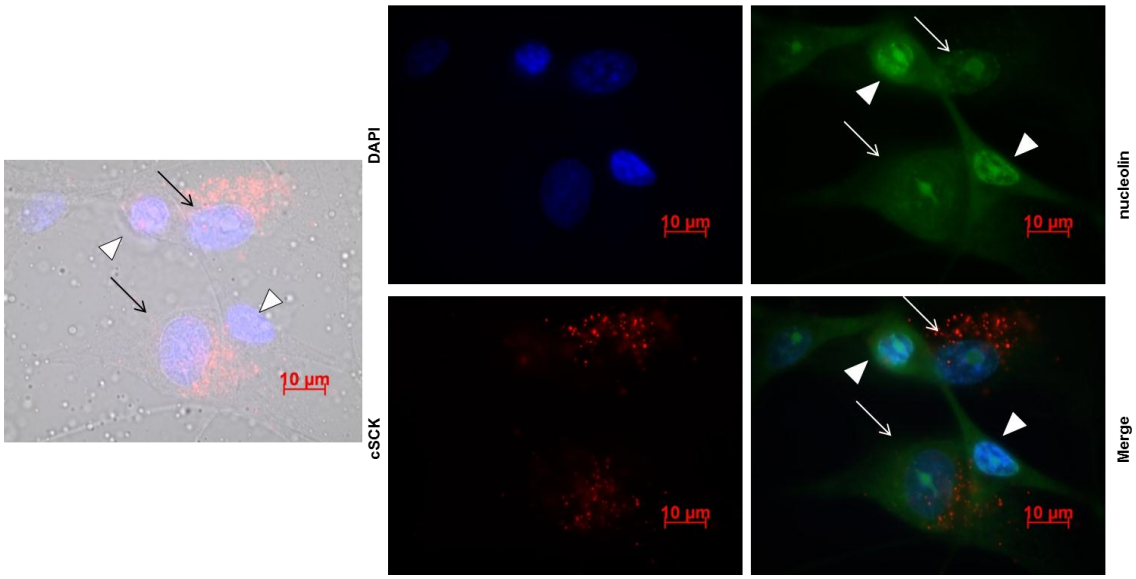

Figure 3.12 Cellular uptake of F3-labeled cSCK-siRNA for knockdown of overexpressed nucleolin in U87MG glioma cells.

Nucleolin is a shuttling protein that plays an important role in tumor cell proliferation. Previously, we have shown that knocking down nucleolin expression in U87MG glioma cells by lentivirus infection approach significantly inhibits tumor cell growth both *in vitro* and *in vivo* cSCK nanoparticles have the potential to deliver siRNA successfully into tumor cells by electrostatic complexation of positively-charged cSCKs with negatively-charged siRNA. We, therefore, mixed a pool of synthesized siRNA molecules specifically against nucleolin with either F3 peptide-conjugated cSCKs or scrambled F3 peptide-conjugated cSCKs, **9** or **10**, and treated U87MG cells *in vitro*. Within 72 h, there was a dramatic knock down of nucleolin expression among those cells treated with nucleolin siRNA-loaded F3-targeted cSCKs, both by immunofluorescence staining (Fig. 3.11 and 3.12) and by immunoblot assay (data not shown). Most

importantly, consistent with our previous observation, cells treated with nucleolin siRNA-loaded and F3-targeted cSCKs (F3-cSCK-Nu-siRNA mixtures) also showed significant decrease of tumor cell survival by MTT assay (Fig. 3.9B), due to their senescent phenotypic changes (Fig. 3.12). At higher magnification, those cells with robust uptake of F3-cSCK-Nu-siRNA mixtures were flat and remarkably enlarged compared to those less targeted populations, consistent with their bona fide morphological changes caused by senescence upon knock-down molecules into glioma-bearing mice will provide us a very useful therapeutic modality of nucleolin protein. Here, by integrating a tumor specific peptide into a cationic nanoparticle system we were able to successfully deliver nucleolin siRNA molecules into human glioma cells that subsequently showed attenuated tumor growth *in vitro*. Future investigation of this system *in vivo* in terms of their biodistribution and efficacy of delivering siRNA are underway.

3.4 Conclusions

Well-defined cSCKs dually labeled with Cy3 and F3 peptides and loaded with nucleolin siRNA have been prepared and their differential uptake and knock down of overexpressed nucleolin in U87MG glioma cells were evaluated. *In vitro* studies demonstrated an enhanced uptake of cSCKs tethered to F3 peptide compared to the scrambled peptide control nanoparticle sample. Additionally, cSCKs showed effective binding to plasmid DNA and were delivered into the cells for efficient knockdown of nucleolin as demonstrated by immunoblot assays. Specific efforts are being made currently to have these biologically-active units presented from the outer most surface of

the SCKs, by employing well-defined multi-step polymerization and polymer modification reactions that involve combinations of stealthy PEG chain grafts.[16] This work is the first step to develop cationic SCKs tethered with targeting ligands for tissue-selective cellular delivery and uptake. With the high levels of sophistication that are possible *via* simple iterations of controlled polymer chemistries, there are several functions that are yet to be incorporated and biological performances to be evaluated. Extended *in vitro* and *in vivo* studies toward employing these materials for gene and nucleic acids toward treatment of acute lung injury are also currently underway.

3.5 Acknowledgements

This material is based upon work supported by the National Heart Lung and Blood Institute of the National Institutes of Health as a Program of Excellence in Nanotechnology (HHSN268201000046C). The Welch Foundation is gratefully acknowledged for support through the W. T. Doherty-Welch Chair in Chemistry, Grant No. A-0001. The authors would like to thank Dr. Mahmoud Elsabahy and Dr. Lily Yun Lin for helpful discussions and support, Ms. Adriana Pavia for creating the Autodesk 3ds Max images, and Mr. Kevin Pollack for assistance with thermal analysis.

CHAPTER IV

ENHANCED ENDOSOMAL ESCAPE AND EFFICIENT SIRNA DELIVERY BY OPTIMIZATION OF CATIONIC SHELL CROSSLINKED KNEDEL-LIKE NANOPARTICLES WITH TUNABLE BUFFERING CAPACITIES

4.1. Introduction

In recent years, the use of small interfering RNAs (siRNAs) has gained much attention as therapeutics for the treatment of various diseases, due to their ability to selectively target and cleave complementary mRNA sequences for efficient gene silencing.[38,118-120] siRNA is composed of double-stranded RNA molecules that are *ca*. 20-25 nucleotides long with inherent negative charge and macromolecular size. The success of siRNA-based therapeutics is largely dependent on the efficient delivery of siRNA into the cytoplasm of the target cells while inducing minimal toxicity. Examples of the hurdles towards the proficient delivery of siRNA include extracellular and intracellular enzymatic degradation, limited cellular uptake, entrapment into endocytic vesicles that form upon the endocytosis of the siRNA, and limited release into the cytoplasm of the transfected cells.[38,39,121] Internalization of siRNA *via* endocytic pathways usually ends into acidified endosomes and later into lysosomes, where enzymatic degradation can occur, in addition to hindering the siRNA from reaching their target sites into the cytoplasm.[1,7] One way to circumvent these challenges is to complex the negatively-charged siRNA with positively-charged lipids/polymers, where electrostatic interactions between siRNA and cationic carriers result in the formation of positively-charged nanocomplexes, which partially protect the siRNA against degradation and enhance cellular uptake.[122-125] In addition, several types of membrane

disruptive polymers and imidazole-containing polymers have been investigated to facilitate escape from the endosomes and achieve efficient transportation of genetic materials into the cytosol.[126-131] In particular, imidazole-containing polymers have gained much attention recently, as they exhibit pK_a ~ 6 and can undergo protonation in the acidic endosomal environment leading, eventually, to efficient endosomal disruption.[130,131]

An intricate system that can electrostatically bind to nucleic acids, mediate cellular entry of the nanocomplexes and trigger mechanisms for endosomal lysis, either by interaction with the endosomal membrane or *via* the proton sponge effect, partially fulfills the design requirements for the cytoplasmic delivery of nucleic acids.[128,132,133] Some of these systems depend on incorporating two functional groups of low and high pK_as, for example, poly(L-Lysine) as a segment with high pK_a and poly[(3-morpholinopropyl) aspartamide] as a low pK_a polymer. The high-pK_a polymer interacts electrostatically with the nucleic acid at physiological pH, whereas the low-pK_a polymer remains mostly non-ionized at this pH. Protonation of the low-pK_a polymer can buffer the endosomes and aid in pumping protons concurrently with chloride ions (*i.e.* endosomal burst *via* the proton sponge effect)[134] or the additional positive charges (unbound to DNA/RNA) provide new sites for electrostatic interactions with the endosomal membrane. Both effects may enhance the ability of the vector to escape from the endosomes and release their cargoes into the cytoplasm.[135,136]

Our group has a long standing interest in designing novel polymeric systems and chemistries to engineer synthetic nanostructures, known as shell-crosslinked knedel-like

nanoparticles (SCKs) that have exhibited promise for a diverse set of biomedical applications, including nucleic acids delivery, due to their versatility in size, shape, and morphology, along with a synthetic approach that allows for ease of chemical modification, orthogonal functionalization and multivalency.[7,9,15,20,31,137-140] SCKs are core-shell nanoparticles composed of amphiphilic block copolymers that self assemble in water, followed by selective crosslinking throughout adjacent chains in the hydrophilic shell layer, which allows SCKs to possess structural and kinetic stabilities. Cationic SCKs (cSCKs), with poly(acrylamidoethylamine) (PAEA) comprising the shells for electrostatic interaction with negatively-charged nucleic acids, have emerged as a promising class of nanomaterials for highly-efficient transfection of nucleic acids of various structures.[83,110,141] In this study, a new class of cSCKs was designed by incorporating various amounts of histamines and primary amines (as low- and high-pK_a functionalities) into their shells to achieve enhanced cell transfection with reduced toxicity, by absorbing protons at pH values between the physiological and endosomal pH range, resulting in disruption of endosomal membranes. These cSCKs were electrostatically complexed with siRNA and investigated for their cellular uptake, cytotoxicity, immunogenicity and endosomal escape in RAW 264.7 mouse macrophages and OVCAR-3 cells.

4.2 Materials and Methods

Polymerizations were performed on a double manifold with glassware and syringes that were dried in an oven (100 °C) for at least 1 h, and with syringes that were washed with N_2 (3 ×), prior to use. *tert*-Butyl acrylate (*t*-BA, 99%, Aldrich), styrene (99%, Aldrich), toluene (anhydrous, 99.8%, Aldrich), *N*,*N*,*N*′,*N*″,*N*″-pentamethyldiethylenetriamine (PMDETA, 99% Aldrich), copper (I) bromide (CuBr, 99.99%, Aldrich), ethyl 2-bromopropionate (99%, Aldrich), trifluoroacetic acid (TFA, 95%; Aldrich), 1-(3′-dimethylaminopropyl)-3-ethylcarbodiimide methiodide (EDCI, 98%, Aldrich), hydroxybenzotriazole (HOBT, Aldrich), 2–(1H–benzotriazol–1–yl)-1,1,3,3-tetramethyluronium hexafluorophosphate (HBTU, Aldrich), N,N-diisopropylethylamine (DIPEA, 99.5%, Aldrich). The amphiphilic block copolymer of poly(acrylic acid)$_{160}$-*block*-polystyrene$_{30}$ (PAA_{160}-*b*-PS_{30}) was prepared using atom transfer radical polymerization (ATRP) of protected monomer precursors followed by deprotection, according to previously reported methods [142]. All other reagents were obtained from Sigma-Aldrich and used as received. Spectra/Por membrane tubes were purchased from Spectrum Medical Industries, Inc. (Waltham, MA), and were used for dialysis. Nanopure water (18 MΩ•cm) was acquired by means of a Barnstead Nanopure ultrapure water purification system (Thermo Scientific, Asheville, NC).

^{1}H NMR and ^{13}C NMR spectra were recorded on an Inova 300 or Mercury 300 MHz interfaced to a UNIX computer using VnmrJ software. Samples were prepared as solutions in $CDCl_3$, CD_2Cl_2, or DMF-d_7 and solvent protons were used as internal standard. Gel permeation chromatography (GPC) was conducted on a system equipped

with a Waters Chromatography, Inc. (Milford, MA) model 1515 isocratic pump and a model 2414 differential refractometer with a three-column set of Polymer Laboratories, Inc. (Amherst, MA) Styragel columns (PL_{gel} 5μm Mixed C, 500 Å, and 10^4 Å, 300 x 7.5 mm columns) and a guard column (PL_{gel} 5μm, 50 x 7.5 mm). The system was equilibrated at 40 °C in tetrahydrofuran (THF), which served as the polymer solvent and eluent (flow rate set to 1.00 mL min^{-1}). The differential refractometer was calibrated with Polymer Laboratories, Inc. polystyrene standards (300 to 467,000 Da). Polymer solutions were prepared at a concentration of *ca*. 3 mg/mL with 0.05% (*v*/*v*) toluene as flow rate marker and an injection volume of 200 µL was used. Data were analyzed using Empower Pro software from Waters Chromatography Inc. IR spectra were recorded on an IR Prestige 21 system (Shimadzu Corp., Japan). A small amount of sample was placed to cover the ATR crystal for IR measurements. Data were analyzed using IRsolution software. Thermogravimetric analysis was performed under N_2 atmosphere using a Mettler Toledo model TGA/DSC1 with a heating rate of 10 °C min^{-1}. Measurements were analyzed using Mettler Toledo STARe software v.10.00.

Samples for TEM were prepared by depositing 5 µL of sample to glow discharged carbon coated copper grids. Excess sample was wicked off using filter paper and the grids were allowed to dry in air for 1 min. The grids were then stained with 5 µL of 2% uranyl acetate and excess stain was wicked off using filter paper. Specimens were observed on a JEOL 1200EX transmission electron microscope operating at 100 kV and micrographs were recorded at calibrated magnifications using an SIA-15C CCD camera. The final pixel size was 0.42 nm/pixel. The number-average particle diameters (D_{av}) and

standard deviations were generated from the analysis of particles from at least two different micrographs (n = 100). Dynamic light scattering (DLS) measurements were conducted using Delsa Nano C from Beckman Coulter, Inc. (Fullerton, CA) equipped with a laser diode operating at 658 nm. Size measurements were made in water (n = 1.3329, η = 0.890 cP at 25 ± 1 °C; n = 1.3293, η = 0.547 cP at 50 ± 1 °C; n = 1.3255, η = 0.404 cP at 70 ± 1 °C). Scattered light was detected at 165° angle and analyzed using a log correlator over 70 accumulations for a 0.5 mL of sample in a glass size cell (0.9 mL capacity). The photomultiplier aperture and the attenuator were automatically adjusted to obtain a photon counting rate of *ca*. 10 kcps. The calculations of the particle size distribution and distribution averages were performed using CONTIN particle size distribution analysis routines. Prior to analysis, the samples were filtered through a 0.45 μm Whatman Nylon membrane filter (Whatman Inc., Piscataway, NJ). The samples in the glass size cell were equilibrated at the desired temperature for 5 min before measurements were made. The peak average of histograms from intensity, volume or number distributions out of *ca.* 70 accumulations was reported as the average diameter of the particles. Absorption measurements were made using a UV-2550 system (Shimadzu Corp., Japan) using PMMA cuvettes. Spectra were analyzed with UV-Probe 2.33 software.

Synthesis of poly(acrylamidoethylamine)$_{160}$-Boc-*b*-polystyrene$_{30}$ (PAEA-Boc$_{160}$-*b*-PS$_{30}$) (1)

PAA$_{160}$-*b*-PS$_{30}$ (150 mg, 9.86 μmol) was allowed to dissolve in DMF (7.50 mL) for 30 min prior to the addition of HOBT (324 mg, 2.39 mmol) and HBTU (912 mg, 2.39 mmol) in a DMF solution. The reaction was allowed to stir for 30 min and diisopropylethylamine (180 mg, 1.34 mmol) was added along with *N*-boc-ethylenediamine (389 mg, 2.39 mmol). The reaction was allowed to stir overnight at room temperature for 24 h and dialyzed against 150 mM NaCl solution for 2 d, then against nanopure water for 5 d. After dialysis, the solution was lyophilized to obtain a white powder (380 mg, 95.0% yield). $(M_n)_{NMR}$ = 38.7 kDa. $(M_n)_{GPC}$ = 47.0 kDa. $(M_w)_{GPC}$ = 60.1 kDa. PDI= 1.27. IR: 3630-3120, 2960, 2910, 1650, 1620, 1540, 1450, 1380, 1260, 1180, 1030, 890, 830 cm^{-1}. ^{1}H-NMR (DMSO-d_6) δ: 1.0 - 2.0 (br, polymer backbone, Boc), 2.2 ((br,-CHC***H***$_2$-), 2.8-3.4 (br,-NC***H***$_2$C***H***$_2$N-) 6.2-7.3 (br, Ar***H***) ppm. ^{13}C NMR (DMSO-d_6) δ: 26.7, 31.6–41.0, 56.5, 80.2, 126.4–128.1, 145.5, 175.3 ppm. DSC: (T_g) = 28 °C, 106 °C. T_{onset} = 132 °C, $T_{decomposition}$: [(132-239 °C) 29 % mass loss; (239-475 °C) 47% mass loss; 24% mass remaining].

Synthesis of poly(acrylamidoethylamine-Boc)$_{0.85}$-*g*-poly(acrylamide ethylimidazole)$_{0.15}$-*b*-polystyrene$_{30}$ ((PAEA-Boc$_{0.85}$-*g*-PAEI$_{0.15}$)$_{160}$-*b*-PS$_{30}$) (2)

General procedure for incorporation of *N*-Boc ethylenediamine and histamine onto the polymer backbone: PAA$_{160}$-*b*-PS$_{30}$ (150 mg, 9.9 μmol) was allowed to dissolve in DMF (7.50 mL) for 30 min prior to the addition of HOBT (324 mg, 2.39 mmol) and HBTU (912 mg, 2.39 mmol) in a DMF solution. The reaction was stirred for 30 min and diisopropylethylamine (180 mg, 1.34 mmol) was added along with *N*-boc-ethylenediamine (330 mg, 2.1 mmol) and histamine (40 mg, 0.2 mmol) from a stock solution in DMF. The reaction was allowed to stir overnight at room temperature for 24 h and dialyzed against 150 mM NaCl solution for 2 d, then against nanopure water for 5 d. After dialysis the solution was lyophilized to obtain a white powder (380 mg, 95.0% yield). $(M_n)_{NMR}$ = 37.2 kDa. IR: 3600-3000, 2965, 1700, 1650, 1538, 1498, 1380, 1288, 1160 cm^{-1}. ^{1}H-NMR (DMSO-d_6) δ: 1.0-2.0 (br, polymer backbone, Boc), 2.2 (br,-CHC***H***$_2$-), 2.8-3.4 (br,-NC***H***$_2$C***H***$_2$N- and -NC***H***$_2$C***H***$_2$C-) 6.2–8.5 (br, Ar***H*****,** styrene and histamine) ppm. ^{13}C NMR (DMSO-d_6) δ: 28.2, 31.6-41.0, 77.6, 117.9, 126.4–128.1, 134.7-136.4, 174.5 ppm. T_{onset} = 186 °C, $T_{decomposition}$: [(186-255 °C) 22 % mass loss; (255-449 °C) 60% mass loss; 18% mass remaining].

Synthesis of poly(acrylamidoethylamine)$_{0.50}$-boc-*g*-poly(acrylamidoethylimidazole)$_{0.50}$-*b*-polystyrene$_{30}$ ((PAEA$_{0.50}$-boc-*g*-PAEI$_{0.50}$)$_{160}$-*b*-PS$_{30}$) (3)

Polymer **3** was synthesized according to the general procedure for preparation of graft copolymer as mentioned above. $(M_n)_{NMR}$ = 34.4 kDa. IR: 3600-3000, 2950, 1700, 1640, 1545, 1460, 1375, 1250, 1160 cm^{-1}.. ^{1}H-NMR (DMSO-d_6) δ: 1.0-2.0 (br, polymer backbone, boc), 2.2 ((br,-CHC***H***$_2$-), 2.8-3.4 (br,-NC***H***$_2$C***H***$_2$N- and -NC***H***$_2$C***H***$_2$C-) 6.2–8.5 (br, Ar***H*****,** styrene and histamine) ppm. ^{13}C NMR (DMSO-d_6): δ: 28.2, 31.6–38.0, 77.7, 117, 126.4–128.1, 134.6, 174.3 ppm. T_{onset} = 183 °C, $T_{decomposition}$: [(183-237 °C) 6 % mass loss; (237-263 °C) 20% mass loss; 74% mass remaining].

Synthesis of poly(acrylamidoethylimidazole)$_{160}$-b-polystyrene$_{31}$ (PAEI$_{160}$-b-PS$_{30}$) (4)

PAA$_{160}$-*b*-PS$_{30}$ (150 mg, 9.86 μmol) was allowed to dissolve in DMF (7.50 mL) for 30 min prior to the addition of HOBT (324 mg, 2.39 mmol) and HBTU (912 mg, 2.39 mmol) in a DMF solution. The reaction was stirred for 30 min and diisopropylethylamine (180 mg, 1.34 mmol) was added along with histamine (270 mg, 2.43 mmol) from a stock solution in DMF. The reaction was allowed to stir overnight at room temperature for 24 h and dialyzed against 150 mM NaCl solution for 2 d, then against nanopure water for 5 d. After dialysis the solution was lyophilized to obtain a white powder (380 mg, 95.0% yield). $(M_n)_{NMR}$ = 30.5 kDa. IR: 3650-3000, 2940, 1630, 1540, 1440, 13750, 1250, 1125 cm^{-1}.^{1}H-NMR (DMSO-d_6) δ: 1.0-2.0 (br, polymer backbone), 2.2 ((br,-CHC***H***$_2$-), 2.8-3.4 (br, -NC***H***$_2$C***H***$_2$C-) 6.2-8.5 (br, Ar***H*****,** styrene and histamine) ppm. ^{13}C NMR (DMSO-d_6): δ: 35-42.3, 117.9, 126.4-128.1, 134.7-136.4,

174.5 ppm. T_{onset} = 108 °C, $T_{decomposition}$: [(108 - 283 °C) 11 % mass loss; (283-500 °C) 48% mass loss; 41% mass remaining].

Synthesis of poly(acrylamidoethylamine)-*b*-polystyrene$_{30}$ (PAEA-$_{160}$-*b*-PS$_{30}$) (5)

General procedure for the removal of Boc groups: A white powder of **1** (153 mg, 3.54 μmol) was allowed to dissolve in TFA (7.00 g, 61.4 mmol) and stirred at room temperature overnight. The following day, TFA was removed under a stream of N_2. The polymer was then dissolved in DMSO and dialyzed against 150 mM NaCl solution for 1 d followed by dialysis against nanopure water for 3 d. The solution was then lyophilized to obtain the deprotected polymer. $(M_n)_{NMR}$ = 22.1 kDa. IR: 4000-2360, 1670, 1560, 1470, 1190, 1130, 855, 810, 750 cm^{-1}. ^{1}H-NMR (DMSO-d_6): δ 1.0-2.0 (br, polymer backbone), 2.2 (br,-CHC***H***$_2$-), 2.8-3.4 (br,-NC***H***$_2$C***H***$_2$N-) 6.2-7.3 (br, Ar***H***), 7.2-8.4 (br, N***H***) ppm. ^{13}C-NMR (DMSO-d_6): δ: 26.7, 31.6-38.0, 40.5, 126.4-128.1, 145.5, 175.0 ppm. T_{onset} = 173 °C, $T_{decomposition}$: [(173 - 296 °C) 14 % mass loss; (296-484 °C) 48% mass loss; 38% mass remaining].

Synthesis of poly(acrylamidoethylamine)$_{0.85}$-*g*-poly(acrylamidoethylimidazole)$_{0.15}$-*b*-polystyrene$_{30}$ ((PAEA$_{0.85}$-*g*-PAEI$_{0.15}$)$_{160}$-*b*-PS$_{30}$) (6)

Polymer **6** was prepared according to the general procedure for removal of Boc groups as mentioned above. $(M_n)_{NMR}$ = 23.4 kDa. IR: 3600-3000, 2940, 1640, 1538, 1450, 1225 cm^{-1}.^{1}H-NMR (DMSO-d_6) δ: 1.0-2.0 (br, polymer backbone), 2.2 ((br,-CHC***H***$_2$-), 2.8-3.4 (br,-NC***H***$_2$C***H***$_2$N- and -NC***H***$_2$C***H***$_2$C-) 6.2–9.5 (br, Ar***H*****,** styrene and histamine, N***H***) ppm. ^{13}C NMR (DMSO-d_6): δ: 31.6–41.0, 117.9, 126.4–128.1, 134.7-

136.4, 174.8 ppm. T_{onset} = 193 °C, $T_{decomposition}$: [(193 - 469 °C) 70 % mass loss; 30% mass remaining].

Synthesis of poly(acrylamidoethylamine)$_{0.50}$-*g*-poly(acrylamidoethylimidazole)$_{0.50}$-*b*-polystyrene$_{30}$ ((PAEA$_{0.50}$-*g*-PAEI$_{0.50}$)$_{160}$-*b*-PS$_{30}$) (7)

Polymer **7** was synthesized according to the general procedure for removal of Boc groups as mentioned above. $(M_n)_{NMR}$ = 26.3 kDa. IR: 3600-3000, 2925, 1750, 1625, 1525, 1450, 1375, 1250, 1160 cm^{-1}. ^{1}H-NMR (DMSO-d_6) δ: 1.0-2.0 (br, polymer backbone), 2.2 ((br,-CHC***H***$_2$-), 2.8-3.4 (br,-NC***H***$_2$C***H***$_2$N- and -NC***H***$_2$C***H***$_2$C-) 6.2-9.5 (br, Ar***H*****,** styrene and histamine, N***H***) ppm. ^{13}C NMR (DMSO-d_6): δ: 31.6–38.0, 117, 126.4–128.1, 134.6, 174.8 ppm. T_{onset} = 188 °C, $T_{decomposition}$: [(188-294 °C) 27 % mass loss; (294-497 °C) 62% mass loss; 11% mass remaining].

General procedure for micellization (8-11)

Each polymer (5.0 mg) was directly dissolved in nanopure water (5.0 mL) and sonicated using a water bath sonicator for 10 min to obtain clear micellar solution at a concentration of 1 mg/mL. The solution was then allowed to stir overnight at room temperature. DLS and zeta-potential measurements are listed in the supporting information (S4-S7).

Preparation of cSCKs of PAEA-$_{160}$-*b*-PS$_{30}$ (12)

General procedure for preparation of cSCKs: To **8** (5.00 mL), sodium carbonate (20 μL of 1.0 M solution) was added to adjust the pH to *ca*. 8.0. A diacid crosslinker, 4,15-dioxo-8,11-dioxa-5,14-diazaoctadecane-1,18-dioic acid, (2.0 mg) was activated with HOBT (1.7 mg, 2.2 equiv. *per* COOH) and HBTU (4.8 mg, 2.2 equiv. per COOH)

in 300 μL of DMF for 30 min. The activated crosslinker solution was slowly added to the micellar solution to crosslink *ca.* 5 % of the amines. The reaction mixture was allowed to stir overnight, and then transferred to a dialysis tube (MWCO *ca.* 6000-8000 Da) and dialyzed against nanopure water for 3 d to obtain clear cSCK solution at 0.88 mg/mL. $(D_h)_{number}$ (DLS) = 21 ± 6 nm; $(D_h)_{volume}$ (DLS) = 30 ± 18 nm; $(D_h)_{intensity}$ (DLS) = 106 ± 81 nm. Zeta potential = 26 ± 2 mV (in nanopure water pH 5.5).

Preparation of cSCKs of $(PAEA_{0.85}$-*g*-$PAEI_{0.15})_{160}$-*b*-PS_{30} (13)

cSCKs of **13** were prepared from the micelles following the general procedure for crosslinking as listed above. $(D_h)_{number}$ (DLS) = 14 ± 4 ; $(D_h)_{volume}$ (DLS) = 21 ± 4 nm; $(D_h)_{intensity}$ (DLS) = 147 ± 61 nm nm. Zeta potential = 35 ± 1 mV (pH 5.5).

Preparation of cSCKs of $(PAEA_{0.50}$-*g*-$PAEI_{0.50})_{160}$-*b*-PS_{30} (14)

cSCKs of **14** were prepared from the micelles following the general procedure for crosslinking as listed above. $(D_h)_{number}$ (DLS) = 19 ± 5 nm; $(D_h)_{volume}$ (DLS) = 29 ± 19 nm; $(D_h)_{intensity}$ (DLS) = 168 ± 163 nm. Zeta potential = 50 ± 2 mV (pH 5.5).

Potentiometric titration experiments

The buffering capacities of the nanoparticles were determined by acid-base titration assays over pH range of 12.0-to-2.0, as reported previously [132]. Briefly, cSCKs (9.0 μmoles of amine) were dissolved in 15 mL NaOH (0.01 N with 150 mM NaCl) and then titrated with HCl (0.01 N with 150 mM NaCl). The buffering capacity was measured as the volume of HCl needed to change pH from 5.1 to 7.4.

Cytotoxicity assays

RAW 264.7 (2 x 10^4 cells/well) mouse macrophages were plated in 96-well plate in Dulbecco's Modified Eagle Medium (DMEM) (10% fetal bovine serum and 1% penicillin/streptomycin). Cells were incubated at 37 °C in a humidified atmosphere containing 5% CO_2 for 24 h to adhere. Then, the medium was replaced with a fresh medium 1-h prior to the addition of 20 μL of the cSCKs and Lipofectamine to 100 μL of the medium (final concentrations ranged from 0-to-100 μg/mL). The cells were incubated with the formulations for 24 h and washed once with phosphate-buffered saline (PBS) and 100 μL of the complete media was added to the cells. MTS combined reagent (20 μL) was added to each well (Cell Titer 96® Aqueous Non-Radioactive Cell Proliferation Assay, Promega Co., Madison, WI). The cells were incubated with the reagent for 2 h at 37 °C in a humidified atmosphere containing 5% CO_2 protected from light. Absorbance was measured at 490 nm using SpectraMax M5 (Molecular Devices Co., Sunnyvale, CA). The cell viability was calculated based on the relative absorbance to the control-untreated cells. The calculation of the IC_{50} values and the statistical analysis were performed using GraphPad Prism four-parameter fit, considering the 0% and 100% cell viabilities are for the control medium (no cells) and cells with no treatment, respectively.

Multi-plex assay

The RAW 264.7 cells were treated with medium (control), unmodified cSCKs and 15%-His-cSCKs (5 μg/mL) for 24 h. The supernatants were then collected and centrifuged for 10 min at 13,000 rpm. Serial dilutions of standards of cytokines were

also prepared in the same diluent utilized for the samples (*i.e.* cell-culture medium). Control, standards and nanoparticle-treated samples (50 μL) were incubated with antibody-conjugated magnetic beads for 30 min in the dark. After washing, the detection antibody was added to the wells and incubated in the dark for 30 min under continuous shaking (300 rpm). After washing, streptavidin-phycoerythrin was added to every well and incubated while protected from light for 10 min under the same shaking conditions. Finally, after several washings and re-suspension in the assay buffer and shaking, the expression of the mouse cytokines, interleukin (IL)-1α, IL-1β, IL-2, IL-3, IL-4, IL-5, IL-6, IL-9, IL-10, IL-12 (P40), IL-12 (P70), IL-13, IL-17, Eotaxin, Granulocyte-colony-stimulating factor (G-CSF), granulocyte macrophage-colony-stimulating factor (GM-CSF), Interferon-γ (IFN-γ), keratinocyte-derived chemokine (KC), monocyte chemotactic protein (MCP)-1, macrophage inflammatory protein (MIP)-1α, MIP-1β, regulated upon activation normal T-cell expressed and presumably secreted (RANTES) and tumor necrosis factor-α (TNF-α) was measured immediately using Bio-plex 200 system with HTF and Pro II Wash station (Bio-Rad Laboratories, Inc., Hercules, CA) and the data were analyzed using the Bio-plex Data Pro software.

Gel shift assay

Agarose gels (1%) were prepared in Tris-acetate-EDTA buffer (Bio-Rad Laboratories, Inc., Hercules, CA). The siRNA (5'-Cy3-(sense strand)-GGCCACAUCGGAUUUCACU, M_w = 13814 g/mol, Dharmacon, Chicago, IL), either free or complexed to the various nanoparticle formulations at nitrogen (total concentrations of the primary amines and histamines)-to-phosphate (N/P) ratios ranging

from 0.25-to-6 (1.3 μg siRNA/25 μL/well), were mixed with glycerol (20% *v*/*v*) prior to the electrophoresis. Gel electrophoresis was carried out using a horizontal apparatus at 100 V for 30 min and fluorescence imaging of the separated siRNA bands was performed using a ChemiDoc XRS (Bio-Rad Laboratories, Inc.).

Death-siRNA transfection assays

RAW 264.7 mouse macrophages (2 x 10^4 cells/well) and human ovarian adenocarcinoma cells (OVCAR-3) (5 x 10^3 cells/well) were plated in a 96-well plate in DMEM and RPMI-1640 medium (10% and 20% fetal bovine serum, for the RAW 264.7 and OVCAR-3, respectively and 1% penicillin/streptomycin). Cells were incubated at 37 °C in a humidified atmosphere containing 5% CO_2 for 24 h to adhere. Then, the medium was replaced with a fresh medium 1-h prior to the addition of the siRNA-loaded cSCKs (100 nM final concentrations of AllStars death- or negative control-siRNA (Qiagen, Valencia, CA)) at N/P ratio of 5, unless otherwise indicated. The cells were incubated with the various formulations for 24 h and washed extensively with PBS and the cell viability was measured 24 h later by measuring the relative cell viability of the cells treated with death-siRNA to the negative control-loaded cSCKs. The cell viabilities were measured as described in the cytotoxicity section. The Lipofectamine-siRNA complexes were prepared according to the manufacturer instructions and the transfection efficiency was measured following the same procedures of the siRNA-cSCKs complexes. The effect of endosomal acidification on transfection efficiency was studied by incubating cells with 200 nM bafilomycin A1 (Sigma-Aldrich, St. Louis, MO) 30-min prior to the transfection and by adding the same concentration of

bafilomycin to the transfection medium. The toxicity of siRNA complexes could be also measured by comparing the cell viability of the cells treated with the negative control-siRNA complexes to that of the control-untreated cells.

Laser scanning confocal microscopy (LSCM)

RAW 264.7 mouse macrophages (1 x 10^5 cells/well) were plated in glass-bottom six-well plate (MatTek Co., Ashland, MA) in DMEM medium. Cells were incubated at 37 °C in a humidified atmosphere containing 5% CO_2 for 24 h to adhere. Then, the medium was replaced with a fresh media 1-h prior to the addition of siRNA-loaded cSCKs or Lipofectamine (100 nM final concentration of the 5'-Cy3-siRNA). The cells were incubated with the formulations for 3 h and washed extensively with PBS. Then, DRAQ-5 (Biostatus Ltd., Shepshed, Leicestershire, UK) was utilized to stain the nucleus (30 min incubation, followed by extensive washing with PBS). Cells were then fixed with 1% formaldehyde for 20 min, washed once with PBS. The cells were then stored in 1 mL PBS in the refrigerator and analyzed by laser scanning confocal microscopy (LSM 510, Zeiss, Jena, Germany). The images were collected under the same conditions (laser power, detector gain, *etc.*) for consistency, and $\lambda_{excitation}$ of 543 and 633 nm were utilized for the Cy3 and DRAQ-5, respectively.

Statistical analysis

Values are presented as mean ± SD of at least three independent experiments. Significance of the differences between two groups was evaluated by Student's t test (unpaired) or between more than two groups by one-way ANOVA followed by Tukey's

multiple comparison tests. Differences between different groups were considered significant for *p* values less than 0.05.

4.3 Results and Discussion

Synthesis of polymers

A library of cationic micelles (**8**-**11**) and shell crosslinked nanoparticles (cSCKs, **12**-**14**) was prepared from amphiphilic block copolymers (**4**-**7**) in a stepwise process, each of which was self-assembled into micelles followed by chemical crosslinking as illustrated in Figures 4.1 and 4.2. Each of the amino- and/or histamine-functionalized amphiphilic block copolymers was derived from the same block copolymer precursor PAA_{160}-*b*-PS_{30}, which was prepared by a two-step ATRP process of *t*BA and styrene, followed by deprotection (S1-S3). Chemical modification reactions onto the PAA backbone and selective acidolysis then introduced the amino and histamine side chain groups. The acrylic acid repeat units were converted to acrylamides, each carrying a protected amino group (0%-His), imidazole (100%-His) or mixture of both at various ratios (85:15 (15%-His) and 50:50 (50%-His)), by using an excess of *N*-Boc ethylene diamine and/or histamine in the presence of HOBT, HBTU and DIPEA in DMF, yielding polymers **1, 2, 3** and **4**. In the final step, the Boc protecting groups were removed by direct dissolution of **1, 2** and **3** in TFA overnight, followed by removal of the TFA under a N_2 stream, to obtain the block copolymers **5, 6** and **7**.

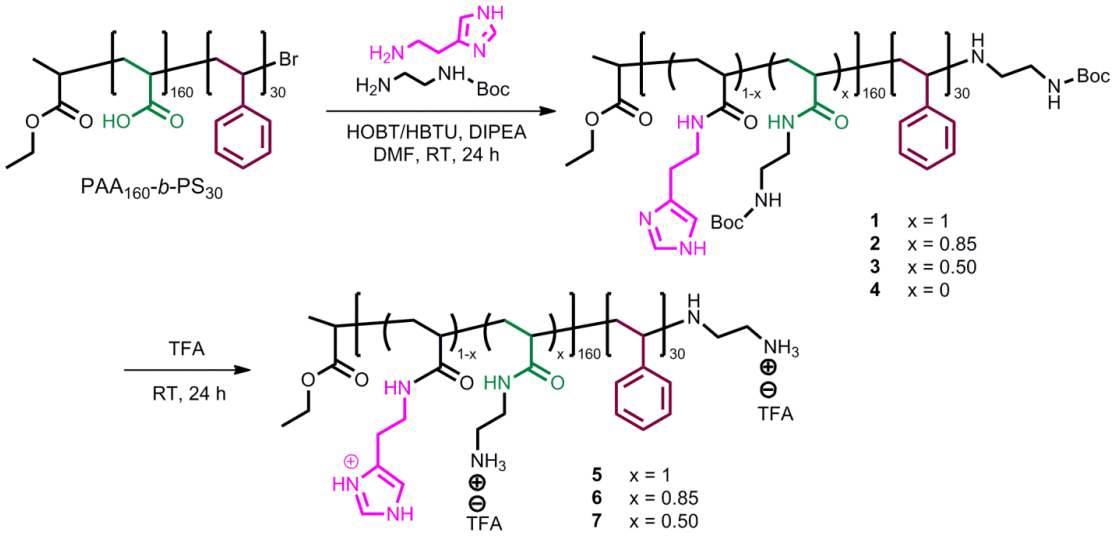

Figure 4.1. Schematic representation of incorporation of various amounts of primary amines and histamines onto a segment of an amphiphilic block copolymer backbone by a sequential two-step process of amidation followed by deprotection.

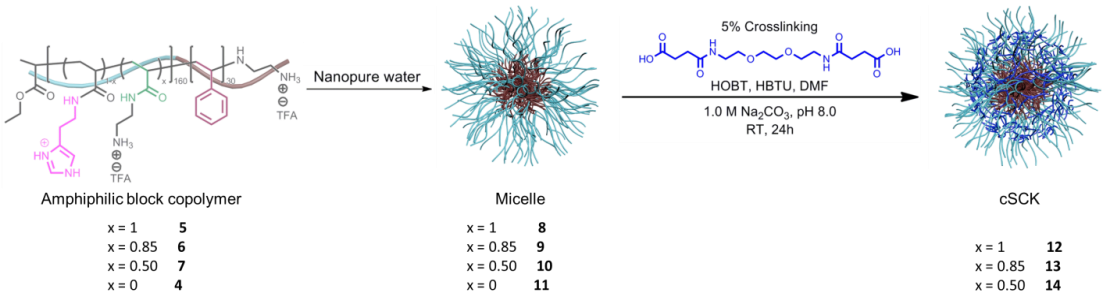

Figure 4.2. Self assembly of polymers with various amounts of primary amines and histamines (**4-7**) into micelles (**8-11**) followed by crosslinking selectively in the hydrophilic shell regions of (**8-10**) to obtain cSCKs (**12-14**).

Preparation and characterization of cSCKs

cSCKs were prepared by the solution-state assembly of amphiphilic block copolymers in water followed by crosslinking selectively throughout the hydrophilic shell layer (Fig. 4.2). Self assembly was induced by the direct dissolution of the amphiphilic block copolymer (**5**, **6**, **7**, and **4**) at 1 mg mL^{-1} in molecular biology grade water to yield micelles **8, 9, 10** and **11**, respectively (0%-His-, 15%-His-, 50%-His- and 100%-His-micelles, respectively)(S4-S7). The series of cSCKs **12**, **13** and **14** (0%-His-, 15%-His-, and 50%-His-cSCKs, respectively) was obtained by crosslinking approximately 5% of the amino groups along the hydrophilic segments of **8**-**10** by amidation with activated carboxylic acids (activated using 2.2 equiv. of both HOBT and HBTU relative to the COOH groups in the crosslinker in DMF) of the diacid crosslinker (4,15-dioxo-8,11-dioxa-5,14-diazaoctadecane-1,18-dioic acid) at pH *ca*. 8 (adjusted using 1.0 M Na_2CO_3 (aq.)). The crosslinking reaction was allowed to proceed overnight, followed by extensive dialysis (MWCO 6-8 kDa) to remove the unreacted small molecule starting materials and reaction by-products. The 100%-His-micelles did not have any crosslinking sites due to the complete incorporation of histamine groups onto the polymer backbone and, hence, were not converted to the corresponding cSCKs; further studies were continued with the micellar form.

To understand the physicochemical properties of the cationic micelles and cSCKs, their sizes and zeta-potential values were determined. Dynamic light scattering (DLS) analysis showed that the hydrodynamic diameters of the micelles and cSCKs decreased slightly with increasing amounts of histamines incorporated. The number-

averaged diameters of the nanoparticles were less than 20 nm in all cases (Fig. 4.3). It was difficult to obtain high quality TEM images for all of the samples, but for those that gave adequate images, the core diameters were measured to be *ca*. 10 nm, consistent with the hydrodynamic DLS-measured overall diameter values (Fig. S2). Zeta potential values of the micelles and cSCKs, each in nanopure water at pH 5.5 were determined initially, and found to be positive for **8-10** and **12-14**, but negative for **11** having only histamines and no primary amino groups. Given the pK_a of histamine groups, typically 6-6.5, the observation of a negative zeta potential at pH 5.5 was hypothesized to be due to the use of nanopure water without high salt content and/or the presence of only histamine groups and, therefore, was then followed by a full study of each of the micellar solutions **8-11** at pH 5.0, 6.0 and 7.4 (PBS buffer, 10 mM NaCl). As the micelles **11** (100%-His) did not have any primary amines in the polymer backbone for crosslinking reaction, this study of zeta potential measurements at different pHs was performed only for the micellar solutions. As expected, at pH 7.4, all of the samples were found to be positively charged except the 100%-His-micelles, which were negatively charged (Figure 4.4 A). Generally, zeta-potential values were found to increase with the decrease in pH, which indicates higher protonation of polymers at acidic pH, corresponding to the endosomal environment. Additionally, nanoparticles with the highest amount of histamine content showed the least zeta potential values at all pHs, and were confirmed to be positively-charged at and below pH 6.0. At pH 7.4, the 50% His-micelles were insoluble and 100% His-micelles exhibited low zeta-potential

values, whereas the 15%-His-micelles demonstrated similar behavior to the unmodified cSCKs.

To determine the buffering capacities of each type of cationic nanostructures, potentiometric titration studies were conducted over a pH range of 12 to 2, with focus over the range of 7.4 to 5.1 of relevance to extracellular to endosomal/lysosomal transitions (Figure 4.4 B). The nanoparticles were dissolved in $NaOH_{(aq)}$ and titrated by gradual addition of HCl. The particles were found to require increasing amounts of HCl to change the pH from 7.4 to 5.1 (17 μmol to 41 μmol) with increasing histamine content (**12** to **14** to **11**, respectively). cSCK nanoparticles with 0% histamines (**12**) required the least amount (1.7 mL) of HCl to change pH from 7.4 to 5.1, while micellar nanoparticles with the highest histamine content (100% His, **11**) needed the highest amount (4.1 mL) of HCl to induce the same change. In general, increasing histamine content directly correlated with the amount of acid needed, demonstrating the increased buffering capacities of nanoparticles with greater histamine content. In comparison to PEI, which contains combinations of primary, secondary and tertiary amines, the primary amino-containing cSCKs, **12**, and the cSCKs with few histamines, **13**, gave lower buffering capacity, whereas each of the cSCK and micelles with 50% and 100% histamines gave higher buffering capacities. Nanoparticles with higher buffering capacity are expected to buffer the endosomes to a greater extent and, hence, result in higher endosomal disruption.[128,133,134]

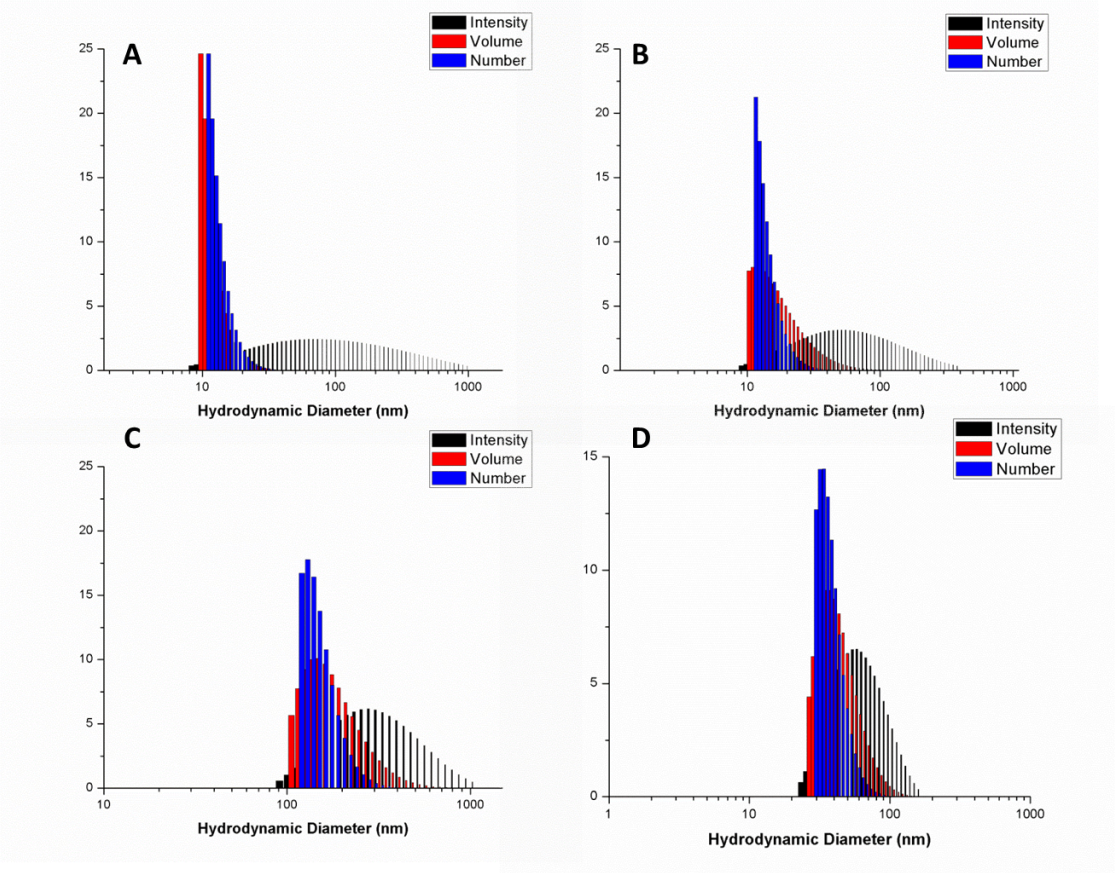

Figure 4.3. DLS histograms from measurements of nanoparticles with various amounts of primary amines and histamines: (**A**) 0%-His-cSCK (**12**), (**B**) 15%-His-cSCK (**13**), (**C**) 50%-His-cSCK (**14**) and (**D**) 100%-His-micelles (**11**).

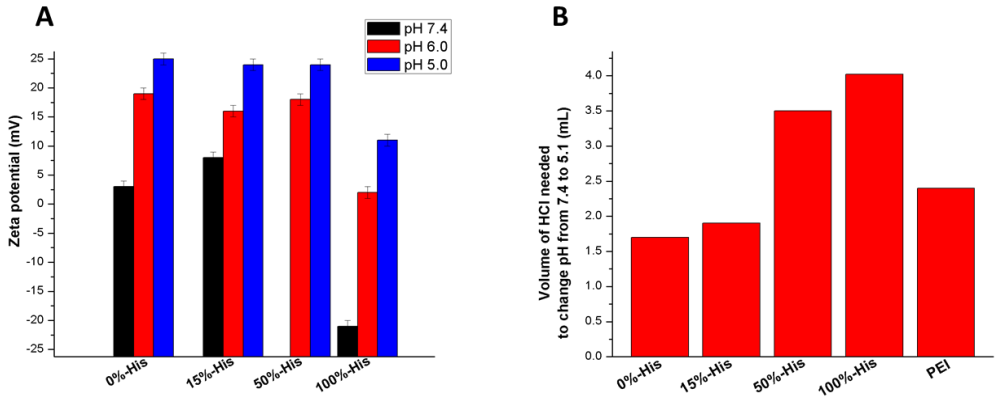

Figure 4.4 (**A**) Zeta-potential measurements of micelles **8**-**11** with increasing histamine content, each at pH 5.0, 6.0 and 7.4. **(B)** Relative buffering capacity of cSCK nanoparticles **12**-**14** and micelles **11** containing various amounts of histamine obtained from potentiometric titration experiments, and comparison with PEI. Each bar represents the amount of HCl (in mL) needed to change the pH of the nanoparticle solutions from pH 7.4 to 5.1.

Toxicity and immunogenicity of cSCKs

The cytotoxicity of nanoparticles containing various amounts of histamine and primary amine groups was evaluated in RAW 264.7 mouse macrophages, and compared to Lipofectamine (Table 4.1). Increasing the histamine contents significantly increased the IC_{50} values of the nanoparticles from 16.3 μg/mL to 20.7 μg/mL ($p < 0.05$), for the cSCKs with 0% and 15% histamines, **12** and **13**, respectively. The IC_{50} values could not be determined for nanoparticles that contained 50% and 100% histamine at the tested concentrations (0-to-100 μg/mL), due to the high cell viability measured over this concentration range. The IC_{50} value of the tested Lipofectamine was significantly higher than the cSCKs of 100% and 85% primary amines (**12** and **13**, respectively), but the cell viabilities were much lower than the cSCK (**14**) and micelles (**11**) with lower amine contents. These results reveal that increasing the histamine content reduced the toxicity

of the nanoparticles, which is in accordance with previously published data from our group showing that reducing the amount of primary amines *per* polymer (by incorporating tertiary amines or carboxylic acids into the polymer structure), reduces the toxicity of the nanoparticles.[7,83] With the higher cytotoxicities observed for the cSCKs having low histamine content, and because the nanoparticles with histamine content greater than 15% demonstrated low cellular uptake and transfection efficiency (*vide infra*), we decided to compare the immunotoxicities of the unmodified- and 15%-His-modified cSCKs.

Table 4.1 The cytotoxicity of Lipofectamine, cSCKs and micelles of various compositions (*i.e.* primary amine and histamine contents).

Formulation	IC_{50} (μg/mL) ± SD	Significance ($p < 0.05$)
Lipofectamine	31.4 ± 5.9	Lipofectamine has significantly higher IC_{50} than 0%-His- and 15%-His-cSCKs
0%-His-cSCKs	16.3 ± 3.2	
15%-His-cSCKs	20.7 ± 0.1	15%-His-cSCKs have significantly higher IC_{50} than 0%-His-cSCKs
50%-His-cSCKs	----------	
100%-His-micelles	----------	

The release of cytokines from cells treated with nanomaterials is usually utilized as an indication of possible immunotoxicity of nanoparticles and their immunomodulatory effects [143-146]. The structure and composition of nanoparticles can greatly impact their ability to interact with the various components of the immune system, where unintentional immunomodulation can be serious and cause severe adverse reactions and complications [147-149]. Cationic liposomes, for instance, are known to induce the secretion of proinflammatory cytokines (*e.g.* TNF-α, IFN-γ and IL-12) [148]. Inorganic anionic zinc oxide nanoparticles also stimulated the release of IL-6 and TNF-α cytokines from dendritic cells treated with the nanoparticles [149].

The immunotoxicities of the 0%- and 15%-His-cSCKs were studied by measuring the levels of 23 cytokines upon treatment of RAW 264.7 mouse macrophages with the nanoparticles for 24 h (Figure 4.5). Generally, lower secretion of the cytokines was observed from cells treated with the histamine-modified cSCKs, **13**, as compared to the cSCKs with 100% primary amines, **12**. A similar trend was observed for most of the tested cytokines, which indicate the potential immunotoxicity of the 0%-His-cSCKs as compared to the histamine modified ones. The differences between the levels of the secreted cytokines were significant for 12 cytokines, IL-3, IL-6, IL-9, IL-10, IL-12(p40), IL-13, Eotaxin, RANTES, MCP-1, MIP-1β, KC and TNF-α (Figure 4.5). The incorporation of histamine into the polymer precursor significantly reduced the toxicity of the nanoparticles and their ability to stimulate the cells and induce the secretions of cytokines, which might be due to the lower charge density, cell-binding affinity and cellular uptake, as will be discussed in the next sections.

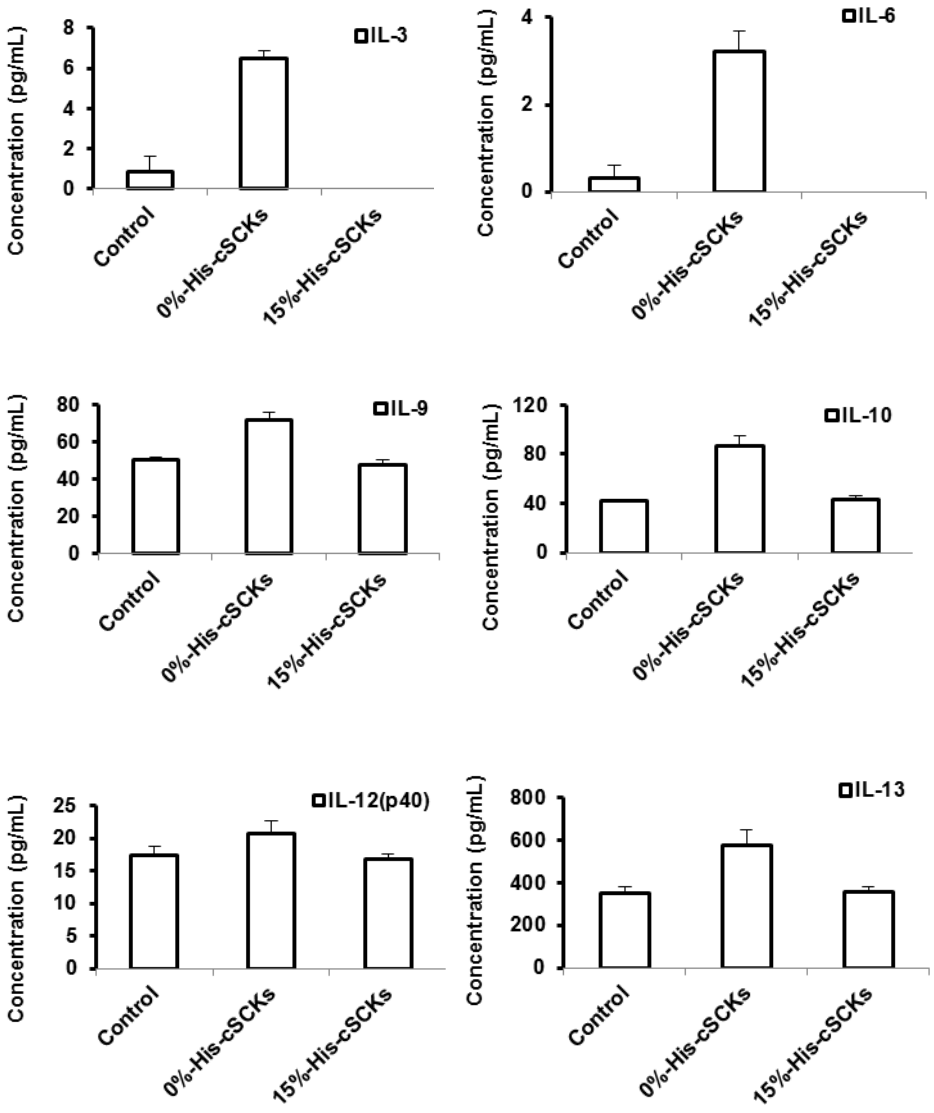

Figure 4.5. The expression of IL-3, IL-6, IL-9, IL-10, IL-12(p40), IL-13, Eotaxin, RANTES, MCP-1, MIP-1β, KC and TNF-α were particularly enhanced upon the treatment of Raw 264.7 mouse macrophages with the unmodified-cSCKs (0%-His-cSCKs) for 24 h, as compared to the 15%-His-cSCKs and the control-untreated cells.

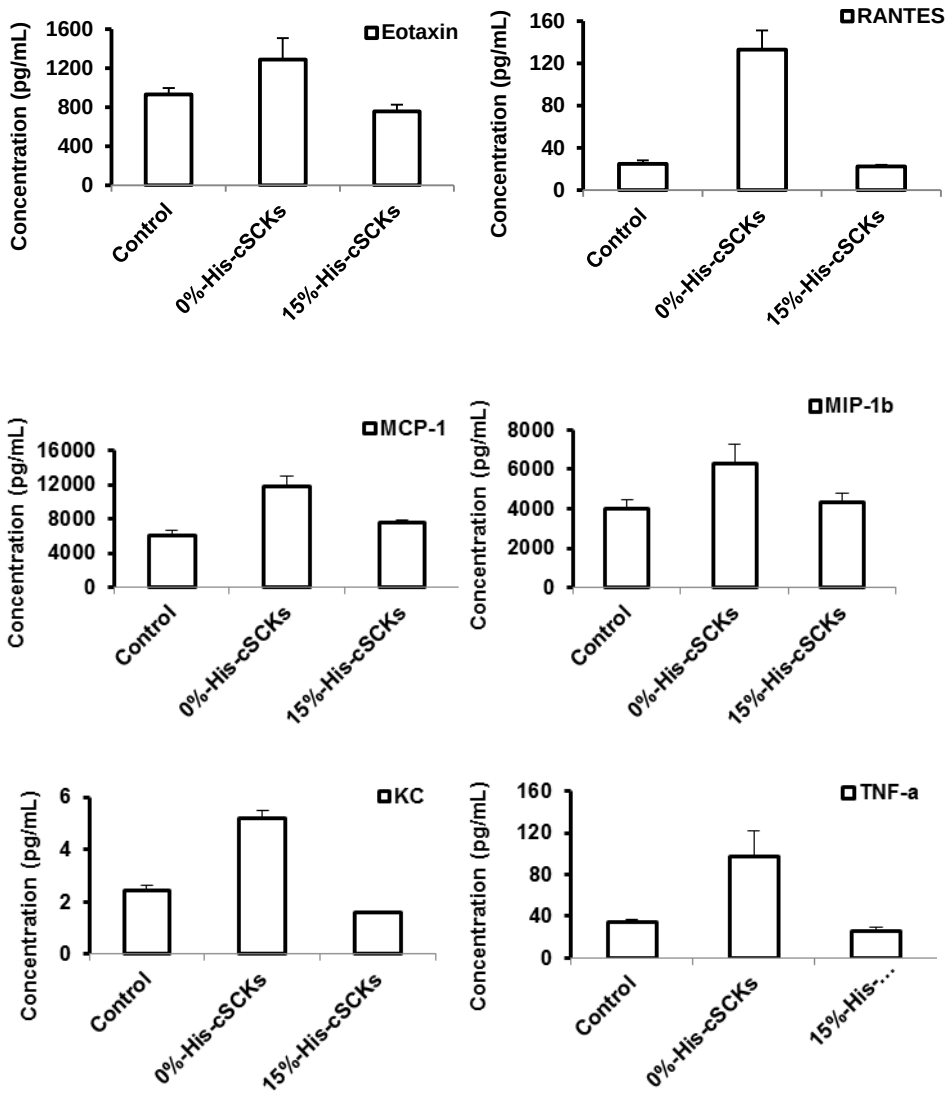

Figure 4.5 continued

Nanocomplexes of siRNA-cSCKs for efficient gene-silencing

The binding affinity of Cy3-labeled siRNA to the micelle and cSCK nanoparticles of various compositions was studied using agarose gel electrophoresis (Fig. 4.6). Only the cSCKs with 0%- and 15%-histamine contents were able to efficiently bind siRNA at N/P ratios of 2 and 4, respectively. The incorporation of histamine reduced the binding affinity of cSCKs and micelles to the siRNA. In a previous study, the reduction of primary amine contents of cSCKs was also correlated with a reduced binding affinity to nucleic acids (plasmid DNA).[83] Increasing the histamine contents reduces the amount of protonated primary amines available to electrostatically interact with the negatively-charged siRNA, and hence decreases the siRNA-binding affinity. The cellular uptake and transfection experiments were then performed at N/P ratio of 5 to ensure the complete siRNA-binding for both kinds of nanoparticles, **12** and **13**.

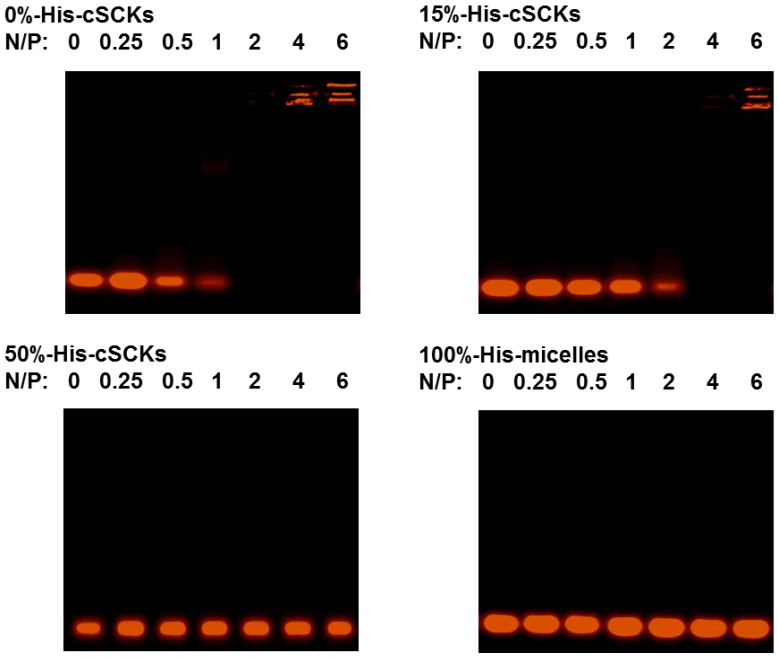

Figure 4.6 Gel-shift assay of Cy3-labeled siRNA, either naked (N/P = 0) or complexed to micelles or cSCKs of various composition at increasing N/P ratios from 0.25-to-6. Complete binding is observed at N/P ratios of 2 and 4, for 0% and 15% histamine-modified cSCKs, whereas no binding was observed for cSCKs and micelles that contain 50% and 100% histamine-modified shells, respectively.

The cellular uptake and transfection efficiency of cSCKs and Lipofectamine were studied using laser scanning confocal microscopy and siRNA-cell death assay using RAW 264.7 mouse macrophages and OVCAR-3 cancer cells (Figure 4.7 and 4.8). The siRNA-cell death assay was performed by measuring the relative viabilities of cells treated with nanoparticles-loaded with siRNA that induces cell death *versus* the cells-treated with the same nanoparticles but loaded with a negative control siRNA. No cellular uptake or transfection efficiency was observed in cells treated with the 50%-His-cSCKs and 100%-His-micelles. Higher cellular uptake was observed for the cells treated with the 0%-His-cSCKs than the cells treated with the 15%-His-cSCKs and

Lipofectamine as indicated by the confocal microscopy images (Fig. 4.7), probably due to the higher binding affinity of the nanoparticles that are fully functionalized with primary amines to the cell membrane as compared to the other nanoparticles. However, the transfection efficiency of the 15%-histamine-modified cSCKs and the Lipofectamine was higher than the 0%-His-cSCKs. The incorporation of histamine increased the buffering capacities of the nanoparticles, as shown by the potentiometric titration experiments (Fig. 4.4B), which is expected to have facilitated greater endosomal release of siRNA/nanoparticles into the cytoplasm and thus resulted in higher intracellular bioavailability. The cellular uptake is not always correlated with transfection efficiency as it does not measure the ability of nanoparticles to reach their target sites into the cytoplasm/nucleus and additionally, does not differentiate between drug molecules that are being delivered into the cytoplasm or entrapped within endosomes/lysosomes. Elsabahy *et al.* [135] have observed higher transfection efficacy and Bcl-2 protein knockdown from antibody fragment-targeted poly(amidoamine)-based polyion complex micelles loaded with Bcl-2 siRNA than the corresponding non-targeted poly(amidoamine)/siRNA complexes, although the latter showed higher cellular uptake as measured by flow cytometric analysis and shown by confocal microscopy images.

The effect of N/P ratio on the transfection efficiency was also measured using the same siRNA-cell death assay and showed a slight increase in transfection efficiency of the cSCKs by increasing the N/P ratio from 5 to 10 (Fig. 4.8B). However, no observable transfection was observed for the 50%-His-cSCKs at both N/P ratios. No toxicities were observed for the siRNA/cSCKs complexes at both N/P ratios (Fig. 4.8C). The role of

endosomal acidification on the transfection of cSCKs was investigated by measuring the effect of bafilomycin A1 (an inhibitor of endosomal acidification) (Fig. 4.9) [134]. The pre-incubation of cells with bafilomycin had a slight effect on the transfection of Lipofectamine and 0%-His-cSCKs, but completely inhibited the transfection of the 15%-His-cSCKs. The non-acidified endosomes partially prevent the protonation of the histamine functionalities, which reduced their ability to destabilize the endosomes and to release a considerable amount of siRNA into the cytoplasm [135,150,151].

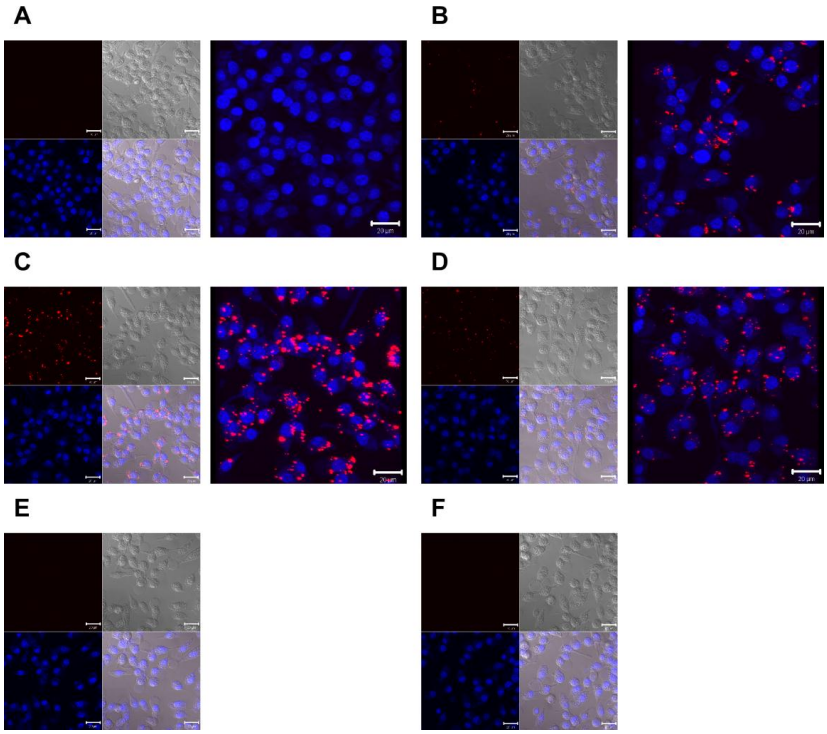

Figure 4.7. Laser scanning confocal microscopy analysis of the control-untreated RAW 264.7 mouse macrophages **(A),** cells treated with Cy3-siRNA (100 nM) complexed with Lipofectamine **(B),** 0%-His- **(C)**, 15%-His- **(D)**, 50%-His- **(E)** and 100%-His-nanoparticles **(F)** at N/P ratio of 5. Two (left panel) and three (right panel)-dimensional images were collected for the cells (**A-D**), while only two-dimensional images were collected for **E** and **F**. On the two-dimensional images, the nucleus were stained with DRAQ5 nuclear stain (blue panel), whereas Cy3-labeled siRNA appears in red. The transmitted light-images and merged images are also indicated.

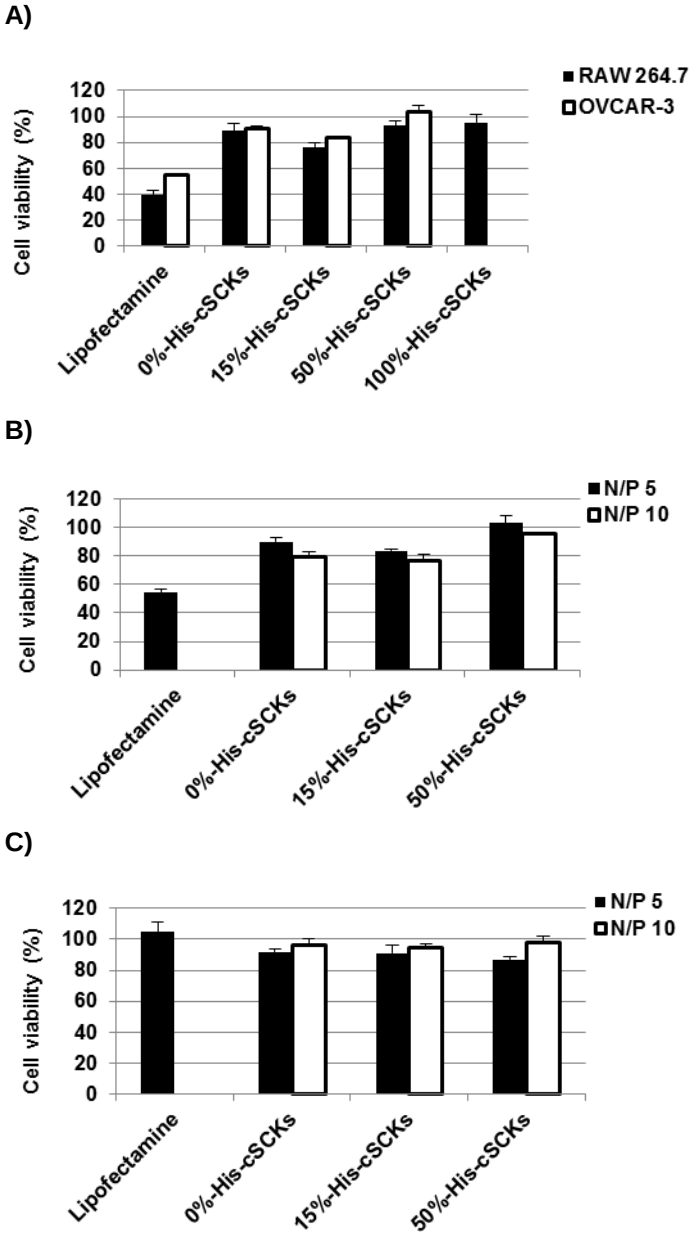

Figure 4.8. Transfection efficiency of death-siRNA complexed with Lipofectamine or cSCKs of varying primary amine and histamine ratios into OVCAR-3 cells and RAW 264.7 mouse macrophages at N/P ratios of 5 and 10. (**A)** The transfection of the death-siRNA/cSCK complexes in the two different cell lines at a N/P ratio of 5. (**B)** The effect of N/P ratio on the transfection efficiency in the OVCAR-3 cells, determined by comparison of death-siRNA/cSCKs *vs*. negative control-siRNA/cSCKs**. (C)** The effect of N/P ratio on the cytotoxicity of cSCKs in OVCAR-3 cells, determine by comparison of negative control-siRNA/cSCKs *vs*. control, untreated cell assays.

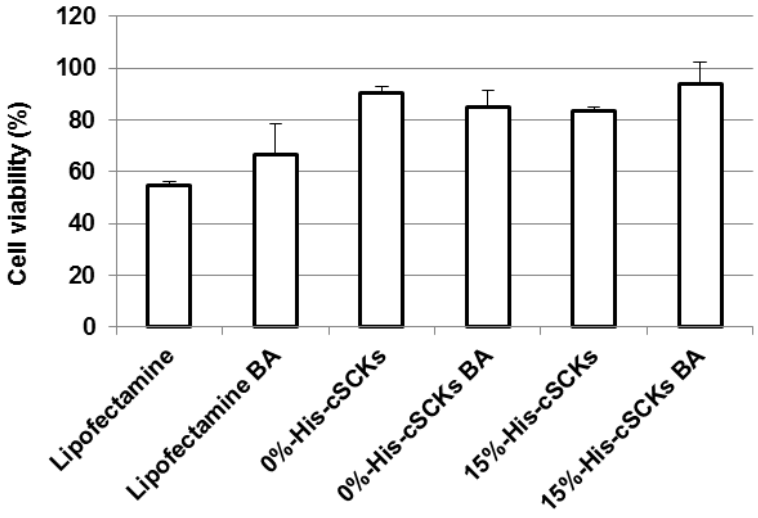

Figure 4.9. Transfection efficiency of death-siRNA (100 nM) complexed with Lipofectamine or cSCKs of varying compositions into OVCAR-3 cells, with and without pre-treatment with bafilomycin A1 (BA, 200 nM for 30 min before the transfection and continued during the transfection).

4.4 Conclusions

In this study, a library of block copolymer micelles and cSCKs has been created with different percentages of primary amines and histamines incorporated into the nanoparticle shells. The 50% and 100%-histamine-modified nanoparticles induced lower cytotoxicity as compared to Lipofectamine, whereas the cSCKs with 85% and 100% primary amines (15% and 0% histamines) were more toxic than Lipofectamine. Treatment of mouse macrophages with the unmodified cSCKs resulted in the secretion of large amounts of several cytokines, as compared to the control-untreated cells and the cells-treated with histamine-modified nanoparticles. Increasing the amount of histamines increased the buffering capacities of the nanoparticles at the expense of the siRNA-binding affinity, due to the reduced contents of primary amines. Intermediate

primary amine and histamine levels resulted in higher intracellular concentrations of the complexed siRNA and higher gene silencing activity. Histamine incorporation of 15% appeared to be a threshold for the series of samples tested, with cSCKs having higher histamine contents completely lost the ability to bind siRNA and to interact with cell membrane and induce gene silencing. These nanoparticles are among the initial steps involved in the development of cSCKs for effective delivery of nucleic acids for clinical applications. However, a further probing of histamine contents between 15% and 50% may better identify the optimum balance of siRNA binding, cellular uptake and buffering capacity. Expansion of the chemical compositional heterogeneity and synthesis of degradable analogs of these cSCKs is currently underway for extended *in vitro* and *in vivo* studies toward development of novel polymeric materials for nucleic acids delivery.

4.5 Acknowledgements

We gratefully acknowledge financial support from the National Heart Lung and Blood Institute of the National Institutes of Health as a Program of Excellence in Nanotechnology (HHSN268201000046C) and the National Institute of Diabetes and Digestive and Kidney Diseases of the National Institutes of Health (R01-DK082546). The authors would like to thank Adriana Pavia for creating the Autodesk 3ds Max images. The Welch Foundation is gratefully acknowledged for support through the W. T. Doherty-Welch Chair in Chemistry, Grant No. A-0001.

4.6 Supporting Information

Synthesis of poly(tert-butyl acrylate)$_{160}$ (P*t*BA$_{160}$) (S1)

Bulk polymerization of *tert*-butyl acrylate by atom transfer radical polymerization: To a flame-dried 100 mL Schlenk flask, *tert*-butyl acrylate (56.6 g, 44.2 mmol) was added along with copper (I) bromide (0.41 g, 2.9 mmol). The reaction mixture was sealed and three freeze pump thaw cycles were performed with N_2 backfilling. N,N,N',N',N''-pentamethyldiethylenetriamine (0.49 g, 2.9 mmol) and 2-ethylbromo propionate (0.40 g, 2.2 mmol) were added to the reaction mixture *via* a syringe and the reaction mixture was allowed to undergo two more freeze pump cycles. The reaction mixture was brought to room temperature and stirred to ensure homogeneity. Following this, the Schlenk flask was immersed into a preheated oil bath at 50 °C. Aliquots were taken at predetermined time interval and conversion was monitored *via* NMR and GPC. After the expected conversion was reached, the polymerization was quenched by immersing the reaction flask into liquid nitrogen. The reaction mixture was passed through a short alumina plug to remove copper and three consecutive precipitations were performed in methanol and ice (80:20). After the final precipitation, removal of solvent and subsequent drying *in vacuo*, a white solid polymer was obtained (18.0 g, 50% yield). $(M_n)_{NMR}$ = 21.2 kDa. $(M_n)_{GPC}$ = 14.9 kDa. $(M_w)_{GPC}$ = 17.7 kDa. PDI= 1.18. IR: 3000-2750, 1710, 1500, 1370, 1220, 1150, 880, 810 cm^{-1}. ^{1}H-NMR (CD_2Cl_2): δ 1.5 (s, ($C\boldsymbol{H}_3$)$_3$COC-), 1.8, (br, -C$\boldsymbol{H}$CH$_2$-), 2.2 ((br, -CHC$\boldsymbol{H}_2$-), 4.1 ($CH_3C\boldsymbol{H}_2$OCO-) ppm. ^{13}C NMR (CD_2Cl_2): δ: 26.7, 31.6–38.0, 80.2, 174.6 ppm. DSC:

(T_g) = 58 °C. TGA: T_{onset} = 118 °C; $T_{decomposition}$: [(118-248 °C) 31 % mass loss; (248-457 °C) 43% mass loss; 26% mass remaining].

Synthesis of poly(*tert*-butyl acrylate)$_{160}$-*b*-poly(styrene)$_{30}$ (P*t*BA$_{160}$-*b*-PS$_{30}$) (S2)

The block copolymer poly(*tert*-butyl acrylate)$_{160}$-*b*-poly(styrene)$_{30}$ (P*t*BA$_{160}$-*b*-PS$_{30}$) was prepared using atom transfer radical polymerization. To a flame-dried 25 mL Schlenk flask, P*t*BA$_{160}$ (8.00 g, 0.37 mmol) was added along with copper (I) bromide (108 mg, 0.75 mmol), styrene (1.96 g, 18.9 mmol) and anisole (8.00 g). The reaction mixture was sealed and three freeze pump thaw cycles were performed with N_2 backfilling. N,N,N',N',N''-pentamethyldiethylenetriamine (130 mg, 0.75 mmol) was added to the reaction mixture *via* a syringe and the reaction mixture was treated by two more freeze pump thaw cycles. The reaction mixture was brought to room temperature and stirred to ensure homogeneity. Following this, the Schlenk flask was immersed into a preheated oil bath at 82 °C. Aliquots were taken at predetermined time intervals and conversions were monitored *via* ^{1}H-NMR spectroscopy and GPC. After the expected conversion was reached, the polymerization was quenched by immersing the reaction flask into liquid nitrogen. The reaction mixture was passed through a short alumina plug to remove copper and three consecutive precipitations were performed in methanol and ice (80:20). After the final precipitation, removal of solvent and subsequent drying *in vacuo*, a white powder was obtained (6.08 g, 97% yield). $(M_n)_{NMR}$ = 24.4 kDa. $(M_n)_{GPC}$ = 23.4 kDa. $(M_w)_{GPC}$ = 25.9 kDa. PDI= 1.11. IR: 3200-3050, 3000-2750, 1730, 1460, 1380, 1280, 1150, 870, 770 cm^{-1}. ^{1}H-NMR (CD_2Cl_2): δ 1.5 (s, (C***H***$_3$)$_3$COC-), 1.8, (br, -CHC***H***$_2$-), 2.2 ((br, -C***H***CH$_2$-), 4.1 (CH$_3$C***H***$_2$OCO-), 6.2-7.3 (br, Ar***H***) ppm. ^{13}C NMR

(CD_2Cl_2): δ: 26.7, 31.6–38.0, 80.2, 126.4–128.1, 174.6 ppm. DSC: $(T_g)_{PtBA}$ = 51 °C; $(T_g)_{PS}$ = not observed. TGA: T_{onset} = 136 °C; $T_{decomposition}$: [(136-245 °C) 36 % mass loss; (245-464 °C) 43% mass loss; 21% mass remaining].

Synthesis of poly(acrylic acid)$_{160}$-*b*-poly(styrene)$_{30}$ (PAA$_{160}$-*b*-PS$_{30}$) (S3)

Block copolymer **S2** (2.1 g, 0.09 mmol) was dissolved in trifluoroacetic acid (70 g, 0.6 mol) and stirred at room temperature for 16 h. The next day, TFA was evaporated under a N2 stream, and the polymer was dissolved in THF and transferred to presoaked dialysis tubing (MWCO 6-8000 Da). The mixture was extensively dialyzed for 4 days against nanopure water followed by lyophilization to obtain white fluffy polymer of PAA_{164}-*b*-PS_{31} (1.0 g, yield = 78%). $(M_n)_{NMR}$ = 15.2 kDa. IR: 3700-2400, 1720, 1488, 1280, 1205, 860 cm^{-1}. ^{1}H-NMR (DMSO-d_6) δ: 1.0-2.0 (br, polymer backbone), 2.2 (br, -CHC***H***$_2$-), 4.1 (CH_3C***H***$_2$OCO-), 6.2 - 7.3 (br, Ar***H***), 12.2 (br, COO***H***) ppm. ^{13}C NMR (DMSO-d_6) δ: 31.6–38.0, 126.4–128.1, 175.6 ppm. DSC: $(T_g)_{PAA}$ = 127 °C; $(T_g)_{PS}$ = not observed. TGA: T_{onset} = 154 °C; $T_{decomposition}$: [(154-289 °C) 6 % mass loss; (289-482 °C) 40% mass loss; 40% mass remaining].

Characterization of micelles of PAEA$_{160}$-*b*-PS$_{30}$ (S4)

$(D_h)_{num}$ (DLS) = 28 ± 5 nm; $(D_h)_{vol}$ (DLS) = 36 ± 23 nm; $(D_h)_{int}$ (DLS) = 170 ± 150 nm. Zeta potential = 47 ± 5 mV (in nanopure water pH 5.5).

Characterization of micelles of (PAEA$_{0.85}$-*g*-PAEI$_{0.15}$)$_{160}$-*b*-PS$_{30}$ (S5)

$(D_h)_{num}$ (DLS) = 14 ± 4 nm; $(D_h)_{vol}$ (DLS) = 21 ± 4 nm; $(D_h)_{int}$ (DLS) = 150 ± 160 nm. Zeta potential = 57 ± 2 mV (in nanopure water pH 5.5).

Characterization of micelles of $(PAEA_{0.50}$-*g*-$PAEI_{0.50})_{160}$-*b*-PS_{30} (S6)

$(D_h)_{num}$ (DLS) = 11 ± 3 nm; $(D_h)_{vol}$ (DLS) = 16 ± 12 nm; $(D_h)_{int}$ (DLS) = 160 ± 170 nm. Zeta potential = 38 ± 1 mV (in nanopure water pH 5.5).

Characterization of micelles of $PAEI_{160}$-*b*-PS_{30} (S7)

$(D_h)_{num}$ (DLS) = 11 ± 3 nm; $(D_h)_{vol}$ (DLS) = 17 ± 11 nm; $(D_h)_{int}$ (DLS) = 100 ± 100 nm. Zeta potential = -34 ± 2 mV (in nanopure water pH 5.5).

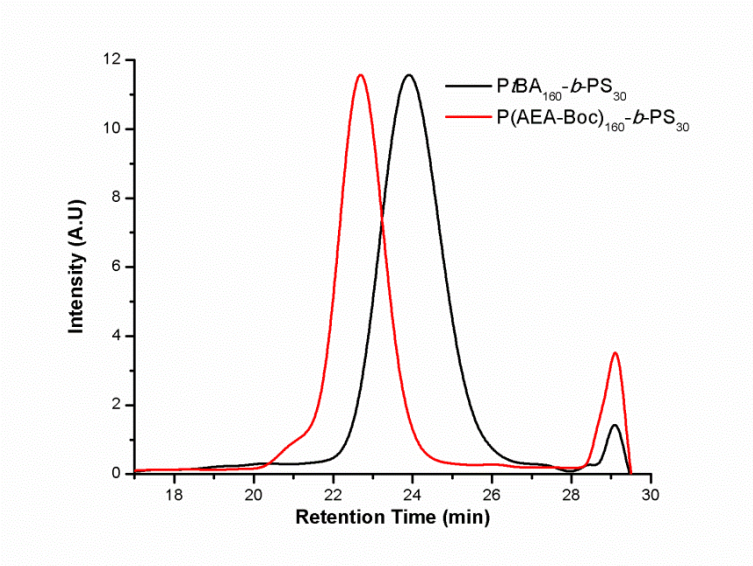

Figure 4.10. GPC of P*t*BA_{160}-*b*-PS_{30} (**S2**) and $P(AEA\text{-}Boc)_{160}$-*b*-PS_{30} (**1**).

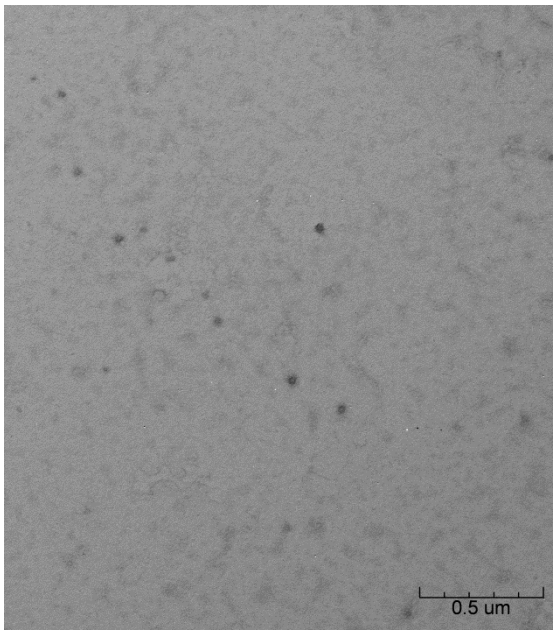

Figure 4.11. TEM micrograph of cSCKs (**12**) composed of $PAEA_{160}$-*b*-PS_{30}.

CHAPTER V

HIERARCHICALLY-ASSEMBLED THERANOSTIC NANOSTRUCTURES FOR SIRNA DELIVERY AND IMAGING APPLICATION

5.1 Introduction

Construction of sophisticated three-dimensional multifunctional nanostructures, such as viruses, in Nature by sequential hierarchical assembly of simpler lower order building blocks (*i.e.*, amino acids to proteins to viral capsid assembly) provides broad inspiration,[2,3,152] and has prompted us to expand our synthetic methodology for the preparation of nanoscopic discrete objects from molecular polymerization and macromolecular assembly to the next level of complexity, involving the hierarchical assembly of nanoscopic building blocks. From a fundamental perspective, the development of strategies by which to construct unique objects in the laboratory setting from nanoscopic materials is of interest to explore advantages of their compositions, structures, overall shapes, and internal morphologies on their biological interactions and properties. Ultimately, multiple levels and types of functional performance may be incorporated. With recent advances in nanotechnologies, there is a high level of attention being directed toward the creation of polymeric nanodevices that can bring together multiple components, for instance to achieve coincident therapy and diagnosis in nanomedicine applications.

Several nanomedical devices incorporate multiple functions within a single entity, where optimization for the integration of various functionalities into nanoparticles plays a critical role in their performance and biological behavior *in vivo*. Current

methods for introduction of multi-functionalities involve manipulation of polymers that are the building blocks of the nanoparticles, which can be iterative and inefficient, as entirely new block copolymers must be synthesized to alter the composition of merely one element contributing to the multi-functionality. Recently, the combination of multiple functions through several individual nanoscopic devices is receiving increased attention, due to the potential for simplification and individualized optimization. As an example, Bhatia *et al*. recently reported the employment of two different nanoparticles in tandem, with each performing a different function to achieve increased drug delivery for the treatment of breast cancer. Firstly, a gold nanorod 'scout' nanoparticle was administered - to accumulate at the tumor site and initiate a clotting cascade after being heated by infrared light irradiation. The clotting process produced additional signals for attracting a second type of nanoparticle loaded with doxorubicin, which led to a 40-fold increase in the amount of drug delivered into the tumor, relative to control studies.[153] Such 'division of labor' allows versatility of each of the nanoparticles to be adjusted for their individual performance for a mutually enhanced function and behavior *in vivo*.

In our continued interest to explore nanoscopic objects designed for various biomedical applications, shell crosslinked knedel-like nanoparticles (SCKs) with tunable size, shape and morphology have been extensively investigated.[9,14,16,17,20,31,72,85,138,154] These SCKs consist of a hydrophobic core and a hydrophilic shell domain, the latter of which can be modified to carry radionuclides, poly(ethylene glycol)s (PEGs), targeting moieties, fluorophore labels, and various payloads to serve as vehicles for combinational therapies. Herein, we have adopted an intermediate approach to bring together

individual components with unique properties by hierarchical assembly of the independent units. Hierarchical assembly of two different modules, one loaded with therapeutic cargo and the other with sites to carry imaging agents, was achieved by templating cationic SCKs (cSCKs) that can electrostatically bind negatively-charged siRNA, onto anionic shell crosslinked rods (SCRs), the core of which provides sites for radiolabeling. These hierarchically hierarchically-assembled theranostic (HAT) nanostructures hold great potential as a platform that allows for merging individual components with independent domains for carrying payloads and radiolabels, optimized as agents for combined therapy and diagnosis. Our initial focus is on the construction of multifunctional nanomaterials that present surface chemistries for transport of nucleic acids as therapeutic cargo into cells, while also possessing an overall shape that provides for long *in vivo* lifetimes. In our laboratory, these have included spherical cSCKs, which have been shown to package negatively-charged nucleic acids *via* electrostatic interactions, protect them from enzymatic degradation and deliver them into cellular target sites.[36,84]

However, many reports of the effects of nanoparticle structure on *in vivo* pharmacokinetics have shown that high aspect ratio nanoparticles provide for extended blood circulation lifetimes,[155,156] while the cell internalization kinetics are dependent on the size, shape and also surface chemistry.[159,160] Although those studies have focused on negatively-charged or neutral materials, examples of cylindrical or rod-shaped nanomaterials having cationic surface characteristics have been produced by engineering[161] or block copolymer crystallization-driven[162] supramolecular assembly

approaches. We have demonstrated that the cSCK property of cell transfection can be transferred onto nanocylinders upon co-assembly, and[111] therefore, in our effort to extend those initial studies to fully functional high aspect ratio nanostructures capable of nucleic acids delivery with radiolabel tracking, we have explored as an alternative approach, hierarchical supramolecular assemblies of cSCKs, produced together with negatively-charged shell crosslinked rods (SCRs), which have sites for radiolabeling in the core.

5.2 Materials and Methods

Polymerizations were performed on a double manifold with glassware and syringes that were dried in an oven (100 °C) for at least 1 h, and with syringes that were washed with N_2 (3 ×), prior to use. *tert*-Butyl acrylate (*t*-BA, 99%, Aldrich), styrene (99%, Aldrich), toluene (anhydrous, 99.8%, Aldrich), *N*,*N*,*N*′,*N*″,*N*″-pentamethyldiethylenetriamine (PMDETA, 99% Aldrich), copper (I) bromide (CuBr, 99.99%, Aldrich), ethyl 2-bromopropionate (99%, Aldrich), trifluoroacetic acid (TFA, 95%; Aldrich), 1-(3′-dimethylaminopropyl)-3-ethylcarbodiimide methiodide (EDCI, 98%, Aldrich), hydroxybenzotriazole (HOBT, Aldrich), 2–(1H–benzotriazol–1–yl)-1,1,3,3-tetramethyluronium hexafluorophosphate (HBTU, Aldrich), N,N-diisopropylethylamine (DIPEA, 99.5%, Aldrich). The amphiphilic block copolymer of poly(acrylic acid)$_{160}$-*block*-polystyrene$_{30}$ (PAA_{160}-*b*-PS_{30}) was prepared using atom transfer radical polymerization (ATRP) of protected monomer precursors followed by deprotection, according to previously reported methods [142]. All other reagents were obtained from Sigma-Aldrich and used as received. Spectra/Por membrane tubes were

purchased from Spectrum Medical Industries, Inc. (Waltham, MA), and were used for dialysis. Nanopure water (18 MΩ•cm) was acquired by means of a Barnstead Nanopure ultrapure water purification system (Thermo Scientific, Asheville, NC).

^{1}H NMR and ^{13}C NMR spectra were recorded on an Inova 300 or Mercury 300 MHz interfaced to a UNIX computer using VnmrJ software. Samples were prepared as solutions in $CDCl_3$, CD_2Cl_2, or DMF-d_7 and solvent protons were used as internal standard. Gel permeation chromatography (GPC) was conducted on a system equipped with a Waters Chromatography, Inc. (Milford, MA) model 1515 isocratic pump and a model 2414 differential refractometer with a three-column set of Polymer Laboratories, Inc. (Amherst, MA) Styragel columns (PL_{gel} 5μm Mixed C, 500 Å, and 10^4 Å, 300 x 7.5 mm columns) and a guard column (PL_{gel} 5μm, 50 x 7.5 mm). The system was equilibrated at 40 °C in tetrahydrofuran (THF), which served as the polymer solvent and eluent (flow rate set to 1.00 mL min^{-1}). The differential refractometer was calibrated with Polymer Laboratories, Inc. polystyrene standards (300 to 467,000 Da). Polymer solutions were prepared at a concentration of *ca*. 3 mg/mL with 0.05% (*v*/*v*) toluene as flow rate marker and an injection volume of 200 μL was used. Data were analyzed using Empower Pro software from Waters Chromatography Inc. IR spectra were recorded on an IR Prestige 21 system (Shimadzu Corp., Japan). A small amount of sample was placed to cover the ATR crystal for IR measurements. Data were analyzed using IRsolution software. Thermogravimetric analysis was performed under N_2 atmosphere using a Mettler Toledo model TGA/DSC1 with a heating rate of 10 °C min^{-1}. Measurements were analyzed using Mettler Toledo STARe software v.10.00.

Samples for TEM were prepared by depositing 5 μL of sample to glow discharged carbon coated copper grids. Excess sample was wicked off using filter paper and the grids were allowed to dry in air for 1 min. The grids were then stained with 5 μL of 2% uranyl acetate and excess stain was wicked off using filter paper. Specimens were observed on a JEOL 1200EX transmission electron microscope operating at 100 kV and micrographs were recorded at calibrated magnifications using an SIA-15C CCD camera. The final pixel size was 0.42 nm/pixel. The number-average particle diameters (D_{av}) and standard deviations were generated from the analysis of particles from at least two different micrographs (n = 100). Dynamic light scattering (DLS) measurements were conducted using Delsa Nano C from Beckman Coulter, Inc. (Fullerton, CA) equipped with a laser diode operating at 658 nm. Size measurements were made in water (n = 1.3329, η = 0.890 cP at 25 ± 1 °C; n = 1.3293, η = 0.547 cP at 50 ± 1 °C; n = 1.3255, η = 0.404 cP at 70 ± 1 °C). Scattered light was detected at 165° angle and analyzed using a log correlator over 70 accumulations for a 0.5 mL of sample in a glass size cell (0.9 mL capacity). The photomultiplier aperture and the attenuator were automatically adjusted to obtain a photon counting rate of *ca*. 10 kcps. The calculations of the particle size distribution and distribution averages were performed using CONTIN particle size distribution analysis routines. Prior to analysis, the samples were filtered through a 0.45 μm Whatman Nylon membrane filter (Whatman Inc., Piscataway, NJ). The samples in the glass size cell were equilibrated at the desired temperature for 5 min before measurements were made. The peak average of histograms from intensity, volume or number distributions out of *ca.* 70 accumulations was reported as the average diameter

of the particles. Absorption measurements were made using a UV-2550 system (Shimadzu Corp., Japan) using PMMA cuvettes. Spectra were analyzed with UV-Probe 2.33 software.

Cytotoxicity assays

RAW 264.7 (2 x 10^4 cells/well) mouse macrophages were plated in 96-well plate in Dulbecco's Modified Eagle Medium (DMEM) (10% fetal bovine serum and 1% penicillin/streptomycin). Cells were incubated at 37 °C in a humidified atmosphere containing 5% CO_2 for 24 h to adhere. Then, the medium was replaced with a fresh medium 1-h prior to the addition of 20 μL of the cSCKs and Lipofectamine to 100 μL of the medium (final concentrations ranged from 0-to-100 μg/mL). The cells were incubated with the formulations for 24 h and washed once with phosphate-buffered saline (PBS) and 100 μL of the complete media was added to the cells. MTS combined reagent (20 μL) was added to each well (Cell Titer 96® Aqueous Non-Radioactive Cell Proliferation Assay, Promega Co., Madison, WI). The cells were incubated with the reagent for 2 h at 37 °C in a humidified atmosphere containing 5% CO_2 protected from light. Absorbance was measured at 490 nm using SpectraMax M5 (Molecular Devices Co., Sunnyvale, CA). The cell viability was calculated based on the relative absorbance to the control-untreated cells. The calculation of the IC_{50} values and the statistical analysis were performed using GraphPad Prism four-parameter fit, considering the 0% and 100% cell viabilities are for the control medium (no cells) and cells with no treatment, respectively.

Gel shift assay

Agarose gels (1%) were prepared in Tris-acetate-EDTA buffer (Bio-Rad Laboratories, Inc., Hercules, CA). The siRNA (5'-Cy3-(sense strand)-GGCCACAUCGGAUUUCACU, M_w = 13814 g/mol, Dharmacon, Chicago, IL), either free or complexed to the various nanoparticle formulations at nitrogen (total concentrations of the primary amines and histamines)-to-phosphate (N/P) ratios ranging from 0.25-to-6 (1.3 μg siRNA/25 μL/well), were mixed with glycerol (20% *v*/*v*) prior to the electrophoresis. Gel electrophoresis was carried out using a horizontal apparatus at 100 V for 30 min and fluorescence imaging of the separated siRNA bands was performed using a ChemiDoc XRS (Bio-Rad Laboratories, Inc.).

Death-siRNA transfection assays

RAW 264.7 mouse macrophages (2 x 10^4 cells/well) and human ovarian adenocarcinoma cells (OVCAR-3) (5 x 10^3 cells/well) were plated in a 96-well plate in DMEM and RPMI-1640 medium (10% and 20% fetal bovine serum, for the RAW 264.7 and OVCAR-3, respectively and 1% penicillin/streptomycin). Cells were incubated at 37 °C in a humidified atmosphere containing 5% CO_2 for 24 h to adhere. Then, the medium was replaced with a fresh medium 1-h prior to the addition of the siRNA-loaded cSCKs (100 nM final concentrations of AllStars death- or negative control-siRNA (Qiagen, Valencia, CA)) at N/P ratio of 5, unless otherwise indicated. The cells were incubated with the various formulations for 24 h and washed extensively with PBS and the cell viability was measured 24 h later by measuring the relative cell viability of the cells treated with death-siRNA to the negative control-loaded cSCKs. The cell

viabilities were measured as described in the cytotoxicity section. The Lipofectamine-siRNA complexes were prepared according to the manufacturer instructions and the transfection efficiency was measured following the same procedures of the siRNA-cSCKs complexes. The effect of endosomal acidification on transfection efficiency was studied by incubating cells with 200 nM bafilomycin A1 (Sigma-Aldrich, St. Louis, MO) 30-min prior to the transfection and by adding the same concentration of bafilomycin to the transfection medium. The toxicity of siRNA complexes could be also measured by comparing the cell viability of the cells treated with the negative control-siRNA complexes to that of the control-untreated cells.

Laser scanning confocal microscopy (LSCM)

RAW 264.7 mouse macrophages (1 x 10^5 cells/well) were plated in glass-bottom six-well plate (MatTek Co., Ashland, MA) in DMEM medium. Cells were incubated at 37 °C in a humidified atmosphere containing 5% CO_2 for 24 h to adhere. Then, the medium was replaced with a fresh media 1-h prior to the addition of siRNA-loaded cSCKs or Lipofectamine (100 nM final concentration of the 5'-Cy3-siRNA). The cells were incubated with the formulations for 3 h and washed extensively with PBS. Then, DRAQ-5 (Biostatus Ltd., Shepshed, Leicestershire, UK) was utilized to stain the nucleus (30 min incubation, followed by extensive washing with PBS). Cells were then fixed with 1% formaldehyde for 20 min, washed once with PBS. The cells were then stored in 1 mL PBS in the refrigerator and analyzed by laser scanning confocal microscopy (LSM 510, Zeiss, Jena, Germany). The images were collected under the same conditions (laser power, detector gain, *etc.*) for consistency, and $\lambda_{excitation}$ of 543 and 633 nm were utilized

for the Cy3 and DRAQ-5, respectively.

5.3 Results and Discussion

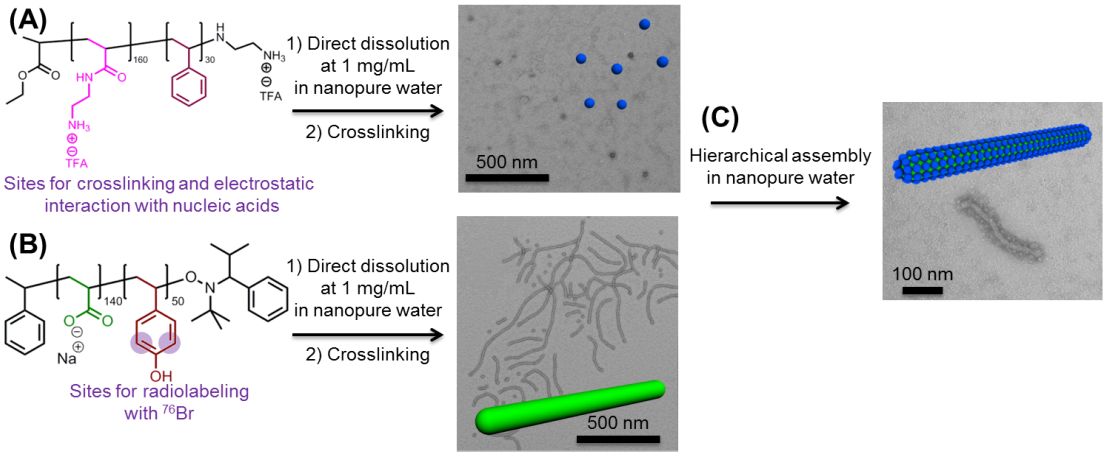

Figure 5.1. Schematic representation of A) Preparation of cationic shell crosslinked nanostructures by directly dissolving polymers into water to obtain micelles followed by crosslinking selectively in the shell region to obtain cSCKs b) Preparation of anionic nanorods by direct dissolution of polymers followed by crosslinking in the shell region C) Hierarchical-assembly of cSCKs on SCRs *via* supramolecular assembly in aqueous medium.

The cSCKs were prepared in a two-step process, first by direct dissolution of poly(acrylamidoethylamine)$_{160}$-*block*-polystyrene$_{30}$ (PAEA$_{160}$-*b*-PS$_{30}$) to obtain a micellar solution, followed by selectively crosslinking 5% of the amines within the hydrophilic shell domain by employing a diacid crosslinker, 4,15-dioxo-8,11-dioxa-5,14-diazaoctadecane-1,18-dioic acid, (activated using O-benzotriazole-N,N,N',N'-tetramethyl-uronium-hexafluoro-phosphate (HBTU) and hydroxybenzotriazole (HOBT) in DMF) in aqueous medium (Fig. 5.1A,S1). Dynamic light scattering (DLS) and transmission electron microscopy (TEM) were used to measure the sizes of the particles

in solution and dry state, and were determined to be *ca*. 20 nm and 15 nm (n = 100), respectively. A zeta potential value of *ca*. 35 mV was determined by electrophoretic light scattering measurements, indicating that the surface of the cationic nanoparticles was positively charged.

Similarly, anionic cylinders were prepared by aqueous self assembly and shell crosslinking of the amphiphilic block copolymer poly(acrylic acid)$_{140}$-*b*-poly(*para*-hydroxystyrene)$_{50}$ (PAA$_{140}$-*b*-P*p*HS$_{50}$), as reported previously,[157] that consisted of PAA as the hydrophilic shell segments and P*p*HS as the hydrophobic core domain. The cylindrical micelles were allowed to undergo crosslinking of approximately 10% of the acrylic acid residues by amidation with the amine groups of the crosslinker (2,2'-ethylenedioxy)bis(ethylamine), in the presence of 1-ethyl-3-(3'-dimethylaminopropyl) carbodiimide methiodide) (EDCI) (Fig. 5.1 B, S2). TEM images confirmed that these nanostructures were rod-like with diameters of *ca*. 10 nm and lengths of *ca*. 1.5 μm (n = 100). Zeta potential measurements were used to evaluate the surface charge of the nanorods and were found to be -30 mV, indicating that they were negatively charged.

The individual cationic spherical and anionic cylindrical nanostructures were co-assembled and further assessed for their performances *in vitro*. The hierarchical assemblies were prepared by mixing cationic spheres with anionic cylinders in aqueous medium at amine-to-carboxylate (N/C) ratio of 10:1. The surfaces of the nanorods were coated with the spheres, as demonstrated by TEM imaging (Fig. 5.1 C,Fig. 5.5). Zeta potential measurements of the complexes were *ca.* 25 mV, indicating a decrease in the net charge of the spheres as a result of electrostatic complexation to the negatively-

charged cylinders, although still maintaining a net positive charge. The abilities of these supramolecular structures to complex siRNA onto the PAEA shell of the spheres and to carry ^{76}Br radiolabels in the P*p*HS core of the cylinders were investigated.

Binding of siRNA to the individual components, and to the HAT nanoassemblies was studied, followed by evaluating the transfection efficiencies of the siRNA nanocomplexes in two different cancer cell lines. It has been demonstrated that the nanoparticle shapes, sizes and charges play a role in cellular internalization. We have previously shown that hierarchical assemblies, as well as cSCKs can be taken up by cells.[84,158] Cylindrical nanoparticles, cSCKs and HAT nanostructures were mixed with Cy3-labeled siRNA and their binding efficiencies were studied by agarose gel electrophoresis at various N/P ratios (Fig. 5.2). Both the cSCKs and the assemblies were able to completely bind the siRNA at a N/P ratio of 2, indicating that the hierarchical assembly process did not adversely affect the electrostatic interactions between cSCKs and nucleic acids. The percentages of free (non-complexed) siRNA at N/P ratios of 0.5 and 1, were 66 *vs.* 62 and 39 *vs.* 20% of the control siRNA for the spherical cSCKs and HAT nanostructures, respectively (Figure 5.2 C and D). These data indicate the ability of both cSCKs and HAT nanostructures to complex siRNA, with slightly higher efficiency for the HAT, probably due to the cooperative electrostatic interactions between the multiple spheres assembled on the surface of the cylinders, as compared to the individual spherical cSCKs. On the contrary, the anionic cylinders were not able to complex the siRNA at a weight ratio up to 5 (cylinders to siRNA; because the anionic cylinders lack amino groups, except for the few that may be present due to incomplete

reaction of the crosslinker, a N/P ratio was not applicable), due to the lack of positively-charged functionalities, which are required for siRNA complexation (Fig. 5.2 A). Worth mentioning is that the amount of cylinders utilized at a weight ratio of 0.5 is higher than the amount of cylinders incorporated into the HAT at a N/P ratio of 5, indicating that the anionic cylinders did not contribute to the binding property of the HAT, but probably clustering of multiple cationic spheres on their surfaces enhanced the electrostatic binding efficiencies with siRNA. In the case of Lipofectamine, complete binding was not observed even at 5-fold the amount recommended by the manufacturer, whereas complete binding of the same amount of siRNA was observed at a N/P ratio of 2 for the cSCKs and HAT (Fig. 5.2). The latter demonstrates the advantage of using nanoparticles for the efficient complexation of nucleic acids, in particular for *in vivo* applications, where complete shielding from extra- and intracellular nucleases is essential for increasing the delivery of intact siRNA to the target sites or intracellularly. For further studies, the nanocomplexes were prepared at N/P ratio of 5.

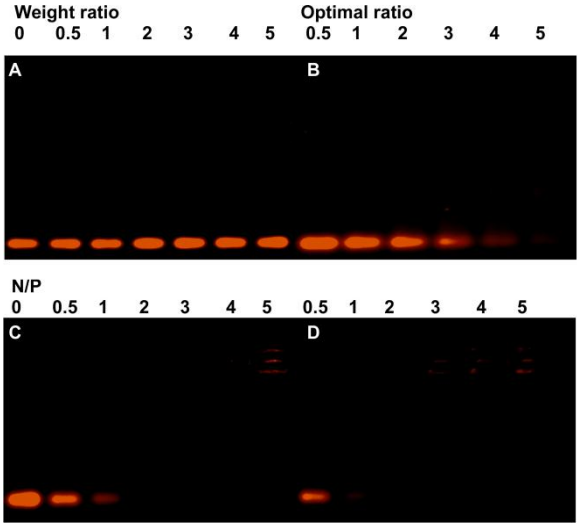

Figure 5.2. Gel-shift assay of Cy3-labeled siRNA, either naked (N/P = 0), mixed with the cylinders (A), Lipofectamine (B) or complexed to cSCKs (C) or HAT (D) at increasing N/P ratios. For cylinders, the weight ratio was used, whereas, for Lipofectamine, the optimal ratio was set according to the manufacturer instructions.

The cellular uptake and transfection efficiencies of the Cy3-labeled siRNA as mixtures/complexes with cylinders, cSCKs, HAT assemblies and Lipofectamine was studied by laser scanning confocal microscopy in human ovarian adenocarcinoma (OVCAR-3) cells (Fig. 5.3). Both cSCKs and assemblies showed comparable cellular uptake (Figure 3A, A4 and A5) that was higher than Lipofectamine (Figure 5.3A, 5.3A3), as indicated by the visual fluorescence intensities and the apparent number of fluorescent cells in the images. No uptake was observed in the control-untreated cells or cells treated with a mixture of siRNA/cylinders (Figure 5.3 A, A1 and A2), which is in agreement with the gel-shift assay results (Fig. 5.2). siRNA-cell death assay was then performed using OVCAR-3 cancer cells and RAW 264.7 mouse macrophages (Fig. 5.3 B), by measuring the relative viabilities of cells treated with nanoparticles-loaded with siRNA that induces cell death *vs.* the cells-treated with the same nanoparticles but loaded

with a negative control siRNA. The nanoparticles showed lower transfection efficiency than Lipofectamine. Our group and others have shown that cellular uptake is not always correlated with transfection efficiency.[163,164] The lower transfection of nanoparticles might be related to the higher stability of the complexes that partially retard the release of siRNA intracellularly. For instance, Leroux and coworkers have found that amine functionalized poly(glycerol methacrylate) linear polymer induced higher bcl-2 oncoprotein knockdown as compared to the star-shaped analogue, although the latter demonstrated higher antisense oligonucleotide binding efficiency.[164] In both cell lines, HAT assemblies induced higher cell-death (transfection), as compared to the cSCKs, and, as expected, no transfection was found for the death-siRNA mixed with the cylinders. The difference in transfection between the cSCKs and the HAT might be related to the multivalent binding of the HAT structures to the cell surface which allowed longer contact period for the intracellular delivery of siRNA. Further studies of the intracellular delivery mechanisms of the cSCKs and assemblies are currently underway.

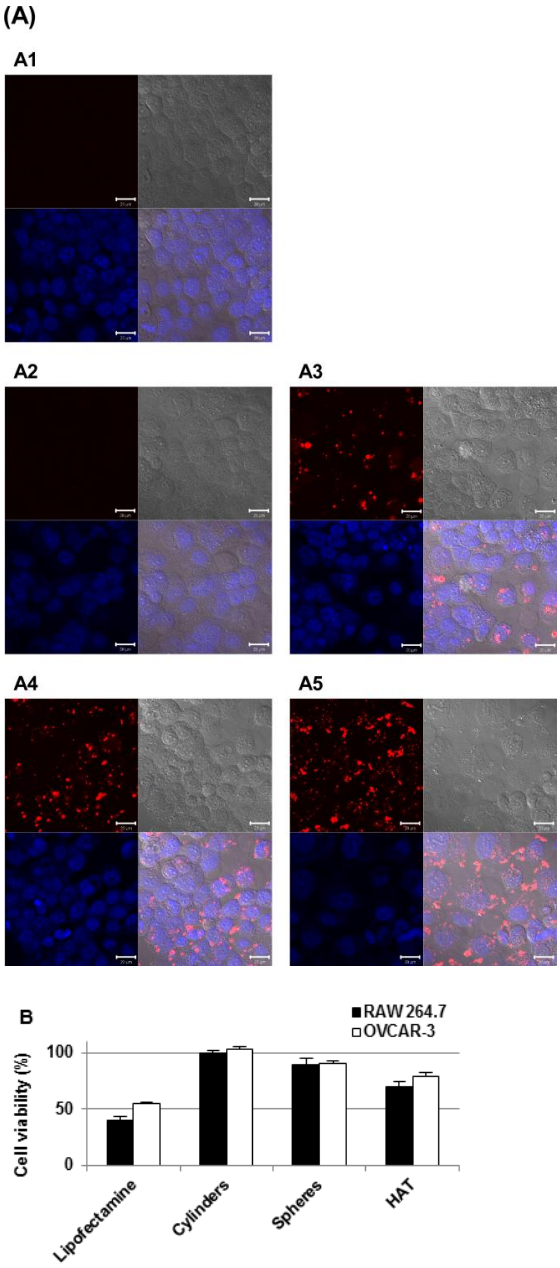

Figure 5.3. (A) Laser scanning confocal microscopy images of OVCAR-3 cells that were either untreated (A1), or treated with Cy3-labeled siRNA (200 nM) mixed with cylinders (A2), or complexed with Lipofectamine (A3), spherical cSCKs (A4) or HAT (A5) for 3 h. The Cy3-siRNA and the nucleus stained with DRAQ-5 appear in the red (upper left) and blue (lower left) panels, respectively. The light transmitted images (upper right) and merged images (lower right) are also presented. (B) Transfection efficiency of the cell-death siRNA (100 nM) mixed with the cylinders, or complexed to Lipofectamine, spherical cSCKs or HAT nanostructures. The complexes were incubated with cells for 24 h and the transfection efficiencies were calculated based on the relative cell viabilities of the cells treated with the nanocomplexes *versus* the cells treated with the same complexes, but prepared with negative control siRNA.

To further evaluate their potential as theranostic candidates, these nanoparticles were radiolabeled with ^{76}Br. cSCKs, HAT nanostructures and SCRs were incubated with 130 μCi ^{76}Br in phosphate-buffered saline (PBS) with the addition of bromoperoxidase (BPO, 0.6 units) in hydrogen peroxide (2.65 pmol) for 1 h at 0 °C (S4). The radiochemical purities of ^{76}Br-radiolabeled nanoparticles were monitored by radio instant thin layer chromatography. Among the three nanoparticles, SCRs had the highest radiolabeling yield (94%) and specific activity (SA = 6.06 μCi/μg) (Fig. 4), which was comparable to the SA of other phenolic-containing nanostructures.[12] Hierarchical assembly by surrounding the anionic SCRs with cSCKs diminished the radiolabeling capability only slightly, giving a radiolabeling yield of 72% and SA of 4.69 μCi/μg. As expected, the PS core-containing cSCKs gave the lowest radiolabeling yield, 30% and SA of 2.01 μCi/μg. Additionally, the chloramine-T method was also used for radiobromination of the three types of nanoparticles and the labeling results were similar to those obtained by the BPO method (Fig 5.4).

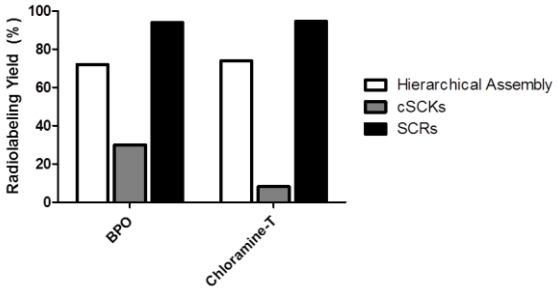

Figure 5.4. Radiolabeling of nanostructures using ^{76}Br. The nanostructures were incubated with 130 μCi ^{76}Br in 1x PBS with the addition of bromoperoxidase (BPO, 0.6 units) in hydrogen peroxide (2.65 pmol) for 1 h at 0 °C and chloramine-T (219.6 nmol) at room temperature for 1 h. The radiochemical purity of ^{76}Br-radiolabeled nanoparticles was monitored by radio instant thin layer chromatography.

5.4 Conclusions

In summary, we have prepared HAT nanostructures where cationic spheres, for complexation of siRNA as a therapeutic cargo, were templated around anionic cylinders with sites for radiolabeling in their hydrophobic cores. These complex nanostructures were able to efficiently complex siRNA and deliver it intracellularly. The HAT structures showed superior siRNA binding affinity and transfection efficiency, in comparison to the individual cationic spheres and anionic cylinders. Additionally, they were radiolabeled with ^{76}Br and exhibited superior radiolabeling efficiency, as compared to the cSCK samples. The HAT nanostructures constitute the first steps toward the development of novel materials that can take advantage of individual components and serve as the next generation of theranostic agents.

5.5 Acknowledgements

We gratefully acknowledge financial support from the National Heart Lung and Blood Institute of the National Institutes of Health as a Program of Excellence in Nanotechnology (HHSN268201000046C) and the National Institute of Diabetes and Digestive and Kidney Diseases of the National Institutes of Health (R01-DK082546). The Welch Foundation is gratefully acknowledged for support through the W. T. Doherty-Welch Chair in Chemistry, Grant No. A-0001.

5.6 Supporting Information

Preparation of cSCKs

The cSCKs were prepared in a two-step process; firstly amphiphilic block copolymer of $PAEA_{160}$-*b*-PS_{30} (5.0 mg) was directly dissolved in nanopure water (5.0 mL) and sonicated using a water bath sonicator for 10 min to obtain clear micellar solution at a concentration of 1 mg/mL. The solution was then allowed to stir overnight at room temperature. To the micellar solution (5.0 mL), sodium carbonate (20 μL of 1.0 M solution) was added to adjust the pH to *ca*. 8.0. A diacid crosslinker, 4,15-dioxo-8,11-dioxa-5,14-diazaoctadecane-1,18-dioic acid, (2.0 mg) was activated with HOBT (1.7 mg, 2.2 equiv. *per* COOH) and HBTU (4.8 mg, 2.2 equiv. *per* COOH) in 300 μL of DMF for 30 min. The activated crosslinker solution was slowly added to the micellar solution to crosslink *ca.* 5 % of the amines. The reaction mixture was allowed to stir overnight, and then transferred to a dialysis tubing (MWCO *ca.* 6000-8000 Da) and dialyzed against nanopure water for 3 d to obtain clear cSCK solution at 0.88 mg/mL.

$(D_h)_{number}$ (DLS) = 21 ± 6 nm; $(D_h)_{volume}$ (DLS) = 48 ± 22 nm; $(D_h)_{intensity}$ (DLS) = 101 ± 59 nm. D_{av} (TEM) = 15 ± 3 nm. Zeta potential = 35 ± 2 mV (nanopure water, pH 5.5).

Preparation of SCRs

Anionic cylinders were prepared by aqueous self assembly of amphiphilic block copolymer of PAA_{140}-*b*-P*p*HS_{50}, as reported previously.[157] To a 100 mL round bottom flask, equipped with a magnetic stir bar, PAA_{140}-*b*-P*p*HS_{50} (25 mg) was added followed by nanopure water (25 mL) to achieve a polymer concentration of 1 mg/mL. The mixture was allowed to stir at room temperature for 2 h followed by addition of nanopure water (60 mL) to achieve a final polymer concentration of *ca* 0.3 mg/mL. The solution was then allowed to stir at room temperature. The following day, cylindrical micelles were allowed to undergo crosslinking of approximately 10% of the acrylic acid segments *via* amidation. To a 50 mL round bottom flask equipped with a magnet stir bar, a solution of cylindrical micelles (25 mL) was added. To this solution, a diamine crosslinker 2, 2'-ethylenedioxy)bis(ethylamine) (1 mg, 1.1 equiv. *per* COOH) was added from a stock solution in nanopure water and the reaction mixture was allowed to stir. After 30 min, 1-ethyl-3-(3-dimethylaminopropyl carbodiimide methiodide) (2.4 mg, 1.3 equiv. per COOH) was slowly added over a period of 2 min from a stock solution in nanopure water. The reaction mixture was allowed to stir overnight, and then transferred to a dialysis tubing (MWCO *ca.* 6000-8000 Da) and dialyzed against nanopure water for 3 d to obtain SCR solution at 0.28 mg/mL. Zeta potential = -30 ± 2 mV (nanopure water, pH 5.5).

Preparation of hierarchical assemblies

Hierarchical assemblies were prepared by mixing cSCKs (600 μL) with SCRs (150 μL) to achieve an amine: carboxylate (N/C) ratio of 10:1. Zeta potential = 25 ± 2 mV (nanopure water, pH 5.5).

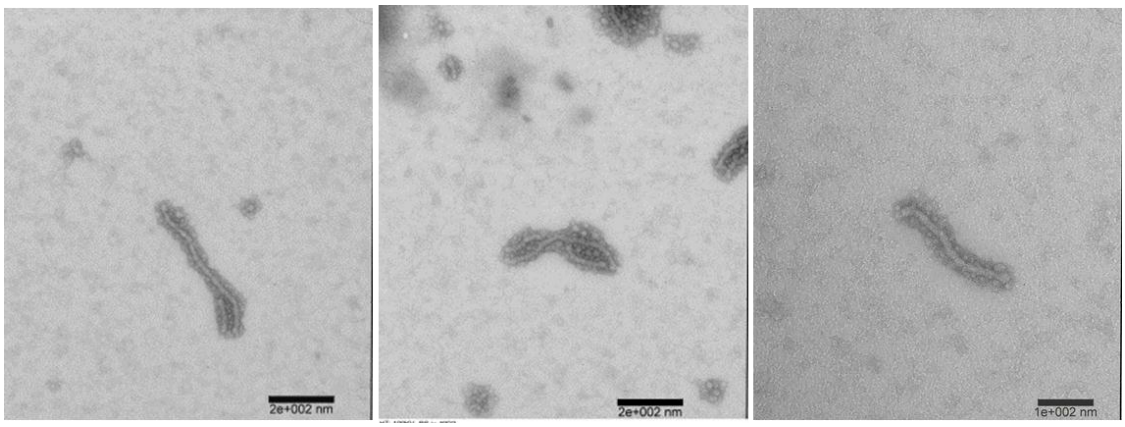

Figure 5.5. TEM micrographs of hierarchically-assembled nanoparticles

Radiolabeling of nanostructures

Bromine-76 ($t_{1/2}$ = 16.2 h, β+ = 57%, EC = 43%) was produced on the Washington University Medical School CS-15 cyclotron by the ^{76}Se (p,n) ^{76}Br nuclear reaction.[2] Hierarchically-assembled HAT nanoparticles, cSCKs, and SCRs (20 μg) were each incubated with 130 μCi ^{76}Br in 1x PBS buffer with the addition of bromoperoxidase (BPO, 0.6 units) in hydrogen peroxide (2.65 pmol) for 1 h at 0 °C. The radiochemical purity of ^{76}Br-radiolabeled nanoparticles was monitored by radio instant thin layer chromatography (radio-ITLC, Bioscan, Washington, DC). Additionally, chloramines-T

method was also employed for ^{76}Br radiolabeling following a previously published procedure.

CHAPTER VI

CONCLUSIONS

This dissertation has focused on the design and development of multifunctional bio-synthetic hybrid nanostructures as theranostic agents for the delivery of nucleic acids toward the treatment of various diseases such as acute lung injury and brain tumor. The main emphasis of this study has been on optimization of nanoparticles to overcome biological barriers toward the efficient delivery of nucleic acids (*e.g.* PNAs and siRNAs) into the cells. We have successfully demonstrated preparation of multifunctional nanoparticle that fulfills the design requirements for imaging and diagnosis. These SCKs consisted of DOTA-lysine to provide sites for chelation of ^{64}Cu for radiolabeling, PEG for prolonged circulation and enhanced biocompatibility *in vivo* and chemical functionalities at the terminus of PEG for tethering targeting ligands (F3 peptide, cell penetrating peptides) or therapeutics cargoes (*e.g.* PNAs) such that they are presented at the outermost surface of the nanostructures. Confirmation of the ability of the PNAs to bind selectively to the target iNOS mRNAs when tethered to the SCK nanoparticles was determined by *in vitro* competition experiments. When attached to the SCKs having a hydrodynamic diameter of 60 ± 16 nm, the K_d values of the PNAs were *ca*. an order of magnitude greater than the free PNAs, while the mismatched PNA showed no significant binding. However, these nanoparticles consisted of PAA as the shell resulting in a net negative charge that potentially could undergo repulsion with the bilayer of the cells hindering its uptake.

Chapters 3 borrowed from the lessons learnt in Chapter 2 to make modification on SCKs for enhanced cellular uptake. In this chapter, facile preparation of cationic SCKs with positive charge on the surface that facilitates cellular entry and enhances binding of nucleic acids for enhancing transfection *in vitro* is discussed. cSCKS were conjugated with a tumor-homing F3 peptide and later complexed with nucleolin targeting siRNA to create a biosynthetic hybrid nanocomplex for improved cellular uptake and knockdown of nucleolin. *In vitro* studies demonstrated an enhanced uptake of cSCKs tethered to F3 peptide compared to the scrambled peptide control nanoparticle sample. Additionally, cSCKs showed effective binding to plasmid DNA and were delivered into the cells for efficient knockdown of nucleolin as demonstrated by immunoblot assays.

Chapter 4 further extends this study to prepare cSCKs optimized for endosomal escape by incorporation of various amounts (0%, 15%, 50% and 100%) of histamine moieties into the polymer precursor of the nanoparticles to afford cSCKs with tunable buffering capacities. The tunable pK_a obtained by conjugation of histamine moieties improved the cytotoxicities of the nanoparticles while also improving the delivery of nucleic acids into the cytosol, as seen by *in vitro* experiments. Histamine incorporation of 15% appeared to be a threshold for the series of samples tested, with cSCKs having higher histamine contents completely lost the ability to bind siRNA and to interact with cell membrane and induce gene silencing. Incorporation of histamine moieties indeed enhanced the cellular delivery of nucleic acids into the cytosol. However, a further

probing of histamine contents between 15% and 50% may better identify the optimum balance of siRNA binding, cellular uptake and buffering capacity.

In Chapter 5, hierarchically-assembled structures were prepared by templating cationic spheres that can electrostatically bind nucleic acid onto anionic cylinders that can be radiolabeled in the hydrophobic core for imaging. This study is an extension to the earlier studies, where only one type of structure was employed for performing multiple functions (radiolabeling, nucleic acid delivery, PEGylation). This system provided an overall advantage over individual nanobjects, as the hierarchically assembled nanostructures exhibited improved siRNA delivery and radiolabeling collectively, compared to the individual nanoparticles which could each only perform one of the separate functions. This provides a facile method to bring together multiple components by simple iterative process to create multifunctional theranostic agents that exhibit great potential as the next generation of theranostic agents.

Nanomedicine is a very promising field that holds a great potential in development of innovative diagnosis and treatment strategies, novel drug candidates and state-of-the-art technologies to revolutionize the fields of healthcare and medicine. However, application of nanotechnology for development of safer and effective medicine and technologies that can be translated from a mere academic curiosity to real-life applications in clinical settings has many hurdles that have to be addressed and overcome. An ideal candidate for biomedical applications *in vivo* has several design requirements ranging from tunability in their sizes, shapes, morphologies, ability to circulate for a pre-determined period of time by mimicking stealth characteristics to

minimize protein adsorption, integration of imaging agents, high loading capacities for drugs followed by competence to release them at a specific sites, either by active or passive targeting strategies, programmed degradability of the nanoparticles by inflicting minimal toxicities, amongst many others. The recent advances in polymer chemistry and nanotechnology has enabled researchers around the world to develop nanoentities that can fulfill one or more of the listed design requirements, however amalgamation of all the components to make an ultimate theranostic agent, known as the "magic bullet" still remains the holy grail of nanomedicine.

This particular study has contributed in advancing the understanding of cellular uptake of nanoparticles complexed with nucleic acids and delivery into cells for theranostics. Efficient delivery into the cytosol is a critical factor that governs the availability of cargo for binding with mRNAs for achieving binding with targeted mRNA for gene suppression. In addition to the current system under investigation, degradable analogues of nanoparticles that can undergo triggered delivery and enhanced clearance *in vivo* will make potential candidates for further studies. It will be important to study the effects of nanoparticles on biological systems *in* vitro and *in vivo* along with the extent, rates and conditions of degradation of the nanoparticles and their degradation products. Furthermore, endosomolytic peptides can be covalently conjugated to the nanoparticles to induce lysis of the endosomal membrane for successful transfection. One of the major challenges in these studies is the ability to quantify the amount of nucleic acids that is delivered into the cells, available in the cytoplasm and those that are available for participating in the binding event *in vitro* and *in vivo*. Determination of the

amount of nucleic acids available is significant in precise quantification and optimization of transfection efficiencies. Novel assays and analytical methods have to be developed for accurate determination nucleic acid available at each stage of investigation that will allow for better understanding of the binding events for development of improved transfection agents.

Nanotechnology is a comparatively new field of study that has been growing by leaps and bounds in the last two decades. Realization of the challenges in the field has opened opportunities for researchers to strive forward toward development of novel therapeutics. The current evolution in physical, biological and analytical sciences will provide opportunities to improve the design, facilitate preparation and extensive characterization of nanomaterials along with an in depth understanding of biological interactions of nanostructures and their ultimate fate *in vitro* and *in vivo* to translate them from bench-to-bedside. There is still "*plenty of room at the bottom*.".[5,6]

REFERENCES

(1) Miyata, K.; Nishiyama, N.; Kataoka, K. *Chem. Soc. Rev.* **2012**, *41*, 2562-2574.

(2) Whitesides, G. M.; Grzybowski, B. *Science* **2002**, *295*, 2418-2421.

(3) Dobon, C. M. *Nature* **2003**, *426*, 884-890.

(4) Miyata, K.; Nishiyama, N.; Kataoka, K. *Chem. Soc. Rev.* **2012**, *41*, 2562-2574.

(5) Feyman, R. P. *Eng. Sci.* **1960**, *23*, 22-36.

(6) Kamaly, N.; Xiao, Z.; Valencia, P. M.; Radovic-Moreno, A. F.; Farokhzad, O. C. *Chem. Soc. Rev.* **2012**, *41*, 2971-3010.

(7) Elsabahy, M.; Wooley, K. L. *Chem. Soc. Rev.* **2012**, *41*, 2545-2561.

(8) Elsabahy, M.; Wooley, K. L. *J. Polym. Sci. Poly. Chem.* **2012**, *50*, 1869-1880.

(9) Nystrom, A. M.; Wooley, K. L. *Accounts Chem. Res.* **2011**, *44*, 969-978.

(10) Petros, R. A.; DeSimone, J. M. *Nat. Rev. Drug. Discov.* **2010**, *9*, 615-627.

(11) Peer, D.; Karp, J. M.; Hong, S.; Farokhzad, O. C.; Margalit, R.; Langer, R. *Nat.Nanotechnol.* **2007**, *2*, 751-760.

(12) Mehnert, W.; Mader, K. *Adv. Drug. Deliv. Rev.* **2001**, *47*, 165-196.

(13) Han, G.; Ghosh, P.; Rotello, V. M. *Nanomedicine -UK* **2007**, *2*, 113-123.

(14) Sun, X. K.; Rossin, R.; Turner, J. L.; Becker, M. L.; Joralemon, M. J.; Welch, M. J.; Wooley, K. L. *Biomacromolecules* **2005**, *6*, 2541-2554.

(15) Sun, G.; Xu, J.; Hagooly, A.; Rossin, R.; Li, Z.; Moore, D. A.; Hawker, C. J.; Welch, M. J.; Wooley, K. L. *Adv Mater* **2007**, *19*, 3157-3162.

(16) Nystrom, A. M.; Wooley, K. L. *Tetrahedron* **2008**, *64*, 8543-8552.

(17) Wooley, K. L.; Lin, L. Y.; Lee, N. S.; Zhu, J. H.; Nystrom, A. M.; Pochan, D. J.; Dorshow, R. B. *J Control Release* **2011**, *152*, 37-48.

(18) Samarajeewa, S.; Shrestha, R.; Li, Y. L.; Wooley, K. L. *J. Am. Chem. Soc.* **2012**, *134*, 1235-1242.

(19) Shrestha, R.; Shen, Y. F.; Pollack, K. A.; Taylor, J. S. A.; Wooley, K. L. *Bioconjugate. Chem.* **2012**, *23*, 574-585.

(20) Sorrells, J. L.; Shrestha, R.; Neumann, W. L.; Wooley, K. L. *J. Mater. Chem.* **2011**, *21*, 8983-8986.

(21) Sun, G.; Hagooly, A.; Xu, J.; Nystrom, A. M.; Li, Z. C.; Rossin, R.; Moore, D. A.; Welch, M. J.; Wooley, K. L. *Biomacromolecules* **2008**, *9*, 1997-2006.

(22) Hawker, C. J.; Wooley, K. L. *Science* **2005**, *309*, 1200-1205.

(23) Braunecker, W. A.; Matyjaszewski, K. *Prog. Polym. Sci.* **2007**, *32*, 93-146.

(24) Cui, H. G.; Chen, Z. Y.; Zhong, S.; Wooley, K. L.; Pochan, D. J. *Science* **2007**, *317*, 647-650.

(25) Zhong, S.; Cui, H. G.; Chen, Z. Y.; Wooley, K. L.; Pochan, D. J. *Soft Matter* **2008**, *4*, 90-93.

(26) Zhu, J. H.; Zhang, K.; Wooley, K. L.; Miesch, C.; Emrick, T.; Pochan, D. J. *Soft Matter* **2011**, *7*, 2500-2506.

(27) Cui, H. G.; Chen, Z. Y.; Wooley, K. L.; Pochan, D. J. *Soft Matter* **2009**, *5*, 1269-1278.

(28) Chen, Z. Y.; Cui, H. G.; Hales, K.; Qi, K.; Wooley, K. L.; Pochan, D. J. *Science* **2004**, *306*, 94-97.

(29) Cui, H. G.; Chen, Z. Y.; Zhong, S.; Pochan, D. J.; Wooley, K. L. *Science* **2007**, *317*, 647-650.

(30) Samarajeewa, S.; Shrestha, R.; Li, Y. L.; Wooley, K. L. *J. Am. Chem. Soc.* **2012**, *134*, 1235-1242.

(31) Shrestha, R.; Shen, Y. F.; Pollack, K. A.; Taylor, J. S. A.; Wooley, K. L. *Bioconjugate Chem.* **2012**, *23*, 574-585.

(32) Zhang, K.; Rossin, R.; Hagooly, A.; Chen, Z.; Welch, M. J.; Wooley, K. L. *J. Polym. Sci. Poly. Chem.* **2008**, *46*, 7578-7583.

(33) Fang, H.; Zhang, K.; Shen, G.; Wooley, K. L.; Taylor, J. S. *Mol. Pharm.* **2009**, *6*, 615-626.

(34) Rossin, R.; Sun, X.; Fang, H.; Turner, J. L.; Li, X.; Wooley, K. L.; Taylor, J. S.; Welch, M. J. *J. Labelled. Compd. Rad.* **2005**, *48*, S35-S35.

(35) Sun, G.; Xu, J.; Hagooly, A.; Rossin, R.; Li, Z.; Moore, D. A.; Hawker, C. J.; Welch, M. J.; Wooley, K. L. *Adv. Mat.* **2007**, *19*, 3157-3162.

(36) Zhang, K.; Fang, H. F.; Wang, Z. H.; Li, Z.; Taylor, J. S. A.; Wooley, K. L. *Biomaterials* **2010**, *31*, 1805-1813.

(37) Nyström, A. M.; Wooley, K. L. *Tetrahedron* **2008**, *64*, 8543-8552.

(38) Whitehead, K. A.; Langer, R.; Anderson, D. G. *Nat. Rev. Drug Discov.* **2009**, *8*, 129-138.

(39) Pack, D. W.; Hoffman, A. S.; Pun, S.; Stayton, P. S. *Nat. Rev. Drug Discov.* **2005**, *4*, 581-593.

(40) Rubenfeld, G. D.; Caldwell, E.; Peabody, E.; Weaver, J.; Martin, D. P.; Neff, M.; Stern, E. J.; Hudson, L. D. *N. Engl. J. Med.* **2005**, *353*, 1685-1693.

(41) Goodman, R. B.; Pugin, J.; Lee, J. S.; Matthay, M. A. *Cytokine Grow. Fac. Rev.* **2003**, *14*, 523-535.

(42) Hemmrich, K.; Kröncke, K.-D.; Suschek, C. V.; Kolb-Bachofen, V. *Nitric Oxide* **2005**, *12*, 183-199.

(43) Guo, F. H.; Deraeve, H. R.; Rice, T. W.; Stuehr, D. J.; Thunnissen, F. B. J. M.; Erzurum, S. C. *Proc. Natl. Acad. Sci. U.S.A.* **1995**, *92*, 7809-7813.

(44) Hosogi, S.; Iwasaki, Y.; Yamada, T.; Komatani-Tamiya, N.; Hiramatsu, A.; Kohno, Y.; Ueda, M.; Arimoto, T.; Marunaka, Y. *Biomed Res-Tokyo* **2008**, *29*, 257-266.

(45) Mehta, S. *Vasc. Pharmacol.* **2005**, *43*, 390-403.

(46) Zhang, J.; McCarthy, T. J.; Moore, W. M.; Currie, M. G.; Welch, M. J. *J Med Chem* **1996**, *39*, 5110-5118.

(47) Panda, K.; Chawla-Sarkar, M.; Santos, C.; Koeck, T.; Erzurum, S. C.; Parkinson, J. F.; Stuehr, D. J. *P Natl Acad Sci USA* **2005**, *102*, 10117-10122.

(48) Towner, R. A.; Smith, N.; Doblas, S.; Garteiser, P.; Watanabe, Y.; He, T.; Saunders, D.; Herlea, O.; Silasi-Mansat, R.; Lupu, F. *Free Rad. Bio. Med.* **2010**, *48*, 691-703.

(49) Hesslinger, C.; Strub, A.; Boer, R.; Ulrich, W. R.; Lehner, M. D.; Braun, C. *Biochem. Soc. Trans.* **2009**, *37*, 886-891.

(50) Lim, M. H.; Xu, D.; Lippard, S. J. *Nat. Chem. Biol.* **2006**, *2*, 375-380.

(51) Ouyang, J.; Hong, H.; Zhao, Y.; Shen, H.; Shen, C.; Zhang, C.; Zhang, J. *Nitric Oxide* **2008**, *19*, 42-49.

(52) Zhou, D.; Lee, H.; Rothfuss, J. M.; Chen, D. L.; Ponde, D. E.; Welch, M. J.; Mach, R. H. *J. Med. Chem.* **2009**, *52*, 2443-2453.

(53) Koppelhus, U.; Nielsen, P. E. *Adv. Drug Deliv.Rev.* **2003**, *55*, 267-280.

(54) Nielsen, P. E.; Egholm, M.; Berg, R. H.; Buchardt, O. *Science* **1991**, *254*, 1497-1500.

(55) Nielsen, P. E. *Mol. Biotechnol.* **2004**, *26*, 233-248.

(56) Lundin, K. E.; Good, L.; Stromberg, R.; Graslund, A.; Smith, C. I. *Adv. Genet.* **2006**, *56*, 1-51.

(57) Nielsen, P. E. *Curr. Pharm. Des.* **2010**, *16*, 3118-3123.

(58) Shi, N.; Boado, R. J.; Pardridge, W. M. *Proc. Natl. Acad. Sci. USA* **2000**, *97*, 14709-14714.

(59) Rao, P. S.; Tian, X.; Qin, W.; Aruva, M. R.; Sauter, E. R.; Thakur, M. L.; Wickstrom, E. *Nucl. Med. Commun.* **2003**, *24*, 857-863.

(60) Sun, X.; Fang, H.; Li, X.; Rossin, R.; Welch, M. J.; Taylor, J. S. *Bioconjugate Chem.* **2005**, *16*, 294-305.

(61) Santangelo, P.; Nitin, N.; Bao, G. *Ann. Biomed. Eng.* **2006**, *34*, 39-50.

(62) Jia, F.; Figueroa, S. D.; Gallazzi, F.; Balaji, B. S.; Hannink, M.; Lever, S. Z.; Hoffman, T. J.; Lewis, M. R. *J. Nucl. Med.* **2008**, *49*, 430-438.

(63) Lendvai, G.; Estrada, S.; Bergstrom, M. *Curr. Med. Chem.* **2009**, *16*, 4445-4461.

(64) Iyer, A. K.; He, J. *Curr. Org. Synth.* **2011**, *8*, 604-614.

(65) Zhilina, Z. V.; Ziemba, A. J.; Ebbinghaus, S. W. *Curr. Top. Med. Chem.* **2005**, *5*, 1119-1131.

(66) Abes, R.; Arzumanov, A. A.; Moulton, H. M.; Abes, S.; Ivanova, G. D.; Iversen, P. L.; Gait, M. J.; Lebleu, B. *Biochem. Soc. Trans.* **2007**, *35*, 775-779.

(67) Thurmond, K. B.; Kowalewski, T.; Wooley, K. L. *J. Am. Chem. Soc.* **1997**, *119*, 6656-6665.

(68) Thurmond, K. B.; Huang, H. Y.; Clark, C. G.; Kowalewski, T.; Wooley, K. L. *Colloid Surface B* **1999**, *16*, 45-54.

(69) Remsen, E. E.; Thurmond, K. B.; Wooley, K. L. *Macromolecules* **1999**, *32*, 3685-3689.

(70) Thurmond, K. B.; Kowalewski, T.; Wooley, K. L. *J. Am. Chem. Soc.* **1996**, *118*, 7239-7240.

(71) Samarajeewa, S.; Shrestha, R.; Li, Y.; Wooley, K. L. *J. Am. Chem. Soc.* **2012**, *134*, 1235-1242.

(72) Cui, H. G.; Chen, Z. Y.; Zhong, S.; Wooley, K. L.; Pochan, D. J. *Science* **2007**, *317*, 647-650.

(73) Becker, M. L.; Bailey, L. O.; Wooley, K. L. *Bioconjugate Chem.* **2004**, *15*, 710-717.

(74) Becker, M. L.; Remsen, E. E.; Pan, D.; Wooley, K. L. *Bioconjugate Chem.* **2004**, *15*, 699-709.

(75) Joralemon, M. J.; Murthy, K. S.; Remsen, E. E.; Becker, M. L.; Wooley, K. L. *Biomacromolecules* **2004**, *5*, 903-913.

(76) Joralemon, M. J.; Smith, N. L.; Holowka, D.; Baird, B.; Wooley, K. L. *Bioconjugate Chem.* **2005**, *16*, 1246-1256.

(77) Lin, L. Y.; Lee, N. S.; Zhu, J.; Nystrom, A. M.; Pochan, D. J.; Dorshow, R. B.; Wooley, K. L. *J. Control. Release* **2011**, *152*, 37-48.

(78) Nystrom, A. M.; Xu, Z. Q.; Xu, J. Q.; Taylor, S.; Nittis, T.; Stewart, S. A.; Leonard, J.; Wooley, K. L. *Chem Commun* **2008**, 3579-3581.

(79) Zhang, S.; Li, Z.; Samarajeewa, S.; Sun, G.; Yang, C.; Wooley, K. L. *J. Am. Chem. Soc.* **2011**, *133*, 11046-11049.

(80) Pan, D.; Turner, J. L.; Wooley, K. L. *Chem. Commun.* **2003**, 2400-2401.

(81) Zhang, K.; Fang, H. F.; Chen, Z. Y.; Taylor, J. S. A.; Wooley, K. L. *Bioconjugate Chem.* **2008**, *19*, 1880-1887.

(82) Turner, J. L.; Becker, M. L.; Li, X. X.; Taylor, J. S. A.; Wooley, K. L. *Soft Matter* **2005**, *1*, 69-78.

(83) Zhang, K.; Fang, H.; Wang, Z.; Li, Z.; Taylor, J. S.; Wooley, K. L. *Biomaterials* **2010**, *31*, 1805-1813.

(84) Zhang, K.; Fang, H.; Wang, Z.; Taylor, J. S.; Wooley, K. L. *Biomaterials* **2009**, *30*, 968-977.

(85) Nystrom, A. M.; Wooley, K. L. *Soft Matter* **2008**, *4*, 849-858.

(86) O'Connor, R. D.; Zhang, Q.; Wooley, K. L.; Schaefer, J. *Helv. Chim. Acta.* **2002**, *85*, 3219-3224.

(87) Zhang, Q.; Clark, C. G.; Wang, M.; Remsen, E. E.; Wooley, K. L. *Nano Lett.* **2002**, *2*, 1051-1054.

(88) Zhang, Q.; Wang, M.; Wooley, K. L. *Curr Org Chem* **2005**, *9*, 1053-1066.

(89) Lai, J. T.; Filla, D.; Shea, R. *Macromolecules* **2002**, *35*, 6754-6756.

(90) Liu, J.; Zhang, Q.; Remsen, E. E.; Wooley, K. L. *Biomacromolecules* **2001**, *2*, 362-368.

(91) Zhang, K.; Fang, H.; Chen, Z.; Taylor, J.-S. A.; Wooley, K. L. *Bioconjugate Chem.* **2008**, *19*, 1880-1887.

(92) Pack, D. W.; Hoffman, A. S.; Pun, S.; Stayton, P. S. *Nat. Rev. Drug Discov.* **2005**, *4*, 581-593.

(93) Rossin, R.; Pan, D. P. J.; Qi, K.; Turner, J. L.; Sun, X. K.; Wooley, K. L.; Welch, M. J. *J. Nucl. Med.* **2005**, *46*, 1210-1218.

(94) Fang, H.; Shen, Y.; Taylor, J. S. *RNA* **2010**, *16*, 1429-1435.

(95) Fang, H.; Yue, X.; Li, X.; Taylor, J. S. *Nucleic Acids Res.* **2005**, *33*, 6700-6711.

(96) Rich, J. N.; Bigner, D. D. *Nature Rev. Drug Discov.* **2004**, *3*, 430-446.

(97) Stupp, R.; Mason, W. P.; van den Bent, M. J.; Weller, M.; Fisher, B.; Taphoorn, M. J.; Belanger, K.; Brandes, A. A.; Marosi, C.; Bogdahn, U.; Curschmann, J.; Janzer, R. C.; Ludwin, S. K.; Gorlia, T.; Allgeier, A.; Lacombe, D.; Cairncross, J. G.; Eisenhauer, E.; Mirimanoff, R. O.*N. Engl. J. Med.* **2005**, *352*, 987-996.

(98) Tokatlian, T.; Segura, T. *Nanomed. and Nanobiotechnol.* **2010**, *2*, 305-315.

(99) Dowdy, S. F.; Eguchi, A.; Meade, B. R.; Chang, Y. C.; Fredrickson, C. T.; Willert, K.; Puri, N. *Nature Biotechnol.* **2009**, *27*, 567-571.

(100) Bhatia, S.; Agrawal, A.; Min, D. H.; Singh, N.; Zhu, H. H.; Birjiniuk, A.; von Maltzahn, G.; Harris, T. J.; Xing, D. Y.; Woolfenden, S. D.; Sharp, P. A.; Charest, A. *ACS Nano* **2009**, *3*, 2495-2504.

(101) Akerman, M. E.; Chan, W. C.; Laakkonen, P.; Bhatia, S. N.; Ruoslahti, E. *Proc. Natl. Acad. Sci. U S A* **2002**, *99*, 12617-12621.

(102) Torchilin, V. P. *Nat. Rev. Drug Discov.* **2005**, *4*, 145-160.

(103) Weissleder, R.; Kelly, K.; Sun, E. Y.; Shtatland, T.; Josephson, L. *Nature Biotechnol.* **2005**, *23*, 1418-1423.

(104) Bao, G.; Nitin, N. *Bioconjugate Chem.* **2008**, *19*, 2205-2211.

(105) Bao, G.; Nitin, N.; Santangelo, P. J.; Kim, G.; Nie, S. M. *Nucleic Acids Res.* **2004**, *32-39*.

(106) Thurmond Ii, K. B.; Huang, H.; Clark Jr, C. G.; Kowalewski, T.; Wooley, K. L. *Colloids and Surface B:* **1999**, *16*, 45-54.

(107) Hawker, C. J.; Fukukawa, K. I.; Rossin, R.; Hagooly, A.; Pressly, E. D.; Hunt, J. N.; Messmore, B. W.; Wooley, K. L.; Welch, M. J. *Biomacromolecules* **2008**, *9*, 1329-1339.

(108) Elsabahy, M.; Wooley, K. L. *J. Polym. Chem. Poly. Sci.* **2012**, *50*, 1869-1880.

(109) Nystrom, A. M.; Xu, Z. Q.; Xu, J. Q.; Taylor, S.; Nittis, T.; Stewart, S. A.; Leonard, J.; Wooley, K. L. *Chem. Commun.* **2008**, 3579-3581.

(110) Zhang, K.; Fang, H.; Wang, Z.; Taylor, J.-S. A.; Wooley, K. L. *Biomaterials* **2009**, *30*, 968-977.

(111) Zhang, K.; Fang, H.; Li, Z.; Ma, J.; Hohlbauch, S. V.; Taylor, J. S. A.; Wooley, K. L. *Soft Matter* **2009**, *5*, 3585-3589.

(112) Christian, S.; Pilch, J.; Akerman, M. E.; Porkka, K.; Laakkonen, P.; Ruoslahti, E. *J. Cell. Biol.* **2003**, *163*, 871-878.

(113) Reddy, G. R.; Bhojani, M. S.; McConville, P.; Moody, J.; Moffat, B. A.; Hall, D. E.; Kim, G.; Koo, Y. E. L.; Woolliscroft, M. J.; Sugai, J. V.; Johnson, T. D.; Philbert, M. A.; Kopelman, R.; Rehemtulla, A.; Ross, B. D. *Clin. Cancer. Res.* **2006**, *12*, 6677-6686.

(114) Park, J. H.; von Maltzahn, G.; Zhang, L. L.; Derfus, A. M.; Simberg, D.; Harris, T. J.; Ruoslahti, E.; Bhatia, S. N.; Sailor, M. J. *Small* **2009**, *5*, 694-700.

(115) Ruoslahti, E.; Bhatia, S. N.; Sailor, M. J. *J. Cell Biol.* **2010**, *188*, 759-768.

(116) Orringer, D. A.; Koo, Y. E. L.; Chen, T.; Kim, G.; Hah, H. J.; Xu, H.; Wang, S. Y.; Keep, R.; Philbert, M. A.; Kopelman, R.; Sagher, O. *Neurosurgery* **2009**, *64*, 965-971.

(117) Orringer, D. A.; Koo, Y. E.; Chen, T.; Kopelman, R.; Sagher, O.; Philbert, M. A. *Clin. Pharmacol. Ther.* **2009**, *85*, 531-534.

(118) Bumcrot, D.; Manoharan, M.; Koteliansky, V.; Sah, D. W. Y. *Nat. Chem. Biol.* **2006**, *2*, 711-719.

(119) Davis, M. E.; Zuckerman, J. E.; Choi, C. H. J.; Seligson, D.; Tolcher, A.; Alabi, C. A.; Yen, Y.; Heidel, J. D.; Ribas, A. *Nature* **2010**, *464*, 1067-1070.

(120) Ferrari, M. *Nat. Rev. Clin. Oncol.* **2010**, *7*, 485-486.

(121) Nishikawa, M.; Huang, L. *Hum. Gene. Ther.* **2001**, *12*, 861-870.

(122) Mastrobattista, E.; Hennink, W. E. *Nat. Mater.* **2012**, *11*, 10-12.

(123) Suma, T.; Miyata, K.; Ishii, T.; Uchida, S.; Uchida, H.; Itaka, K.; Nishiyama, N.; Kataoka, K. *Biomaterials* **2012**, *33*, 2770-2779.

(124) Takemoto, H.; Ishii, A.; Miyata, K.; Nakanishi, M.; Oba, M.; Ishii, T.; Yamasaki, Y.; Nishiyama, N.; Kataoka, K. *Biomaterials* **2010**, *31*, 8097-8105.

(125) Li, W. J.; Szoka, F. C. *Pharm. Res.* **2007**, *24*, 438-449.

(126) Murthy, N.; Robichaud, J. R.; Tirrell, D. A.; Stayton, P. S.; Hoffman, A. S. *J. Control Release.* **1999**, *61*, 137-143.

(127) Chen, T.; McIntosh, D.; He, Y.; Kim, J.; Tirrell, D. A.; Scherrer, P.; Fenske, D. B.; Sandhu, A. P.; Cullis, P. R. *Mol.Membr.Biol.* **2004**, *21*, 385-393.

(128) Itaka, K.; Kanayama, N.; Nishiyama, N.; Jang, W. D.; Yamasaki, Y.; Nakamura, K.; Kawaguchi, H.; Kataoka, K. *J. Am. Chem. Soc.* **2004**, *126*, 13612-13613.

(129) Cho, Y. W.; Kim, J. D.; Park, K. *J. Pharm. Pharmacol.* **2003**, *55*, 721-734.

(130) Putnam, D.; Gentry, C. A.; Pack, D. W.; Langer, R. *Proc. Natl. Acad. Sci. USA.* **2001**, *98*, 1200-1205.

(131) Luo, S. B.; Cheng, R.; Meng, F. H.; Park, T. G.; Zhong, Z. Y. *J. Polym. Sci. Pol. Chem.* **2011**, *49*, 3366-3373.

(132) Kanayama, N.; Fukushima, S.; Nishiyama, N.; Itaka, K.; Jang, W. D.; Miyata, K.; Yamasaki, Y.; Chung, U. I.; Kataoka, K. *Chem. Med. Chem.* **2006**, *1*, 439-444.

(133) Fukushima, S.; Miyata, K.; Nishiyama, N.; Kanayama, N.; Yamasaki, Y.; Kataoka, K. *J. Am. Chem. Soc.* **2005**, *127*, 2810-2811.

(134) Akinc, A.; Thomas, M.; Klibanov, A. M.; Langer, R. *J. Gene. Med.* **2005**, *7*, 657-663.

(135) Elsabahy, M.; Wazen, N.; Bayo-Puxan, N.; Deleavey, G.; Servant, M.; Damha, M. J.; Leroux, J. C. *Adv. Funct. Mater.* **2009**, *19*, 3862-3867.

(136) Elsabahy M; Dufresne M-H; J-C, L. *Handbook of Materials for Nanomedicine* **2012**, 169-227.

(137) Elsabahy, M.; Wooley, K. L. *J. Polym. Sci. Pol. Chem.* **2012**, *50*, 1869-1880.

(138) Samarajeewa, S.; Shrestha, R.; Li, Y. L.; Wooley, K. L. *J. Am. Chem. Soc.* **2012**, *134*, 1235-1242.

(139) Welch, M. J.; Pressly, E. D.; Rossin, R.; Hagooly, A.; Fukukawa, K. I.; Messmore, B. W.; Wooley, K. L.; Lamm, M. S.; Hule, R. A.; Pochan, D. J.; Hawker, C. J. *Biomacromolecules* **2007**, *8*, 3126-3134.

(140) Thurmond, K. B.; Huang, H.; Clark Jr, C. G.; Kowalewski, T.; Wooley, K. L. *Colloids and Surface B* **1999**, *16*, 45-54.

(141) Zhang, K.; Fang, H.; Shen, G.; Taylor, J. S.; Wooley, K. L. *Proc. Am. Thorac. Soc.* **2009**, *6*, 450-457.

(142) Ma, Q. G.; Wooley, K. L. *J. Polym. Sci. Pol. Chem.* **2000**, *38*, 4805-4820.

(143) Heng, B. C.; Zhao, X.; Tan, E. C.; Khamis, N.; Assodani, A.; Xiong, S.; Ruedl, C.; Ng, K. W.; Loo, J. S. *Arch Toxicol* **2011**, *85*, 1517-1528.

(144) Hussain, S.; Boland, S.; Baeza-Squiban, A.; Hamel, R.; Thomassen, L. C.; Martens, J. A.; Billon-Galland, M. A.; Fleury-Feith, J.; Moisan, F.; Pairon, J. C.; Marano, F. *Toxicology* **2009**, *260*, 142-149.

(145) Rettig, L.; Haen, S. P.; Bittermann, A. G.; von Boehmer, L.; Curioni, A.; Kramer, S. D.; Knuth, A.; Pascolo, S. *Blood* **2010**, *115*, 4533-4541.

(146) Poland, C. A.; Duffin, R.; Kinloch, I.; Maynard, A.; Wallace, W. A. H.; Seaton, A.; Stone, V.; Brown, S.; MacNee, W.; Donaldson, K. *Nat. Nanotechnol.* **2008**, *3*, 423-428.

(147) Tao, W. K.; Mao, X. Z.; Davide, J. P.; Ng, B.; Cai, M. M.; Burke, P. A.; Sachs, A. B.; Sepp-Lorenzino, L. *Mol. Ther.* **2011**, *19*, 567-575.

(148) Cui, Z. R.; Han, S. J.; Vangasseri, D. P.; Huang, L. *Mol. Pharm.* **2005**, *2*, 22-28.

(149) Heng, B. C.; Zhao, X. X.; Tan, E. C.; Khamis, N.; Assodani, A.; Xiong, S. J.; Ruedl, C.; Ng, K. W.; Loo, J. S. C. *Arch. Toxicol.* **2011**, *85*, 1517-1528.

(150) Dufes, C.; Uchegbu, I. F.; Schatzlein, A. G. *Adv. Drug Deliver. Rev.* **2005**, *57*, 2177-2202.

(151) Hong, S. P.; Leroueil, P. R.; Janus, E. K.; Peters, J. L.; Kober, M. M.; Islam, M. T.; Orr, B. G.; Baker, J. R.; Holl, M. M. B. *Bioconjugate Chem.* **2006**, *17*, 728-734.

(152) Zhang, S. G. *Nat. Nanotechnol.* **2006**, *1*, 169-170.

(153) Maltzahn, G. V.; Park, J.-H.; Lin, K. Y.; Singh, N.; Schwoppe, C.; Mesters, R.; Berdel, W. E.; Ruoslahti, E.; Sailor, M. J.; Bhatia, S. N. *Nat. Mater.* **2011**, *10*, 545-552.

(154) Welch, M. J.; Rossin, R.; Pan, D. P. J.; Qi, K.; Turner, J. L.; Sun, X. K.; Wooley, K. L. *J. Nucl. Med.* **2005**, *46*, 1210-1218.

(155) Geng, Y.; Dalhaimer, P.; Cai, S. S.; Tsai, R.; Tewari, M.; Minko, T.; Discher, D. E. *Nat. Nanotechnol.* **2007**, *2*, 249-255.

(156) Decuzzi, P.; Godin, B.; Tanaka, T.; Lee, S. Y.; Chiappini, C.; Liu, X.; Ferrari, M. *J. Control. Release* **2010**, *141*, 320-327.

(157) Lee, N. S.; Lin, L. Y.; Neumann, W. L.; Freskos, J. N.; Karwa, A.; Shieh, J. J.; Dorshow, R. B.; Wooley, K. L. *Small* **2011**, *7*, 1998-2003.

(158) Zhang, K.; Fang, H. F.; Li, Z.; Ma, J.; Hohlbauch, S. V.; Taylor, J. S. A.; Wooley, K. L. *Soft Matter* **2009**, *5*, 5045-5045.

(159) Zhang, K.; Rossin, R.; Hagooly, A.; Chen, Z.; Welch, M. J.; Wooley, K. L. *J. Polym.Sci. Poly. Chem.* **2008**, *46*, 7578-7583.

(161) Doshi, N.; Mitragotri, S. *Interface* **2010**, *7*, 403-410.

(162) Petzetakis, N.; Dove, A. P.; O'Reilly, R. K. *Chem Sci* 2011, *2*, 955-960.

(163) Nam, H. Y.; Nam, K.; Hahn, H. J.; Kim, B. H.; Lim, H. J.; Kim, H. J.; Choi, J. S.; Park, J. S. *Biomaterials* **2009**, *30*, 665-670.

(164) Gao, H.; Elsabahy, M.; Giger, E. V.; Li, D. K.; Prud'homme, R. E.; Leroux, J. C. *Biomacromolecules* **2010**, *11*, 889-895.

(165) Almutairi, A.; Rossin, R.; Shokeen, M.; Hagooly, A.; Ananth, A.; Capoccia, B.; Guillaudeu, S.; Abendschein, D.; Anderson, C. J.; Welch, M. J.; Frechet, J. M. *Proc Natl Acad Sci U S A* **2009**, *106*, 685-690.

APPENDIX A

HIGHLY SPECIFIC *IN VIVO* TARGETING OF INOS MRNA AND ENHANCED CELLULAR UPTAKE OF ANTISENSE PNAS MEDIATED BY CATIONIC SHELL CROSSLINKED NANOPARTICLES*

Acute lung injury (ALI) is a complex lung disease characterized by the up-regulation of inflammatory mediators in the host followed by dyspnea, hypoxemia and pulmonary edema. Over expression of inducible nitric oxide synthase (iNOS) results in production of high levels of nitric oxide, which in turn plays a crucial role in mediating acute lung injury. Thus, there is a great interest in developing probes for sensitive and specific imaging of iNOS expression toward diagnosis of ALI. In this study, we employ peptide nucleic acids (PNAs) as a candidate, which have several advantages including *in vivo* stability and superior binding affinity that make them an ideal platform for development of antisense theranostic agents. However, their membrane impermeability that results in poor cellular uptake limits their biological applications. Herein, we report the preparation of an iNOS imaging probe through electrostatic complexation between a PNA-oligodeoxynucleotide (ODN) hybrid and cationic shell-crosslinked knedel-like nanoparticle (cSCK) that allows for enhanced cellular uptake of PNA.

In collaboration with Yuefei Shen[†], Aida Ibricevic[§], Sean P. Gunsten[§], Michael J. Welch[#], Steven L. Brody[§,#], John-Stephen A. Taylor[,†] and Yongjian Liu*[,#] [†]Department of Chemistry, Washington University in Saint Louis, [§] Department of Medicine, Washington University in Saint Louis, [#] Department of Radiology, Washington University in Saint Louis.

We found complete binding of cSCK amine to ODN phosphate (ratio of cSCK nitrogen to ODN phosphate, N/P) was achieved at 8:1 ratio as shown by gel retardation assay. PNA-ODN-cSCK nanocomplexes showed efficient cellular entry in RAW 264.7 cell line, compared to naked PNA. Additionally, to determine the specific targeting of iNOS

mRNA, antisense or scramble PNAs radiolabeled with ^{123}I were complexed with cSCKs. ^{123}I-PNA$_{antisense}$-ODN-cSCK nanocomplexes demonstrated significantly higher retention in iNOS-induced RAW cell model when compared to ^{123}I-PNA$_{scramble}$-ODN-cSCK. Moreover, increased retention of radiolabeled PNA$_{antisense}$-ODN-cSCK was also observed *in vivo* in iNOS-induced mouse lung after intratracheal administration of nanocomplexes. This work shows specific and sensitive *in vitro* and *in vivo* detection of iNOS mRNA with radiolabeled nanocomplexes and their potential in early diagnosis of ALI.

APPENDIX B

PEGYLATION OF CATIONIC, SHELL-CROSSLINKED-KNEDEL-LIKE NANOPARTICLES MODULATES INFLAMMATION AND ENHANCES CELLULAR UPTAKE IN THE LUNG *

The airway provides a major route for delivery of nanoparticles bearing therapeutic or diagnostic payloads with advantages for local and systemic applications, however optimizing a nanoplatform for this application remains challenging. Poly(ethylene glycol) (PEG) surface modification is commonly used to improve the performance of intravenously-administered nanoparticles but less is known about the behavior of PEGylated nanoparticles delivered to the airway, where complex interactions with innate immune and barrier functions must be considered. We assess the behavior of a library of cationic, shell crosslinked knedel-like nanoparticles (cSCKs), constructed with varying amounts of primary and tertiary amines or PEG (1.5 kDa PEG with 2, 5 or 10 molecules/polymer arms) on the outer shell. Following delivery of cSCK to the lung *via* the trachea, the acute inflammatory response and nanoparticle fate were studied.

In collaboration with Aida Ibricevic[§], Sean P. Gunsten[§], Ke Zhang, Jing Yi Sun, Michael J. Welch[#], Yongjian Liu[#] and Steven L. Brody[§,#,] [§] Department of Medicine, Washington University in Saint Louis, [#] Department of Radiology, Washington University in Saint Louis.

Assay of immune cells and cytokines recovered in bronchoalveolar lavage after 24 h showed that non-PEGylated cSCKs with any modification induced marked inflammation, whereas PEGylation of particles resulted in significantly less inflammation, in a PEG dose-dependent manner. PEGylation also enhanced the entry of cSCKs in lung alveolar epithelial cells and improved penetration through surfactant and mucosal barriers. Endocytosis inhibitor studies showed that PEGylation altered the mechanism of uptake in lung epithelial cells. Non-PEGylated cSCKs used clathrin- and dynamin-dependent pathways, whereas PEGylated cSCKs utilized predominantly non-clathrin, dynamin-independent routes of endocytosis. These results indicate that PEGylation favorably affect the *in vivo* properties of nanoparticles and enhanced the performance following airway delivery.